• U C •

FCTUC FACULDADE DE CIÊNCIAS
E TECNOLOGIA
UNIVERSIDADE DE COIMBRA

Lea Cristele Rosa Velez

Computational model of the effect of alpha oscillatory phase on the timing of neuronal activations and resulting motor responses

Dissertation presented to University of Coimbra in fulfilment of the requirements to obtain a Master's degree in Biomedical Engineering

Supervisors:

Dr. Maria Ribeiro (Institute for Biomedical Imaging and Life Sciences, Faculty of Medicine, University of Coimbra)

Coimbra, 2017

This project was developed in collaboration with:

Institute for Biomedical Imaging and Life Sciences,
Faculty of Medicine, Universidade de Coimbra

Faculty of Medicine, Universidade de Coimbra

Acknowledgements

Tenho absolutamente de começar por agradecer à minha orientadora, Maria, não só pela proposta de um projecto numa área tão especial e fascinante para mim, computação em neurociências, como, e acima de tudo, pela quantidade incrível de apoio, paciência, ajuda e motivação que me cedeu durante este ano.

À minha família, a quem devo tudo, pelo esforço constante de tornar os meus sonhos em realidade, e pelos abraços que me esvaziam de angústia e stress.

À Bethoven, cujo apoio incondicional é digno de irmã e foi crucial para poder estar a escrever isto hoje, de cabeça erguida.

À Lu, que me ensinou o que era a verdadeira amizade.

À Nice, pelo exemplo de força e perseverança que foi para mim, e pelos silêncios de cumplicidade total.

Ao Manel, pelos dons da música e da palavra, ambos capazes de me erguer após tudo e mais alguma coisa.

À Estudantina Feminina de Coimbra, pela beleza que foi criá-la e vê-la crescer, e pelo que me ensinou nesse processo.

Ao Grupo de Cordas, pela clara demonstração que foi, na minha vida, do quão incrivelmente melhor é amar o que fazemos.

Aos três P's progressivos, pelo que significaram para mim nesta etapa.

A toda a Luz que há na minha vida.

E, por fim, aos tantos sorrisos de amizade que tornaram tudo possível, e que tornaram esta experiência tão lindamente única e marcante!

Abstract

Human behaviour presents high moment-to-moment variability. In fact, when repeatedly performing the same sensorimotor task, subjects' response times vary from one moment to the next. This high within-subject variability in human behavioural response timing has long encouraged researchers to uncover the underlying mechanisms of cognition and sensory stimulus neural processing. Current reaction time (RT) models attribute the source of this variability to variability in the evidence accumulation process, before making a response. Yet, recent findings suggest that the phase of alpha oscillations in the brain modulates the timing of neuronal population activity, opening the possibility that, in alternative to current models, reaction time variability arises from variability in the timing of information transmission in the brain. We propose a computational model focusing on this very aspect, by simulating the neural mechanisms behind information transmission during sensory processing in the brain, while focusing on an alpha oscillatory phase-dependent neuronal population activation. Notably, our model was able to predict important associations between alpha oscillations and response times. Furthermore, we were able to successfully fit our simulated data to empirical RT data from two auditory tasks (simple RT and go/no-go), with subjects from two different age groups (young and older adults), and obtained differences in the model's parameters that appear to align with what is known from the literature.

Resumo

O comportamento humano varia de um momento para o outro. Na realidade, quando uma tarefa sensório-motora é repetida várias vezes, os tempos de reacção de um sujeito variam ao longo da tarefa. Esta alta variabilidade, para cada sujeito, que existe no tempo de resposta comportamental humana, tem motivado investigadores a estudar os mecanismos que estão por trás da cognição e processamento de estímulos sensoriais. Os modelos de tempo de reacção actuais atribuem como causa desta variabilidade a variabilidade no processo de acumulação de evidência, antes da formulação de uma resposta. No entanto, descobertas recentes sugerem que a fase de oscilação das ondas alfa no cérebro modulam o tempo de activação das populações neuronais, abrindo a possibilidade de esta variabilidade nos tempos de reacção surgir da variabilidade nos tempos de transmissão de informação no cérebro. Aqui propomos um modelo computacional focado neste mesmo aspecto, simulando os mecanismos neurais por trás da transmissão de informação durante o processamento sensorial no cérebro, e assumindo uma activação de populações neuronais dependente da fase das ondas alfa. Notavelmente, o nosso modelo conseguiu prever associações importantes entre a frequência das ondas alfa e os tempos de reacção. Para além disso, conseguimos fazer o ajuste, com sucesso, de dados de tempo de reacção simulados a dados de tempo de reacção empíricos obtidos usando duas tarefas experimentais ("simple RT" e "go/no-go"), com sujeitos de dois grupos etários (jovens adultos e adultos seniores). Nesta análise, obtivemos diferenças nos parâmetros do modelo que aparentam estar de acordo com o que se sabe da literatura sobre as diferenças de processamento neuronal nestes dois tipos de tarefas experimentais.

Contents

1 Introduction

1.1 Motivation & goals

The high within-subject variability in human behavioural response timing, when performing the same task repeatedly, has long motivated scientists to study the underlying mechanisms of cognition. The analysis of how different experimental conditions affect reaction times (RTs) has proven useful for testing models and hypotheses about the underlying processes and structures of mental architecture (Ratcliff R. , 2006) (Ratcliff, Thapar, & McKoon, 2001) (Smith, 1995). One of the main types of RT data comes from one-choice tasks, namely "simple RT" tasks, where a subject must detect the onset of a sensory stimulus and respond, as quickly as possible, to indicate its detection. In a typical reaction time experiment, each subject repeats the trials several times producing a different RT each time. The distribution of RTs from the same subject reveals several characteristics of RT data. This within-subject variability inherent to this type of data makes for very characteristic RT distributions, which suggest several hypotheses regarding the neural mechanisms underlying these types of cognitive processes. Computational RT models can help test hypotheses regarding the components of the cognitive processing underlying performance on these tasks by fitting RT distributions to its simulated data. Models can then be tested for their ability to predict the observed shape of RT distributions from empirical data (Van Zandt, 2000). RT distributions are characterized by their positive skewness (Ratcliff R. , 1979), i.e. their ex-Gaussian form, which plays an important role in RT model fitting. In order to be successful, a model must correctly reproduce the shape of the distribution and, specifically, must capture the behaviour of the distribution's right tail (Ratcliff & Van Dongen, 2011). Many models have arisen for choice RT data, such as the diffusion decision model (DDM) (Ratcliff & McKoon, 2008) or the linear ballistic accumulator (LBA) (Brown & Heathcote, The Simplest Complete Model of Choice Response Time: Linear Ballistic Accumulation, 2008),

with focus on the evidence accumulation needed for a subject to make a choice and, then, respond.

Although a few models have successfully been applied to simple detection (one-choice) RT tasks (Ratcliff & Van Dongen, 2011) (Fisher, Walsh, Blaha, & Gunzelmann, 2015), these also focus on the accumulation of evidence until a threshold is reached to produce a response. However, neurophysiological measurements of brain activity during task processing suggest an alternative mechanism where reaction time variability arises from variability in the timing of information transfer across cortical areas. To our knowledge, no computational model has arisen that can both produce successful RT distributions and satisfyingly explain how the successive processing of a stimulus along the cortex works, what components of processing are involved, or how these vary under different conditions, such as task difficulty.

When it comes to stimulus processing, as is for auditory or visual stimuli, much is known about the cortical regions involved in the process, but not about the timing of this processing, specifically about what modulates the timing of communication between the involved brain processing areas. Coon et al. (2016) showed that the phase of alpha oscillations modulates the timing of neuronal activity. Specifically, they showed that the variability in latency incurred in communication between neuronal populations is a function of alpha oscillatory phase, and that reaction time variability can be totally accounted for by this intrinsic variability. We saw this as a possible foundation for explaining variability found in response timing for very simple, straight-forward, tasks, such as the simple detection tasks where decision processes are minimized.

In order to test this hypothesis that reaction time variability can be accounted for by the variability in latency incurred in communication between neuronal populations as a function of alpha oscillatory phase, we developed a new computational reaction time model that computes the mathematics underlying sensory stimulus processing by assuming a phase-dependent transmission of activity between neuronal populations responsible for processing the said

stimulus. This model is designed for one-choice RT tasks, focusing on the neural aspects of processing a stimulus in the brain, instead of on the intuitive evidence accumulation aspect required for making a decision when comparing two or more different responses.

Our model produced reaction time distributions that were similar to empirical data, suggesting that this mechanism could indeed account for the reaction time variability observed in simple reaction time tasks. Furthermore, our model was tested against different experimental conditions and with data from different groups of subjects, a group of young and a group of older adults, and was able to successfully provide insights on how ageing and task differences might produce different reaction time distributions.

1.2 Theoretical background

1.2.1 Within-subject trial-by-trial reaction time variability

When we perform multiple trials of a simple reaction-time task, where in each trial a subject must execute a motor response as soon as he/she detects a presented stimulus, we obtain highly variable values for the resulting reaction times of each subject. This variability is what we refer to when we mention high variability in the timing of human behavioural responses. Great efforts have been put into discovering the origin of this variability. Since the task remains the same between trials, something in the neural processing of the task must explain these variations in the timing of reactions. Considering the example of a simple auditory-motor task, where a subject presses a button to indicate the detection of an auditory stimulus, information needs to be processed over a trajectory of cortical areas, namely the auditory and motor cortices. Although research over the past decades has shown evidence towards brain plasticity (i.e. the ability of the brain to change its structure throughout life) in processes such as learning (Moser,

Moser, & Andersen, 1994) (Piccioli & Littleton, 2014) and neurorehabilitation (Kelly, Foxe, & Garavan, 2006), such plastic changes in anatomy cannot explain these alterations in brain processes on the time scale of seconds. This leads to the assumption that these changes are caused by trial-by-trial variations in function.

1.2.1.1 RT distributions

In a typical RT experiment, each subject repeats the trials several times, and in each trial the RT obtained is slightly different. This within-subject variability inherent to RT data makes for very characteristic distributions. RT distributions are characterized by their positive skewness (Ratcliff R. , 1979), i.e. their ex-Gaussian form. Several models have been proposed testing the neural mechanisms underlying the RT variability that results in this characteristic shape of RT distribution. Ratcliff (1979) suggested characterizing the shape of empirical distributions by fitting an explicit density function (probability density function, PDF), and the ex-Gaussian density has been largely adopted (Andrews & Heathcote, 2001). Researchers have shown increased interest in characterizing the shape of RT distributions instead of focusing only on a measure of the distribution's central tendency (e.g. the mean). Fitting a model to the mean RT only can mask important details of the data that can be revealed by examining the entire distribution, such as the behaviour of fast and slow responses across experimental conditions (Heathcote, Popiel, & Mewhort, 1991). Furthermore, the RT distribution can provide an important interface between theory and data, since the ability of a model to predict the observed shape of a RT distribution is considered a critical test of that model (Luce, 1986).

To provide further insight into what defines an ex-Gaussian distribution, a visual representation is displayed in Figure 1. Ex-Gaussian distributions are mainly characterized by three parameters: μ [represents the mean of the normal (Gaussian) portion of the distribution] – reflects average performance –, σ [the standard deviation of the normal portion of the distribution] – reflects variability

in performance –, and τ [the mean and standard deviation of the exponential part of the distribution – which characterizes the behaviour of the tail, resulting in a positive skew, for RT distributions] – reflects extremes in performance, more specifically, extremely slow responses. (Heathcote, Popiel, & Mewhort, 1991). The main interest of RT studies lies in how RT changes with experimental manipulations. Therefore, when comparing RT distributions obtained from different experimental conditions, the ex-Gaussian approach (i.e. fitting the ex-Gaussian to data) allows us to determine whether the effects of those conditions are attributable to shift (μ), spread (σ), or skew (τ) in RT distributions, which sets the ex-Gaussian approach as one with great interpretative power (McAuley, Yap, Christ, & White, 2006).

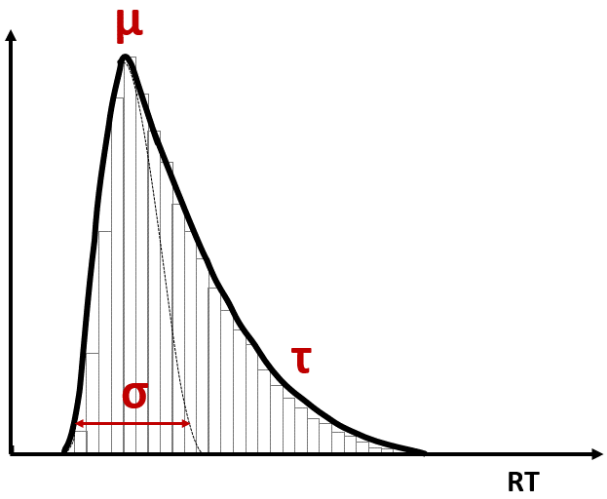

Figure 1. Schematic representation of a RT distribution (histogram of RT values obtained from the same subject performing an RT task repeatedly) and its ex-Gaussian fit. The ex-Gaussian distribution (displayed through its density function by the black line) can be fit to RT data (characterized by the histogram). Ex-Gaussian parameters (μ, σ, τ), and their contribution to the final curve are also displayed. μ is the mean of the Gaussian portion of the distribution, σ the standard deviation of that same portion, and τ the mean and standard deviation of the exponential part of the distribution (thus, characterizes the behaviour of the distribution's tail).

1.2.1.2 How RT distributions change with experimental conditions

There are many experimental paradigms to obtain RT data (see Sternberg's (2004) discussion on reaction-time experimentation for an explanation on different approaches and considerations in obtaining RT data), namely the "simple RT" task, where only one stimulus is presented to the subject, and only one response (which is known in advance) is required, the "choice RT: 1-1 mapping" task, where there is more than one type of stimulus, and each stimulus demands a unique response, the "choice RT: Go/No-go" task, where two different stimuli exist, but only one response is demanded for one of the stimulus types (i.e. one of the stimuli, the "no-go" component, requires no response from the subject), and the "choice RT: many-one mapping" task, also known as the RT categorizing task, where multiple stimuli exist for only one type of response, and all stimuli are categorized as either "critical" or "non-critical", requiring a response from the subject indicating those who are "critical".

The main interest in studying reaction times is mostly in studying how experimental variables (factors) change RT, i.e. the effects of the factors and how these effects combine. An increasing number of studies has arisen reporting the effects of aging on reaction tasks (Ratcliff, Thapar, & McKoon, 2001) (Ben-David, Eidels, & Donkin, 2014) (McAuley, Yap, Christ, & White, 2006) (Gottsdanker, 1982) (Dykiert, Der, Starr, & Deary, 2012). Ratcliff et al. (2001) reported slower responses and wider distributions of RTs for older subjects, compared to younger subjects, across conditions, and were able to attribute this difference to older subjects having longer motor execution times and more conservative response criteria than their younger counterparts. In a study performed by Ben-David et al. (2014), to study the effects of aging and distractors on the detection of redundant visual targets, they reported overall slower RTs for older subjects, compared to young subjects, but attributed those differences to the older subjects' incapacity of filtering out the distractors. A study on the effect of age on the efficiency of inhibitory control using the ex-Gaussian approach (i.e. fitting the ex-Gaussian to

data) also revealed significant changes in RT distributions (reflected by the ex-Gaussian parameters, μ, σ and τ) between young adults and older adults. Specifically, they found that the performance of older adults was slower (higher μ), more variable (higher σ), and more extreme (higher τ) than that of young adults (McAuley, Yap, Christ, & White, 2006). It has also been reported that RT increases (i.e. slows) with increasing number of alternatives for a single choice (Hyman, 1953), i.e. with more alternatives to process for a decision, and with increasing difficulty of a decision (Ratcliff & McKoon, 2008).

RT distributions are a common focus in RT analysis, and it is them that provide the data for modelling. Computational RT models are useful for testing different mechanisms of the cognitive processing underlying performance on RT tasks by fitting distributions to its simulated data. Models can then be tested for their ability to predict the observed shape of RT distributions from empirical data (Van Zandt, 2000). In order to be successful, a model must correctly reproduce the shape of the distribution and, specifically, must capture the behaviour of the distribution's right tail (Ratcliff & Van Dongen, 2011). We will briefly review existing reaction time models below.

1.2.2 Reaction time models

A great number of models have arisen for choice RT data, such as the diffusion decision model (DDM) (Ratcliff & McKoon, 2008), the leaky competing accumulator (Usher & McClelland, 2001), or the linear ballistic accumulator (LBA) (Brown & Heathcote, The Simplest Complete Model of Choice Response Time: Linear Ballistic Accumulation, 2008), all with focus on the evidence accumulation needed for a subject to make a choice and, then, respond. These models focus on choice RT, dealing not only with the mean RTs and their distributions, but also with the accuracy (correct/incorrect) of the responses.

Diffusion models for simple, two-choice decision processes have received increasing attention over the last years, for their ability to account for several behavioural data (and for several experimental paradigms), for their successful application to practical domains (such as aging), allowing new interpretations for well-known empirical phenomena, and for their shown potential in linking neurophysiological and behavioural data, when applied to neurophysiological data (Ratcliff & McKoon, 2008). Diffusion models divide decision processes into a number of components: the quality of the information from a stimulus that drives the decision process, the variability in the quality of information, the criteria that set boundaries on the amount of information (or evidence) that must be accumulated in order for a response to be made, and the non-decisional (encoding and response execution) parts of response time (Ratcliff, Thapar, & McKoon, 2001). These components are largely adopted by several other models.

The complicated effects observed in the shape of RT distributions, the relative speed of correct and incorrect responses, and the interaction of all these with error rates has led to increasingly complicated models of choice RT. In an attempt to simplify the leading models in the field, Brown & Heathcote (2008) proposed a new theory of choice RT – the linear ballistic accumulator (LBA). The LBA is a greatly simplified instance of sequential sampling, which is the dominant theoretical framework of choice RT models, that assumes a decision is made by the accumulation of "evidence" that varies randomly from moment to moment (considering this stochastic accumulation the main reason behind within-subject variability in choice RT) (Brown & Heathcote, The Simplest Complete Model of Choice Response Time: Linear Ballistic Accumulation, 2008). Figure 2 presents a schematic representation of three different versions of models proposed from the stochastic leaky competing accumulator to the LBA. All three models assume accumulators of evidence for each possible response, and a threshold of minimum evidence required to formulate, or choose, a response. The first evidence accumulator to reach this threshold leads to the execution of its associated response. Usher & McClelland's (2001) leaky competing accumulator assumes stochastic accumulation of evidence, i.e. evidence accumulation that varies randomly from moment to moment (Figure 2, left panel). Brown & Heathcote

(2005) proposed a simplification of the leaky competitor accumulator by omitting the within-trial randomness from the evidence accumulation process – the ballistic accumulator (Figure 2, centre panel). The linear ballistic accumulator model further simplified the evidence accumulation process by omitting the nonlinearities from the ballistic accumulator (Figure 2, right panel), assuming a linear evidence accumulation (Brown & Heathcote, 2008). The LBA is explained in detail below.

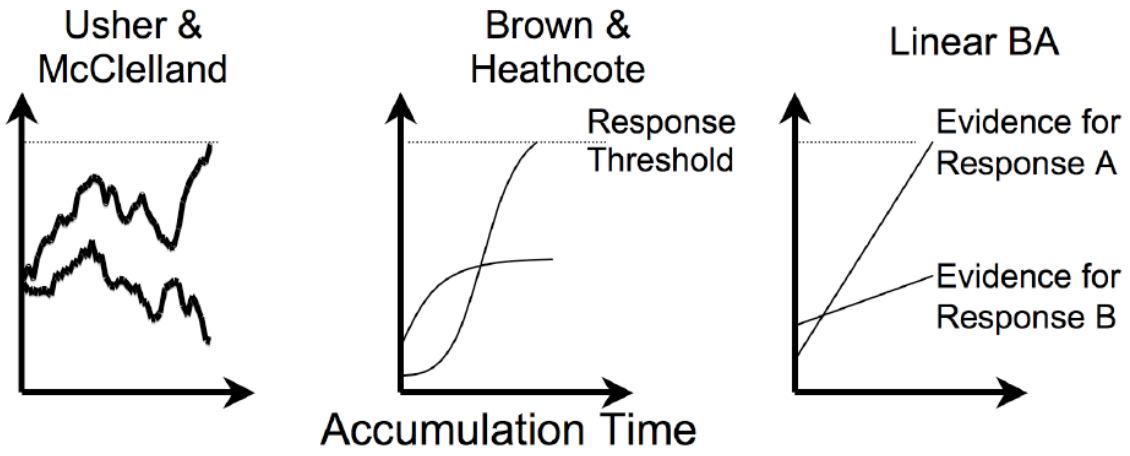

Figure 2. Schematic illustration of Usher & McClelland's (2001, left panel) stochastic accumulator panel. Brown and Heathcote's (2005, centre panel) ballistic accumulator was simplified by omitting within-trial stochastic variation. The linear ballistic accumulator was further simplified by assuming a linear evidence accumulation. From Brown & Heathcote (2008).

The LBA's mathematical simplicity, which still allows for complete analytic solutions (Brown & Heathcote, The Simplest Complete Model of Choice Response Time: Linear Ballistic Accumulation, 2008), highly motivated its choice from our behalf (details explained further ahead, in Chapter 2 – Methods) as a possible means of comparison with our proposed model. As a model of choice RT, it assumes that, for any decision to be made, evidence must accumulate until it reaches a "decision" threshold. Figure 3 displays a schematic representation of a typical LBA decision between two choices. The LBA assumes a linear accumulation of evidence in separate, independent, evidence accumulators for each possible response. These accumulators gather evidence until a threshold (b) is reached for one response. The choice corresponding to that accumulator is then produced, and the

decision time is equal to the time it took for the accumulator to reach the response threshold. An additional, constant, time t_0 is added to the final response time to represent non-decision processes, such as stimulus arrival at the cortex and motor response execution. The speed at which evidence accumulates in each separate accumulator is given by its drift-rate, different for each accumulator, represented by the slopes of the lines in Figure 3. The LBA assumes drift rates to vary randomly and independently between accumulators from trial-to-trial according to a normal distribution with mean v and standard deviation s. The decision process is assumed to begin with each accumulator at its own starting point of evidence accumulation. This starting evidence also varies between trials, and has a randomly assigned value between zero and A. A cannot be higher than b to ensure that evidence needs to be accumulated for a response to be triggered.

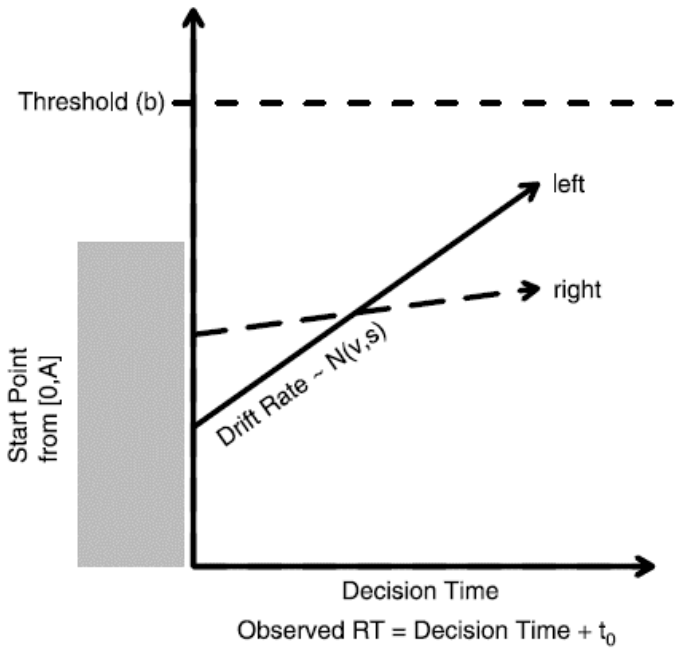

Figure 3. Schematic representation of a typical LBA decision for a two-choice RT task. In the task here considered, subjects must decide whether a cloud of dots appears to be moving to the left or to the right. In the illustrated trial, a left-moving stimulus has been presented. Each choice is represented by a different accumulator (continuous line arrow for "left", dashed arrow for "right"), and the drift rates for the left and right accumulators have been sampled normal distributions with means v and $1 - v$, respectively, and a common standard deviation, s. The usage of $1 - v$ for incorrect responses has become a common practice in LBA application (Donkin, Brown, & Heathcote, 2011). From Donkin, Brown & Heathcote (2011).

Although the above-mentioned models are choice RT models, i.e. designed for choice paradigms, between two or more possible responses, a few models using the same rationale have successfully been applied to simple detection (one-choice) RT tasks (Ratcliff & Van Dongen, 2011) (Fisher, Walsh, Blaha, & Gunzelmann, 2015). However, recent neurophysiological measurements of human brain activity during task processing suggest an alternative mechanism. Namely Coon et al.'s (2016) findings suggest that the phase of alpha oscillations in the brain modulates the timing of neural population activity, opening a possibility that RT variability arises from variability in the timing of information transmission in the brain, instead of variability in the time it takes for evidence to accumulate in the brain. To allow for a more comprehensive analysis of Coon et al.'s results (which motivated our proposed model), described further ahead, we now focus on the sensory information processing mechanisms in the human brain.

1.2.3 The brain

1.2.3.1 General organization of the nervous system

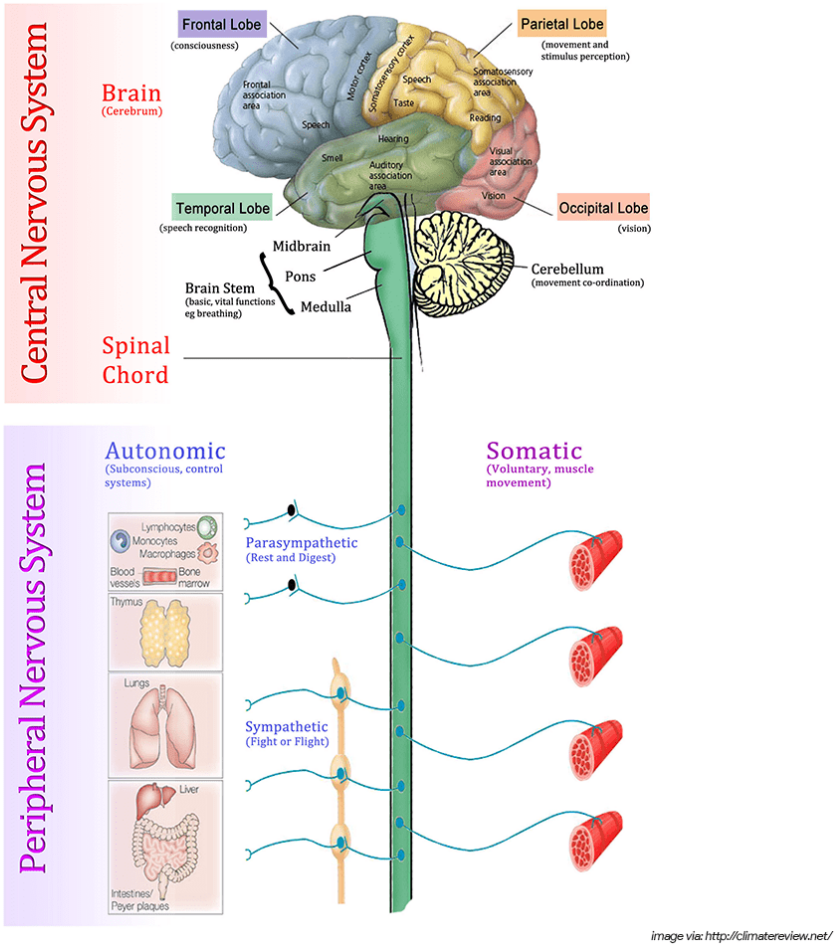

Figure 4. The Nervous System, by James Follet.

The nervous system can be divided in two parts: the central nervous system (CNS), composed by the encephalon and spinal cord, and the peripheral nervous system (PNS), encompassing the cranial and spinal nerves and their associated ganglia (see Figure 4 for a schematic representation of the organization of the nervous system). Neuronal circuits, composed by interconnected neurons that mutually influence each other, are the functional entity of the nervous system (Purves, et al., 2001). Nervous cells, or neurons, are excitable cells specialized in the reception of stimuli and in the conduction of nervous impulses (through their capability of producing action potentials), and are the basic components of neuronal circuits (Snell, 2010). Groups of neuronal circuits with similar function are called neuronal systems, and can be divided in sensorial systems (e.g. visual

and auditory systems), motor systems, that control behavioural responses, and association systems, which are intermediary systems between sensorial and motor systems. The sensory division of the nervous system can, therefore, be considered as the afferent division (information entering the CNS), and the motor division as the efferent division (information is sent from the CNS to the rest of the body). The CNS can be subdivided into the spinal cord and the encephalon, where the latter can be further subdivided into many other structures, such as the cerebellum, the brainstem, the diencephalon (thalamus and hypothalamus), and the telencephalon (cerebral hemispheres). The cerebral cortex is divided in two cerebral hemispheres, which, in turn, are divided into four lobes: frontal, parietal, temporal and occipital (Purves, et al., 2001). Within each lobe there are several cortical areas, and some are, currently, largely associated with certain cortical functions, e.g. the auditory cortex in the temporal lobe and the visual cortex in the occipital lobe (Snell, 2010). Figure 5 displays a representation of the organization of the human brain, including the cortical division into functional lobes. Within the aim of our project, we will focus mainly on the areas in the nervous system involved in stimulus processing, namely auditory stimuli, and in the execution of a motor response.

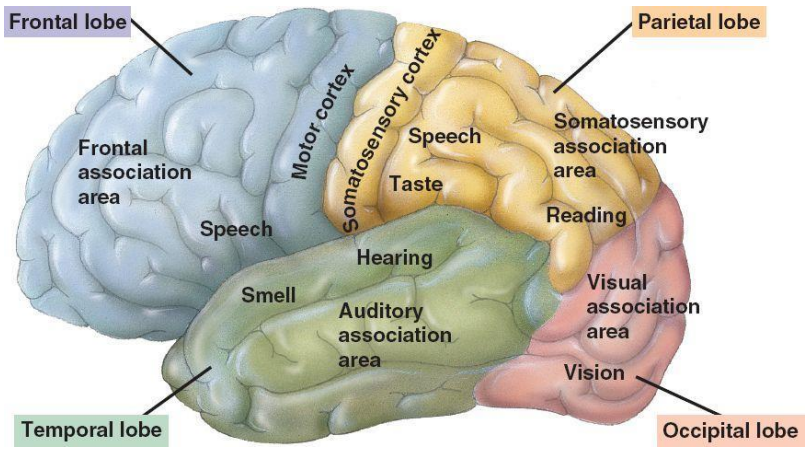

Figure 5. Division of the cortical hemisphere into lobes, and some of their functional areas. Copyright © 2008 Pearson Education, Inc.

1.2.3.2 Hierarchical organization of cortical sensory systems

There is a general hierarchical organization when it comes to sensory processing in the nervous system. Stimuli are detected and transmitted to the peripheral nervous system, which sends the sensory information to the central nervous system for processing. It has become generally understood that, within the CNS, there is also a hierarchy for sensory information processing, such as in the visual system (Hochstein & Ahissar, 2002), auditory system (Okada, et al., 2010), or olfactory system (Savic, Gulyas, Larsson, & Roland, 2000). This means that, within the sensory pathway, there is somewhat of an order of information transmission between cortical areas and neuronal populations. A well-studied example of this is the visual system (Hochstein & Ahissar, 2002) (Rousselet, Thorpe, & Fabre-Thorpe, 2004) (Silvanto, 2015). The visual pathway has a well-defined hierarchical structure for stimulus processing, including the pathway from the retinal cells, which are sensitive to light and fire electrical impulses according with the received input, to the lateral geniculate nucleus (LGN) in the thalamus (the area in the thalamus responsible for relaying visual information to the cortex), which then transmits information to the occipital lobe, namely to the primary visual cortex (V1) (Snell, 2010). Within the visual cortex, it is now generally understood that visual input is processed in a hierarchical fashion, giving rise to conscious perception (Silvanto, 2015). Without getting into too much detail, it is known that V1 has a very well-defined map of the spatial information in vision, and sends much of its input to the next visual cortical region, area V2 (visual area 2), which, in turn, projects to at least three occipital regions: medio-temporal region (MT), visual area 3 (V3), and visual area 4 (V4), and so it goes, with each area projecting forward to several other areas (Rousselet, Thorpe, & Fabre-Thorpe, 2004) (Silvanto, 2015). V1 and V2 are generally considered as "low-level" areas (Hochstein & Ahissar, 2002), receiving visual input and representing simple features of vision, such as lines, or edges, or specific orientation and location. Their outputs are integrated by their successive cortical levels (MT, V3, V4), which gradually generalize over spatial parameters and specialize to represent global features. Finally, further levels integrate their outputs to

represent more abstract forms, objects, and categories. In summary, higher-level cortical areas represent increasingly complex characteristics of images, objects, and categories (Hochstein & Ahissar, 2002). A simple example would be the processing of an image of a chair. The lower-level visual areas would mainly process the overall lines and spatial orientation of the visual input, and as their output would be processed by higher-level areas, it would gradually process the visual input as the overall shape of the chair, finally leading to our acknowledgement that the image we just saw was, indeed, a representation of our concept of "chair". It has been proposed that, aside from this forward hierarchy, which acts implicitly, there is also a reverse hierarchy, which acts explicitly, returning to lower-level areas for higher detailed information, within the general idea perceived by the higher-level areas (Hochstein & Ahissar, 2002). In our example, it would allow the subject to perceive the type of wood of the chair, the details of its edges, etc. Figure 6 provides a schematic diagram of these two types of hierarchy in the visual system.

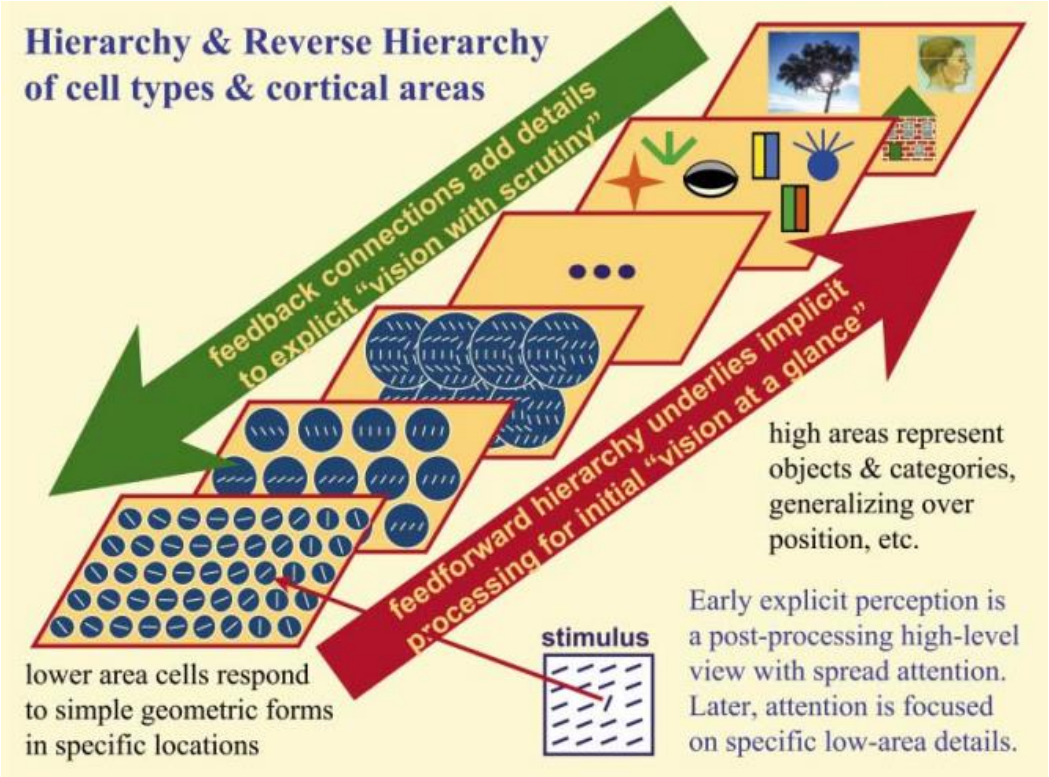

Figure 6. Schematic diagram of classical (forward) hierarchy and reverse hierarchy theory. From Hochstein & Ahissar (2002). With feedforward hierarchy, higher-level cortical areas represent increasingly complex characteristics of the images, objects, and categories.

It is worth noting that, within the frame of this project, for the simple detection of a visual input, simple forward hierarchy would be the main pathway needed for generating a motor response indicating stimulus detection.

The hierarchical organization of the auditory cortex has also been the subject of various studies, and is now generally understood that core regions of the auditory cortex respond to simple auditory stimuli (e.g. tones) whereas downstream regions are selectively responsive to more complex stimuli (e.g. speech). We get into further detail regarding the processing of auditory stimuli, due to the fact that our empirically obtained RT data were a result of an auditory-motor task.

1.2.3.3 Auditory stimulus processing

The auditory cortex (AC), located in the temporal lobe (see Figure 5), is the main area responsible for processing auditory information. When an auditory stimulus is presented, it is detected by the ear where its vibrations are converted into electrical impulses by the cochlea (in the inner ear) (Purves, et al., 2001). These impulses are sent through the brainstem into the cortex. Specifically, this ascending auditory pathway is composed by the spiral ganglion, auditory nerve, cochlear nucleus, olivary nucleus, lateral lemniscus, inferior colliculus, medial geniculate body (in the thalamus), and, finally, the auditory cortex. The auditory cortex is divided into primary auditory cortex (A1) and secondary auditory cortex (or auditory association area, A2). A1 is associated with the primary processing of the auditory information, and sounds are processed in different locations (within A1) according to their frequency (Ehret, 1997). It is believed that A1 performs sound analysis by combining spatially distributed coincident or by time-coordinated neuronal responses (Ehret, 1997). Furthermore, there is now reasonable evidence for the existence of hierarchical processing within the AC – where the A1, receiving direct input from the thalamus, provides input to surrounding areas (Wessinger, et al., 2001). A2 is thought to be essential to the

interpretation of sounds and to its association with other sensory information (Snell, 2010).

When we consider a task such as detecting a sound and pressing a button to indicate its detection, much like the task used in this study (which is further described in Chapter 2 – Methods), we must consider not only the processing of the auditory stimulus by the AC, but also how the information of the stimulus is processed by cortical areas regarding conscious decision upon receiving sensory input (the decision to press the button) and motor response (the button press), both in different areas of the frontal lobe (Snell, 2010). This implicates some level of communication between cortical areas, sending information from one to another, in order to process the information and formulate a response. We discuss considerations on how neuronal populations communicate below.

Although much is known regarding the processing of auditory information in the brain, there are still many unanswered questions, namely regarding the modulation of timing within information processing.

1.2.3.4 Brain oscillations – alpha rhythm

The understanding of how neuronal populations communicate with each other has long been a subject of interest for neuroscientists. Hans Berger (1929) discovered that cortical activity can be captured by electroencephalography in the form of electrical activity. This technique led to the discovery of brain oscillations, and since then electroencephalograms (EEGs) have been used to further understand the different rhythms behind brain function. There are several frequency bands, or ranges, that have been identified throughout the years, and here we will focus on the alpha frequency band (for reasons explained below), also first described by Berger (1929). The alpha rhythm stands for frequencies within the 8 – 13 Hz range, shows the highest amplitude in the human brain and is known for its high prevalence in the posterior regions of the head (mainly occipital, parietal and posterior temporal regions), despite not being limited to those areas

(Niedermeyer & Lopes da Silva, 1982). As an example, studies have shown that voluntary movement tends to be timed in relation to the phase of the alpha rhythm (Bates, 1951). It reaches a mean of about 10 Hz in childhood, which stands as, essentially, the mean alpha frequency of adulthood. The frequency of alpha rhythm tends to decline in the elderly (Niedermeyer & Lopes da Silva, 1982) (Klimesch, 1999), although this decrease was shown to reflect some degree of cerebral pathology, and healthy elderly individuals appear to show little to no decline in alpha frequency (Niedermeyer & Lopes da Silva, 1982) (Grandy, et al., 2013). Since this project focuses on brain waves within the alpha frequency range, and on sensory-motor tasks, it might interest the reader that rhythmic activity in the alpha frequency range has been found strongly related to functions of the motor cortex (the mu rhythm), of the visual cortex in the occipital lobe, and of the auditory cortex in the temporal lobe (the tau rhythm) (Niedermeyer & Lopes da Silva, 1982) (Klimesch, 1999). These were found to be independent from each other. The interest this represents to our project relies on the fact that, not only do all of these independent rhythms have activity related to the cortical areas that would be affected in an auditory-motor task, but they also exhibit frequencies within a similar range, and, as will become apparent in the description of our model (Chapter 2 – Methods), frequency is the main factor contributing to wave distinguishability between tests of our presented model.

Over the last decades an increasing interest has arisen into discovering which components of these oscillatory activities influence neural activity and how. Recent findings suggest that synchronous neural activity, induced by oscillatory activity, modulates sensory and cognitive processes (Herrmann, Munk, & Engel, 2004) (Kahana, 2006) (Klimesch, EEG alpha and theta oscillations reflect cognitive and memory performance: a review and analysis, 1999) (Klimesch, Sauseng, Hanslmayr, Gruber, & Freunberger, 2007). Klimesch et al. (2007) stated in their review a phase-dependent timing of neuronal activity, stating that a neuron is very likely to fire during the phase of high excitability, as opposed to the phase of low excitability, where neurons are unlikely to fire. They stated a crucial principle that, during oscillatory activity, neurons fire synchronously in the excitatory phase, leading to synchronized neural activity being received by

common target cells, which leads to a spread of neural firing through a cell assembly. They further stated their assumption that the functional interaction between units of the same assembly or between units of different assemblies is the result of coordinated timing, which is enabled by oscillations.

There are currently several hypotheses that attempt to explain not only how active neuronal groups interact with each other, but also how this communication is flexibly modulated to originate our cognitive dynamics, such as Fries' (2005) communication through coherence (CTC), which suggests that the oscillation of activated neuronal populations produce temporal windows for communication, where only coherently oscillating neuronal groups are able to interact effectively, or Schalk's (2015) function-through-biased-oscillations (FBO), which hypothesizes that oscillatory voltage amplitude is the main measurement that directly reflects cortical excitability, namely variations in its asymmetric nature. More recently, Coon et al. (2016) showed an important role for the phase of alpha oscillations in modulating the timing of the neural trajectory of task-related population-level activity. Specifically, they showed that the onset of neuronal population activity tends to occur in the trough of alpha oscillations, and that deviations from this relationship were related to changes in the timing of the behavioural response. We agree with their proposal that these findings may provide the basis for a model of variability in the effective speed of information transmission across the brain and for variability in the timing of human behaviour. Further insights are provided below on Coon et al.'s (2016) discoveries and how they inspired our proposed model.

1.2.4 Modulation of the timing of neuronal activations and resulting behaviour by alpha oscillatory phase: a description of Coon et al. (2016)'s study

Although an increasing number of reports showed evidence of a role of oscillatory activity in the gating of neural signal transmission (Fries, 2005) (Hanslmayr, Volberg, Wimber, Dalal, & Greenlee, 2013) (Klimesch, Sauseng, & Hanslmayr, 2007) (Schalk, 2015), and that oscillatory phase in primary motor and visual areas may alter the timing of behaviour (Bates, 1951) (Haegens, Nácher, Luna, Romo, & Jensen, 2011) (Hanslmayr, Volberg, Wimber, Dalal, & Greenlee, 2013) (van Dijk, Schoffelen, Osstenveld, & Jensen, 2008), it remained unknown whether the phase of alpha oscillations modulates the timing of signal propagation across widely distributed neuronal populations that connect a sensory stimulus to a behaviour, thus possibly being responsible for the timing of the observed behavioural responses. In an attempt to answer this question, Coon et al. (2016) used recordings from the cortical surface (electrocorticography, ECoG) to chart the trajectory of task-related neuronal population activity across the cortex in single trials. Following this, they proceeded to examine whether the timing of that population activity, and the timing of the consequent behaviour, was modulated by the phase of low-frequency oscillations, discovering that such was true for oscillations in the alpha band in all subjects and across all task-related cortical areas.

The task used in the experimental trials was a modified Posner cueing task, where subjects maintained a fixed gaze on a central fixation cross throughout the entire experimental run, until presented with a visual cue and, after a random interval (3.5 to 4.5 s), a visual stimulus prompted them to respond with a button press as soon as possible.

They were able to successfully identify the trajectory of neuronal activity across the cortex in single trials (see Figure 7 for exemplary time courses of broadband gamma activity – which has been shown to correspond closely to the

average firing rate of neuronal populations – at five different locations in occipital, temporal, parietal and frontal locations). In fact, they were able to see a clear temporal progression of neuronal activity from occipital, to temporal, to frontal and finally parietal cortices, as would be expected in such a task. This temporal progression can be seen in Figure 7, where clearly different (and progressive) timings of population activity for each location can be observed.

To further validate the physiological relevance of the onset times identified, they established their relationship at individual locations with the phase of oscillatory activity. They found task-related modulation in and around the alpha band, but not in other frequency bands, to be a common feature across all task-related locations. Additionally, they confirmed that the onset of population activity occurred preferentially in the trough of alpha oscillations (see Figures 7b and 8 for a visual representation), preferentially during the falling slope of the trough.

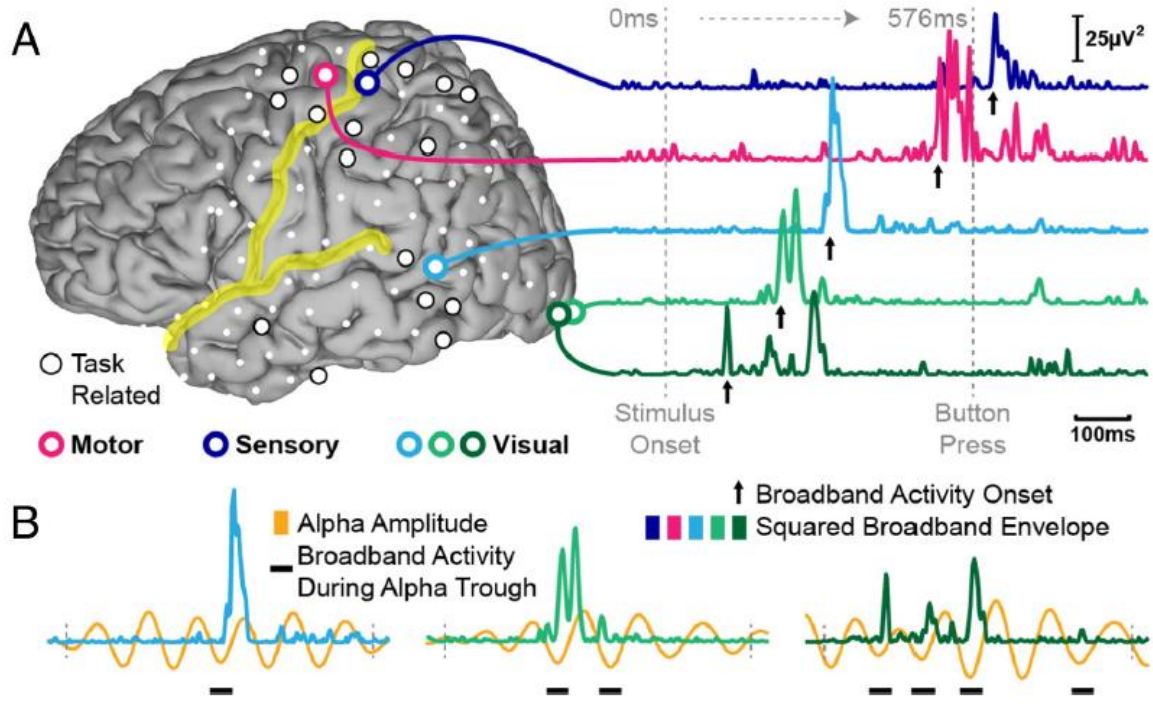

Figure 7. Exemplary spatiotemporal trajectory of task-related neuronal population activity in one single trial. A. Task-related cortical locations from one subject (left), and the time course of neuronal population activity in exemplary locations (right). B. Population-level activity occurs during the trough of alpha oscillations. From Coon et al. (2016).

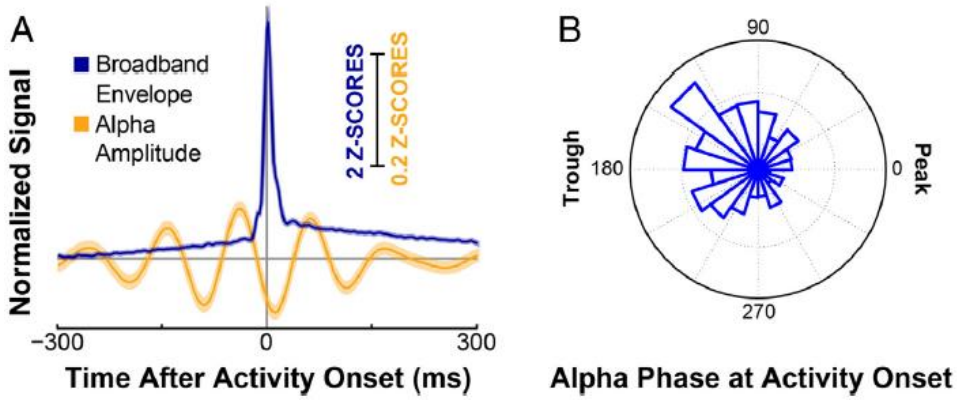

Figure 8. The onset time of neuronal population activity tends to occur during the falling phase of the trough of alpha oscillations. A. Traces show normalized time courses of the amplitude of neuronal population activity (blue) and the amplitude of the activity in the alpha band (orange), averaged across all trials, all task-related locations and across all subjects, and time-locked to the onset of population activity in each corresponding trial (traces show mean ± standard error). B. Polar histogram of alpha phases at the time of detected activity onset from all trials, all locations and all subjects. From Coon et al. (2016).

Supported by the refined relationship between oscillatory phase and the onset of population-level activity, they were able to formulate a hypothesis to explain how oscillatory phase can explain variability in the timing of information transfer between brain areas and, thus, variability in the resulting behaviour. Supported by evidence that information about visual stimuli is propagated across neuronal populations through series of population-level spike volleys (Thorpe, Delorme, & Van Rullen, 2001), that communication between neuronal populations depends on the excitability of the receiving population, and that such cortical excitability is modulated by low-frequency oscillations (Schalk, 2015), they differentiated two distinct possibilities of neuronal communication (Figure 9).

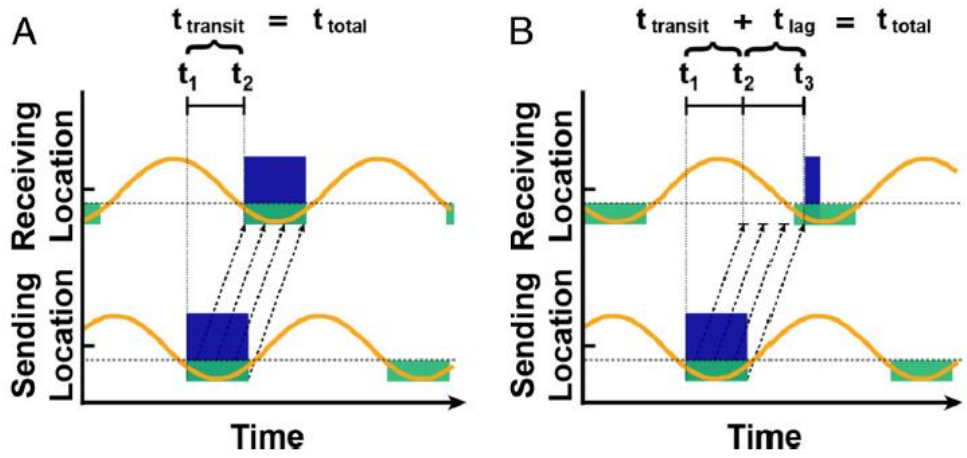

Figure 9. Communication between neuronal populations may be modulated by alpha oscillatory activity. As alpha amplitude (orange lines) decreases past a threshold voltage (dotted grey lines), a neuronal population may process and transmit information (permissive window represented by the green boxes) to the following population. In this attempt to signal the receiving neuronal population, the time it takes for a series of spike volleys (black dotted arrows) to excite population activity (blue boxes) depends on the phase of the receiving population's oscillatory activity. In A, the first spike immediately results in excitation of the receiving population. In B, most spikes do not arrive during a permissive window, delaying excitation by t_{lag} milliseconds. From Coon, et al. (2016).

In the first case (Figure 9a), the phase relationship of oscillatory activity between the sending and receiving locations is such that the first of a series of spike volleys to reach neuronal populations at the receiving location immediately excites them. This means the total amount of time between the start of the neuronal excitation at the sending site and the information being received in the receiving site (t_{total}) is the amount of time it takes to transmit a spike volley from the sending to the receiving site ($t_{transit}$). In contrast, in the second case (Figure 9b), the phase relationship of oscillatory activity at the sending and receiving sites is such that not the first but only a subsequent volley in a series of spike volleys results in cortical excitation at the receiving location. In this scenario, the time between the start of the neuronal excitation at the sending site and the information being received in the receiving site may incur a variable lag (t_{lag}) of up to several tens of milliseconds, after the arrival of the first spike volley. Assuming that the neural trajectory connecting a stimulus to a behaviour is

composed of successive activation of neuronal populations, all in communication with each other, these variable lags at individual locations would accumulate, thus contributing to the observed variability in the behavioural response latency.

These findings lead to the possibility that within-subject variability in response timing in a sensorimotor task can be explained by alpha-band oscillatory activity, namely by having alpha phase-dependent permissive windows for neuronal population activity onset (excitation) in each cortical location of the neural trajectory associated with sensorimotor function.

In order to test the hypothesis proposed by Coon et al, that their findings may provide the basis for a general model of variability in the effective speed of information transmission in the brain, and for variability in the timing of human behaviour, we propose here a computational model that models reaction time variability arising from alpha phase dependent variability in the timing of information transfer in the brain. We proceed by providing a general introduction to our model's proposal, which is thoroughly described in Chapter 2 – Methods.

1.2.4.1 Computational model proposal

As mentioned above, there are a few models that have been successfully applied to simple detection (one-choice) RT tasks (Ratcliff & Van Dongen, 2011) (Fisher, Walsh, Blaha, & Gunzelmann, 2015). However, all of these focus on evidence accumulation processes of cognition. Having been presented with the possibility of an alternative mechanism, based on neurophysiological measurements of human brain activity, and since, to our knowledge, no computational model has arisen that can both successfully reproduce RT distributions and satisfyingly explain how the successive processing of a stimulus along the cortex works, what components of processing are involved, or how these vary under different conditions, such as task difficulty, we were inspired to propose a new model that accommodated these neurophysiological findings.

To test the hypothesis that reaction time variability can be accounted for by the variability in latency incurred in communication between neuronal populations as a function of alpha oscillatory phase, we developed a new computational reaction time model that computes the mathematics underlying the timing of sensorimotor processing by assuming a phase-dependent transmission of activity between neuronal populations responsible for processing the sensorimotor task.

Figure 10 provides a simple schematic representation of the model's approach on information processing throughout the cortex. Our proposed model assumes the presentation of a sensory stimulus, which takes t_0 milliseconds to reach the cortex. Having found reports using auditory event-related potentials reporting latency for the first peak (in the auditory cortex) approximate to 40 ms in adults (Mahajan & McArthur, 2012), although smaller values have been reported (Jain, Bansal, Kumar, & Singh, 2015), we define t_0 as a constant time interval throughout all trials and all model tests, set equal to 30 ms. We assume a hierarchical sensory stimulus processing, by modelling unidirectional communications only, i.e. by having a successive, orderly transmission of information throughout all modelled cortical regions. The total number of cortical regions modelled is dependent on the characteristics of the sensorimotor task being modelled and is given by parameter N, whose value is selected by the user in each run. For each cortical area, an alpha-band sinusoidal oscillation is generated with random phase offset, ϕ (randomly attributed by the model at the beginning of each trial), and alpha-band (8 – 13 Hz) frequency, which is also selected by the user, and attributed to parameter f. All waves are generated with the same amplitude value (= 1), due to our interest in focusing on frequency and phase as the characteristic wave parameters, as suggested by Coon et al.'s discoveries. With focus on Coon et al.'s (2016) findings, we assume a phase-dependent permissive window for neuronal population activity by establishing a threshold under which the onset of population activity can occur at the receiving population (i.e. the neuronal population receiving the information, in series of spike volleys, from the sending neuronal population). Specifically, this threshold

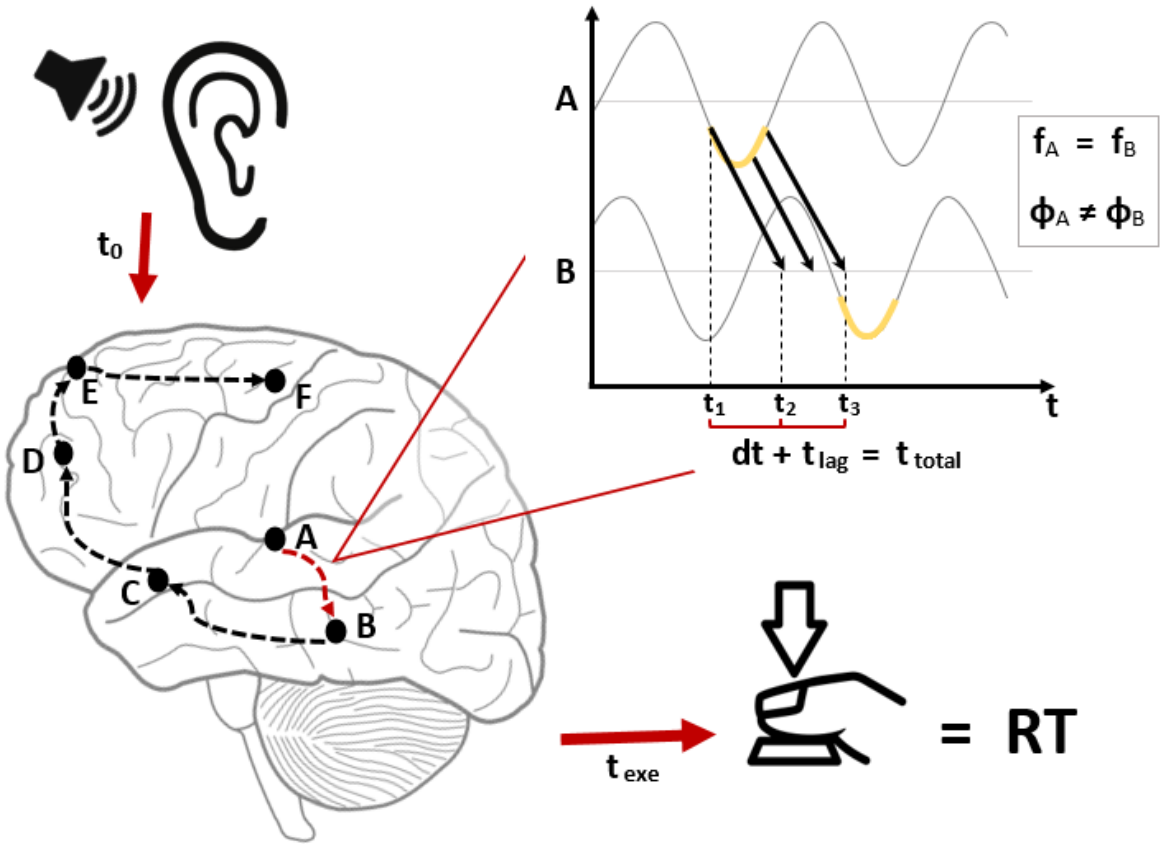

Figure 10. Schematic representation of the model's consideration of the stimulus detection process. An auditory stimulus is presented and takes t_0 seconds to reach the cortex. It is then processed sequentially by several cortical areas. The speed of the information transmission from one area to the other is dependent on the phase of the alpha oscillations. In our model, we considered the alpha-band neuronal activity, with a specific frequency (f) and oscillation phase (ϕ), where only the latter varies across locations. Calculating the instant of time when the onset of population activity on a location occurs, a time lag, t_{lag}, can be added to the minimum amount of time it takes for the stimulus to reach the receiving population, dt, here considered equal for all paths. This lag occurs when the two current oscillations are out of phase with each other and the stimulus does not arrive during the trough of oscillatory activity of the receiving population. After all N brain locations initiate activity, a time constant (t_{exe}) is added, resulting in the final reaction time, RT.

is created for an optimal phase permissive window between 120 – 240º (suggested by Figures 8b and 9 retrieved from Coon et al. (2016)). As suggested by Coon et al.'s (2016) explanations (Figure 9), there is a minimum amount of time for a sending neuronal population to be able to excite the neuronal populations at the receiving site, which they name $t_{transit}$. This value represents the time it takes for

information to be sent between areas, regardless of immediate excitation on the receiving site's population of neurons. In our model, this parameter (*dt*) is defined by the user, thus concluding the three main parameters that are studied in our model tests: *f*, *N* and *dt*. When the last of the *N* cortical areas' neuronal population has initiated cortical activity (which we assume to be immediate, as long as it originates within the phase-dependent permissive window), a time constant (t_{exe}) is added to final time, originating a reaction time. This time constant, t_{exe}, reflects the effective motor response only. We consider t_{exe} = 15 ms, as a rough estimation based on the fastest recorded electromyographic responses for humans (Sourakov, 2009).

Further detail into how the model computes simulated RT data is provided in Chapter 2 – Methods.

Our model produced reaction time distributions that resembled those from empirical data, suggesting that this mechanism could indeed account for the reaction time variability observed in simple reaction time tasks. Furthermore, our model was tested against different experimental conditions (two types of task: simple RT and go/no-go task) and with data from different groups of subjects, a group of young and a group of older adults, and was able to successfully provide insights on how ageing and task differences might produce different reaction time distributions.

2 Methods

2.1 Computational model of the effect of alpha oscillatory phase on the timing of neuronal activations and resulting motor responses

What our model, essentially, aims to do is reproduce what occurs in the brain during a simple auditory-motor detection task, i.e. when a person detects an auditory stimulus and provides a motor response (such as a button press) to indicate its detection. To do this, we need to simulate a mathematical approach to how a sensorimotor task is processed in the brain. In particular, we were interested in modelling the effect of the phase of alpha oscillations in cortico-cortical information transmission, as proposed by Coon et al (2016).

When a stimulus is detected by the brain, sensory information is conveyed into the brain through the sensory organs. This information is then sent through several brain regions for processing. In the scenario of this task, a command for a motor response must then be sent to indicate stimulus detection.

In real life, as studied with empirical data, a simple detection task like the one described, when repeated many times, results in different response times (i.e. time that takes from stimulus onset to button press) or, as henceforth mentioned, reaction times (RT). These variations in RT, which result in an ex-Gaussian distribution (Ratcliff (1979), Heathcote & Brown (2002)) (see Figures 1 or 14 for an example and explanation of an ex-Gaussian distribution), imply some level of variability in the neural processes. Since brain anatomy can be considered to remain unchanged in a time interval of seconds (Coon, et al., 2016), we consider this variation to originate in the actual stimulus and motor processing, occurring between all the neuronal populations it crosses. Specifically, we consider Coon et

al.'s proposal on how alpha-band activity modulates the onset of neuronal population activity (Coon, et al., 2016).

For a matter of simplicity, and as a first approach, we represent alpha-band oscillations as sinusoidal waves, since the general focus of our model is on the wave's frequency and phase offset, both crucial definers of a sinusoidal wave. Specifically, our model generates cosine waves, due to Coon et al.'s graphic representation of brain alpha oscillations, on which we based our alpha modulation research (Coon, et al., 2016). A sinusoidal wave is defined by its frequency, phase offset and amplitude. We fixed the amplitude value for all waves, in the interest of focusing on frequency and phase offset for our study. In each stimulus detection simulation, we consider the frequency of alpha oscillations to be equal in all neuronal populations that process and propagate the stimulus information. The total number of cortical regions that process the stimulus is defined by the user. Phase offset for each brain wave in each brain location is randomly attributed by the model at the moment of sensory information's arrival at the cortex.

We now explain how the model simulates the sensorimotor processing. Primarily, when a neural signal coding a certain sensory stimulus enters the cortex, it is processed by a specific number of cortical regions, being sent from one to another, and, once the final area (motor cortex) is activated, the subject executes a motor response, also considered by our model.

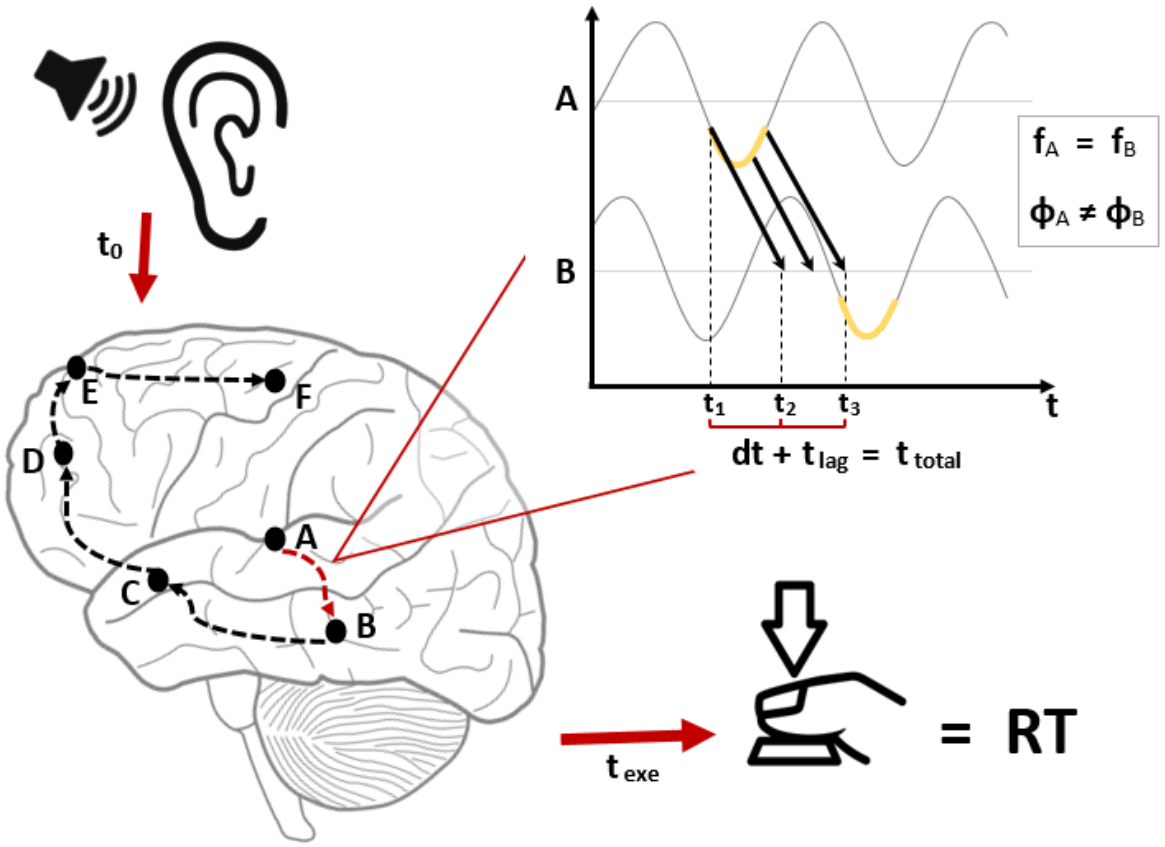

Figure 11. Schematic representation of the model's consideration of the stimulus detection process. An auditory stimulus is presented and takes t_0 seconds to reach the cortex. It is then processed sequentially by several cortical areas. The speed of the information transmission from one area to the other is dependent on the phase of the alpha oscillations. In our model we considered the alpha-band neuronal activity, with a specific frequency (f) and oscillation phase (ϕ), where only the latter varies across locations. Calculating the instant of time when the onset of population activity on a location occurs, a time lag, t_{lag}, can be added to the minimum amount of time it takes for the stimulus to reach the receiving population, dt, here considered equal for all paths. This lag occurs when the two current oscillations are out of phase with each other and the stimulus does not arrive during the trough of oscillatory activity of the receiving population. After all N brain locations initiate activity, a time constant (t_{exe}) is added, resulting in the final reaction time, RT.

Figure 11 displays a schematic representation of how the model obtains a reaction time value. An auditory stimulus is presented to the subject at time $\underline{t} = 0$ s. We consider a constant amount of time, t_0, from the stimulus onset until it reaches the cortex equal to 30 ms. By this time, $t = t_0$, the stimulus begins to travel from one cortical location to the next, in a total of N brain locations. The

excitability of each location's neuronal population is modulated by oscillatory activity in the alpha-band frequency (8-13 Hz). Here we simplify the model by assuming that the alpha frequency is the same in all brain areas and across all trials. This frequency value, *f*, within the alpha band, is defined by the user each time the model is tested. The model also assumes a constant time interval, *dt*, for neuronal activity to reach the subsequent brain location. This parameter represents the minimum amount of time it takes for information to travel from the sending area to the receiving cortical location. In reality, it depends on the distance between brain areas. However, here, we assumed that this value was the same across all pairs of areas modelled. In fact, the chosen value can be considered as the average time of information transfer between areas. Further delays that accumulate as neural activity advances from one population to the next originate in the alpha phase of the receiving location at the time the information arrives at that location (see Figures 11 and 12 for better detail).

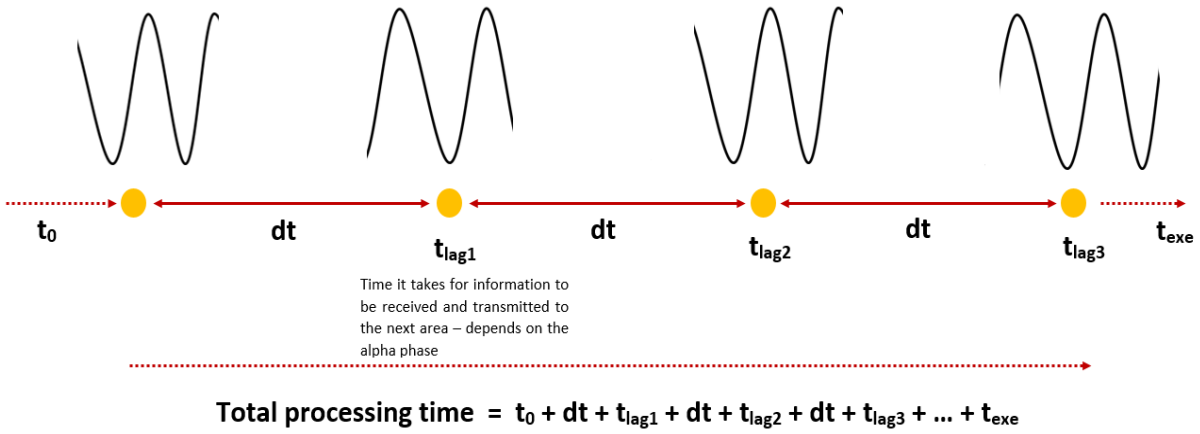

Figure 12. Schematic representation of the timing of stimulus processing. Information reaches the cortex at time t_0. It reaches the following area after *dt* ms (this interval of time is always the same between areas). The time it takes from the stimulus being processed to the onset of the receiving neuronal population activity is represented by t_{lag}, which is different in each area and dependent on the alpha phase. The total stimulus processing time results from the accumulation of all these lags (t_{lag1}, …, t_{lagN}) summed to the minimum time needed for sending information between all *N* areas (*dt* × *N*). After all areas have processed the stimulus, t_{exe} is added for motor execution purposes.

Based on Coon et al.'s (2016) findings, our model assumes that information can only be received or sent when the phase of the modelled alpha oscillations is between 120º and 240º – at the trough of alpha oscillations (represented by the green boxes in Figure 13).

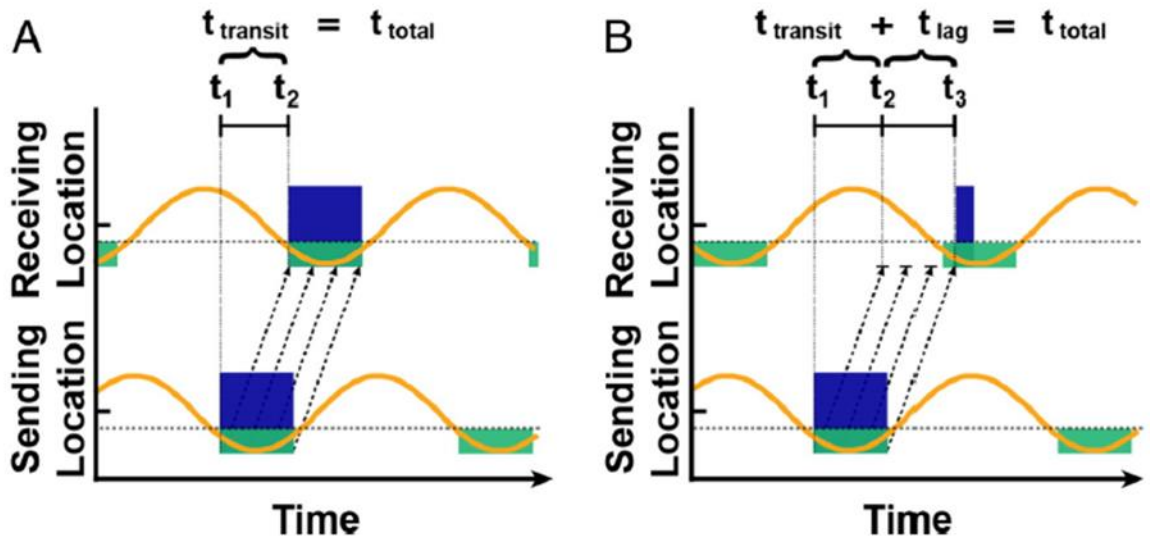

Figure 13. Communication between neuronal populations may be modulated by alpha oscillatory activity. As alpha activity (orange lines) decreases past a threshold voltage (dotted grey lines), a neuronal population may process and transmit information (permissive window represented by the green boxes) to the following population. In this attempt to signal the receiving neuronal population, the time it takes for a series of spike volleys (black dotted arrows) to excite population activity (blue boxes) depends on the phase of the receiving population's oscillatory activity. In A, the first spike immediately results in excitation of the receiving population. In B, most spikes do not arrive during a permissive window, delaying excitation by t_{lag} milliseconds. From Coon, et al. (2016).

Mathematically the model was developed as follows (see Figure 14). A cosine wave is generated for each brain location, all of which have equal amplitude A (= 1) and frequency and a randomly assigned phase offset (ϕ). These waves represent the alpha oscillations at each brain area modelled. All waves are generated across the same time interval of one second (1000 ms – this interval of time is enough for information to travel across all areas) with a frequency of discretization of 1000 Hz, generating a time vector, t, composed of one thousand 1 ms time intervals.

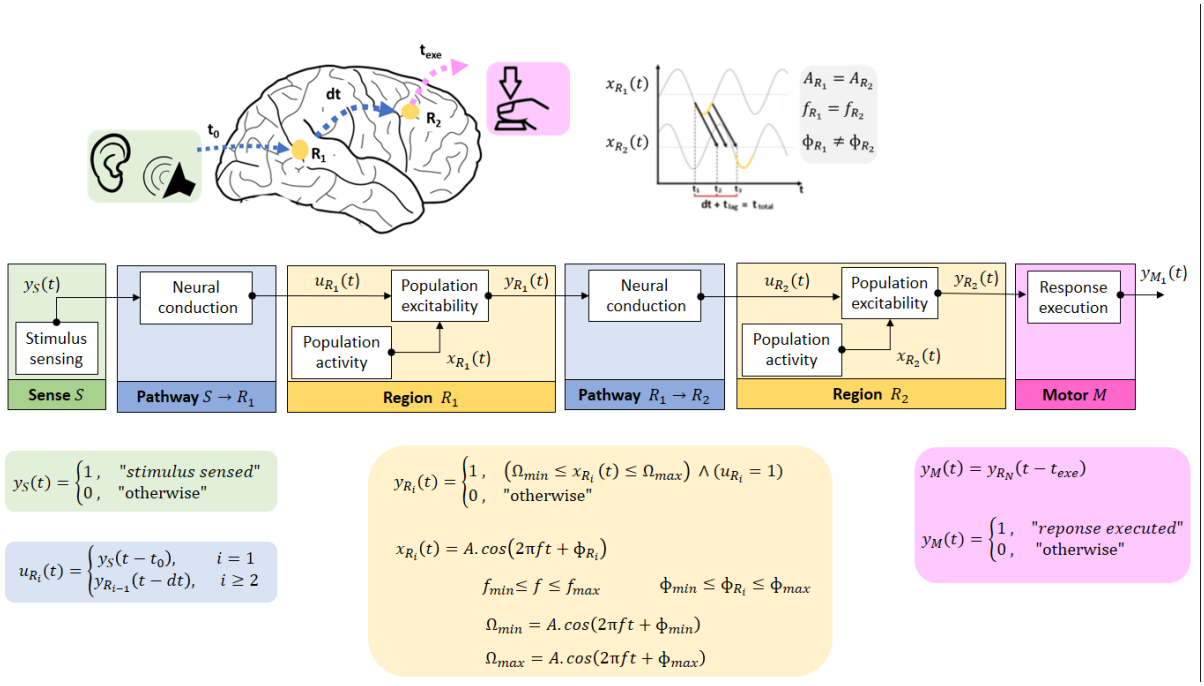

Figure 14. Schematic representation of the model's computational process, considering a two-area stimulus processing.

When an area sends information to the next area, the signal takes *dt* seconds to reach the following neuronal population. At this point, the model checks if the phase of the receiving location's alpha-band oscillatory activity at that time instant is at its trough, i.e. between 120º and 240º. Specifically, since cos (120º) = cos (240º) = -0.5, the model verifies whether the inverse cosine of the local phase is below -0.5, as represented by the yellow bolder portion of the alpha oscillations in Figure 11, and the green boxes (and threshold – dotted grey lines) in Figure 13. If the phase of the alpha oscillations of the receiving location is not within the specified interval, the model iterates through time instants until the alpha phase reaches 120º, at which point it returns the time instant where information can be received, processed and sent to the next area. These three processes are assumed by the model to occur instantly. When all *N* brain locations have been excited by their precedents, a time constant, t_{exe}, of 15 ms for motor response execution purposes is added to the final time, resulting in the final reaction time (RT).

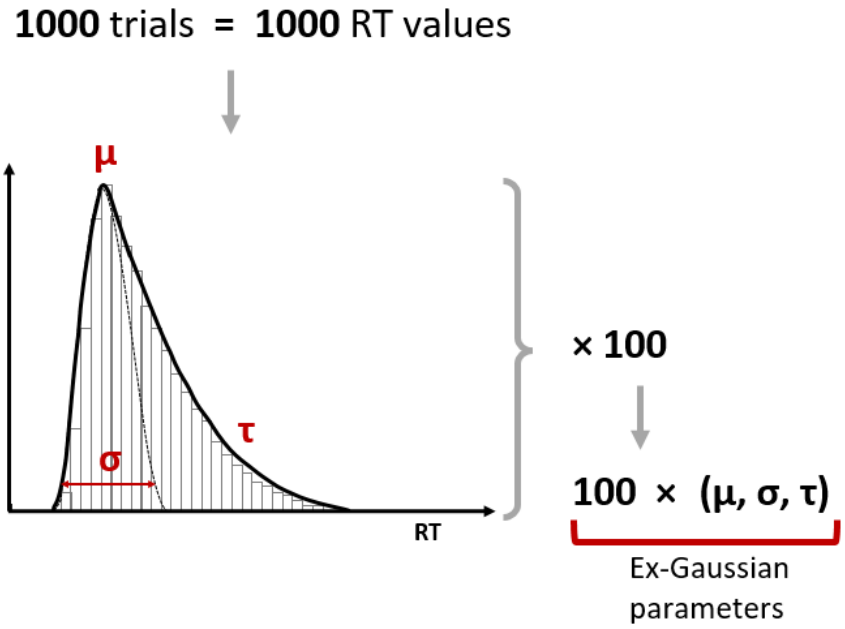

Figure 15. Schematic representation of the model output. For each set of model parameters, the model was run 1000 times, producing 1000 values of reaction time. The graph represents the histogram of these output values. An ex-Gaussian was then fit to the histogram, thereby producing for each histogram the ex-Gaussian parameters, μ, σ, and τ. This procedure was repeated 100 times to produce 100 ex-Gaussian parameters per set of model parameters.

For each set of parameters (frequency, *dt*, and number of areas), the model was run 1000 times. This originates 1000 RT values that are then plotted in a histogram and fitted for the ex-Gaussian distribution (Figure 15). The ex-Gaussian fitting was done with Bram Zandbelt's MATLAB toolbox Exgauss (https://github.com/bramzandbelt/exgauss). This toolbox returns the three ex-Gaussian parameters μ, σ and τ, where μ stands for the mean of the normal (Gaussian) portion of the distribution, σ for the standard deviation of the normal portion of the distribution and τ for the mean and standard deviation of the exponential component of the distribution (Heathcote, Popiel, & Mewhort, 1991) (Parris, Dienes, & Hodgson, 2013). This means for every run we obtain 1000 RT values and one of each ex-Gaussian parameters. Moreover, in order to have an estimate of the results consistency, for each set of parameters the model is run 100

times. This originates 100 combinations of ex-Gaussian parameters, that were then used for statistical analyses.

2.1.1 Parameter value variation

Table 1 provides a general description of how each parameter was studied, by providing the minimum and maximum values that were used for each parameter, the increments considered between model runs that studied one parameter's variation and the type of input necessary for each parameter. The "fixed" type is defined and fixed across all model variations, the "random" type is randomly generated by the model and the "chosen by user" type is defined in each model by the user, meaning those are the parameters that vary across different runs. In summary, we studied the effect of varying the frequency of alpha oscillations (*f*) – that varies from person to person and with parameters such as age or gender –, the total number of brain areas involved in stimulus processing (*N*) – that will depend on the task – and the amount of time information being sent from a particular brain location takes to reach the following one (*dt*) – that depends on the average distance between cortical areas involved in the task.

Table 1. Value range of each model parameter, defined by its minimum value (Min), maximum value (Max), increment of the value between different runs and the type of value input the model considers.

Parameter	Min	Max	Increment	Type of value input
f (Hz)	8	13	0.2	Chosen by user
N	10	30	5	Chosen by user
dt (ms)	5	20	5	Chosen by user
ϕ (degrees)	0^o	360^o	-	Random
A	1	-	-	Fixed
t_{exe} (ms)	15	-	-	Fixed
t_0 (ms)	30	-	-	Fixed

2.1.2 MATLAB computation

MATLAB (2014a, The MathWorks, Natick, Massachusetts, United States of America, 2014) was used to compute the model. Each variation of the model (parameter-wise) was saved to a different MATLAB® script, using custom made MATLAB® functions. All custom scripts can be found on Appendix A.II.

For each brain location, MATLAB® runs `generate_random_phase()`, a function that generates a random phase offset between 0º and 360º, i.e. between 0 and 2π radians, using MATLAB®'s `rand()` function, for each run, for each brain node a different random phase is assigned at the beginning t = t0. Having all model parameters defined, MATLAB® then generates *N* alpha-band frequency waves, for all *N* brain locations and across the entire length of the time vector, and places them within a matrix. This is done by running `generate_wave()` in an iteration loop with *N* iterations. The `in_trough_at()` function calculates whether, at a particular instant of the time vector, the phase of the introduced wave is between 120º and 240º. Specifically, it creates a threshold under which excitation can occur. This threshold is the result of the multiplication of the wave's amplitude (*A*) and the cosine of 120º (which is equal to the cosine of 240º), equal to -0.5. If the wave is not under that threshold, the function iterates through time intervals until this is accomplished, at which time it returns the instant of time at which excitation can occur.

Between each brain location the model runs the `in_trough_at()` function and adds *dt* into the instant of time returned by the function. This is done in an iteration loop of *N* iterations. When the final brain location is excited, i.e. when the final iteration of this loop is concluded and the last instant of time is returned, the model adds t_{exe} to the total time of response, generating the final reaction time.

For each set of parameters chosen, the `temp_run.m` script creates a folder and generates 100 runs. Each run calls MATLAB® function `get_1000rt()`, which runs 1000 trials of that model version.

Because MATLAB® resets the random (used by `rand()`) state at start-up, the `get_1000rt()` function begins by changing the value of the state input, ensuring true random values each time a model is run. Then it runs the specified model version one thousand times, saving the 1000 RT values and the frequency and phase of alpha oscillations at each brain location, for each trial, into a MATLAB® structure `result`, which is then returned.

The RT data is then used by the Exgauss toolbox described above, resulting in one ex-Gaussian parameter combination (μ, σ, τ) for each 1000 RT values. Bram Zandbelt's Exgauss toolbox also provides three figures (using the best fitting parameters): a histogram of the data with a line plot of the ex-Gaussian probability density function (PDF), a plot of quantiles (0.1, 0.3, 0.5, 0.7, and 0.9) of the data with a line plot of the ex-Gaussian cumulative distribution function (CDF), and a figure of these two plots side by side. These figures are saved into separate folders, generated automatically, for each run of the specific model. MATLAB® structures containing the resulting ex-Gaussian parameters, RT's, phase offsets and frequencies are also saved into these folders. A total of 238 model variations were created, a summary of which's specific parameters can be found in Appendix A.III.

A script `model2csv.m` converts the selected models' *.mat* data files into *.csv* (comma separated values) files, that can then be imported into SPSS Statistics or Microsoft Excel. Initially, an `all_data_into_csv.m` script was also created to generate a *.csv* file containing all the data relative to the models for dt = 10 ms.

2.2 Empirical reaction time data

2.2.1 Task

Empirical reaction time data was previously collected by other researchers in the lab, and involved data from two types of tasks: a simple detection task and a go/no-go task. Both sensorimotor tasks, these were of an auditory type. The simple detection task involved the plain detection of an auditory stimulus (see Figure 16a). This stimulus onset would occur at a random period of time (between 1.5 – 2.2 s) after a cue. For validation, 83% of the trials had an auditory stimulus, and 17% were catch (blank) trials, with the cue presentation only, and no target present. Upon the detection of the auditory stimulus, the subject was required to press a button, so as to communicate that detection, providing a resulting reaction time (time from stimulus onset until button press). The go/no-go task was, essentially, a choice task between two different types of auditory stimuli (see Figure 16b). One for which the subjects were instructed to press the button, indicating detection, and another where no button press should occur. 67% of trials had the first stimulus and 17% had the latter. Again, 17% of trials were catch trials, with the cue presentation only. Both "go" and "no-go" stimuli were preceded by an auditory cue. Both tasks were executed by all subjects, and the order by which these tasks were performed (i.e. which was executed first) was not the same for all subjects.

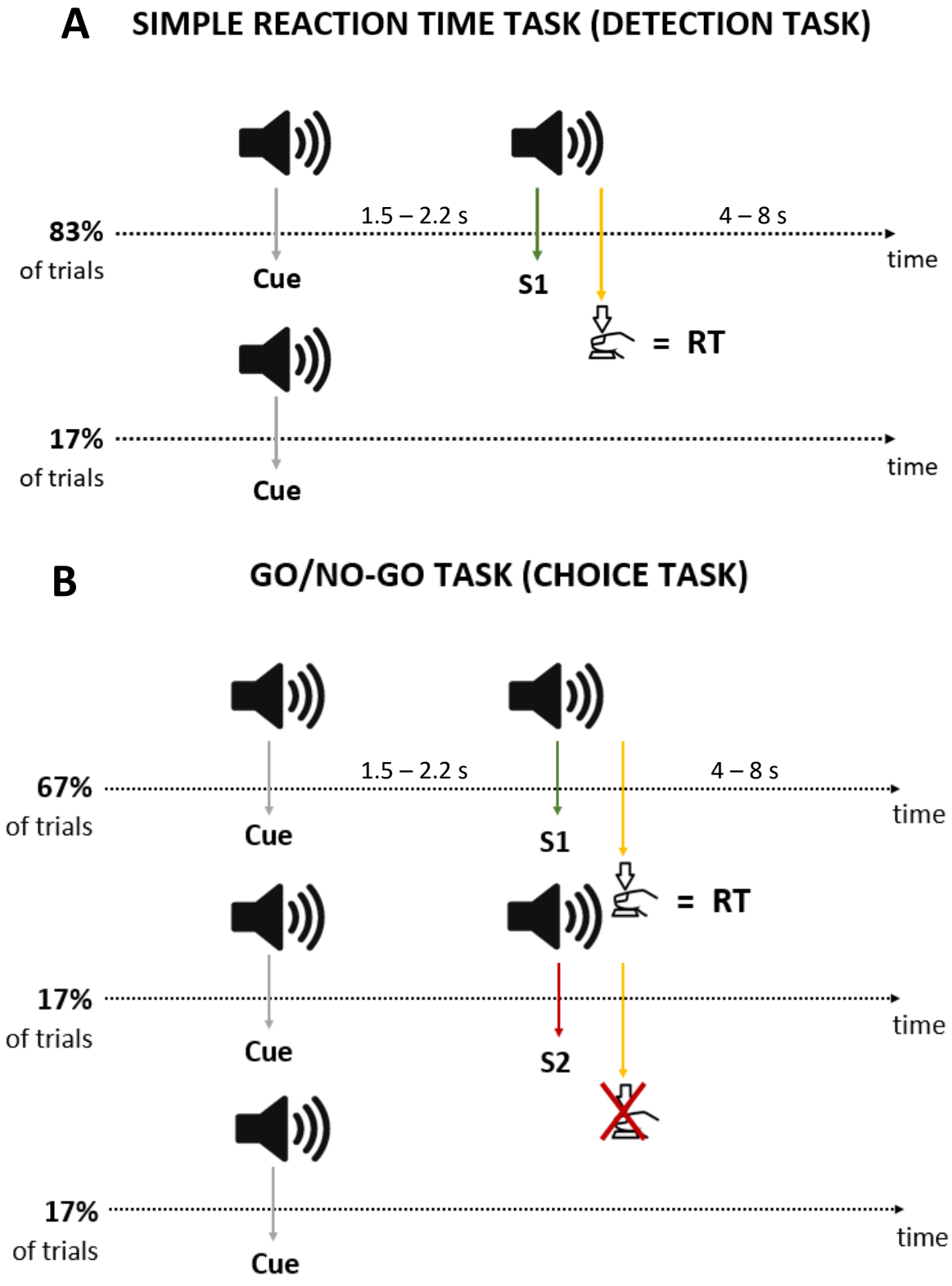

Figure 16. Schematic representations of both experimental tasks. A. Simple detection task where, following an auditory cue, an auditory stimulus is presented (S1) after a random interval of time, and the subject responds by pressing a button, resulting in a reaction time (RT). B. Go/No-go task where two different auditory stimuli exist (S1 and S2), but only for one (S1) is a response required.

Behavioural data from 65 subjects were included in our analyses. Participants belonged to two different age groups. The younger age group comprised ages between 19 and 30 years old, and the older group between 52 and 70 years old. Subjects from both male and female genders performed the experiment.

Each subject performed a total of 120 trials per task. Trials with wrong responses (namely false positives in the go/no-go task) were removed from the data. Outliers were also removed from the data, resulting in different numbers of trials for each subject, in each task, i.e. the resulting RT matrices did not have the same length. The resulting data had two columns: one with the reaction times, and another with the cue-target interval of time. Since in previous studies it had been observed that, for cue-target time intervals longer than 1.9 s, RTs became slower (i.e. higher), these were then excluded from the original data, in order to have data where the RT variability did not depend on the cue-target interval.

2.2.2 Ex-Gaussian fitting to empirical data

In order to fit the ex-Gaussian distribution to our empirical RT data and obtain the respective ex-Gaussian parameters, data from each subject were submitted to the Exgauss MATLAB® toolbox. After obtaining the ex-Gaussian parameters and graphic fitting for both the probability density function (PDF) superimposed on the histogram of the data and the cumulative distributive function (CDF) superimposed on a quantile plot of the observed data, results were inspected for deviations from the typical ex-Gaussian distribution curve and outlier values in the parameters. This initially lead to three subsets of data being created for further analysis: one excluding subjects whom visual inspection identified as having poor ex-Gaussian fitting, another where subjects with calculated absolute z-scores (for each parameter) above 3 were excluded, and a subset where all the above subjects were excluded (either by one criterion or another, or both).

Z-score outlier exclusion

The standard score, or z-score, is the number of standard deviations by which the value of an observation is above or below the sample mean. Z-scores were calculated in MS Excel using the formula:

$$z = \frac{x - \bar{x}}{SD}$$

, where z is the z-score, x the observation data point, $\bar{x}$ the sample mean and SD the sample standard deviation. The absolute value of the z-score provides a measure of how many standard deviations the observed value is from the mean. We considered subjects whose absolute z-scores were above 3 to be possible outliers, and excluded these from this data subset. For this exclusion, 3 subjects were eliminated.

Poor ex-Gaussian fitting exclusion

Figure 17 gives examples of what a poor ex-Gaussian fitting looks like compared to a good fit. For this exclusion, a total of 7 subjects were eliminated.

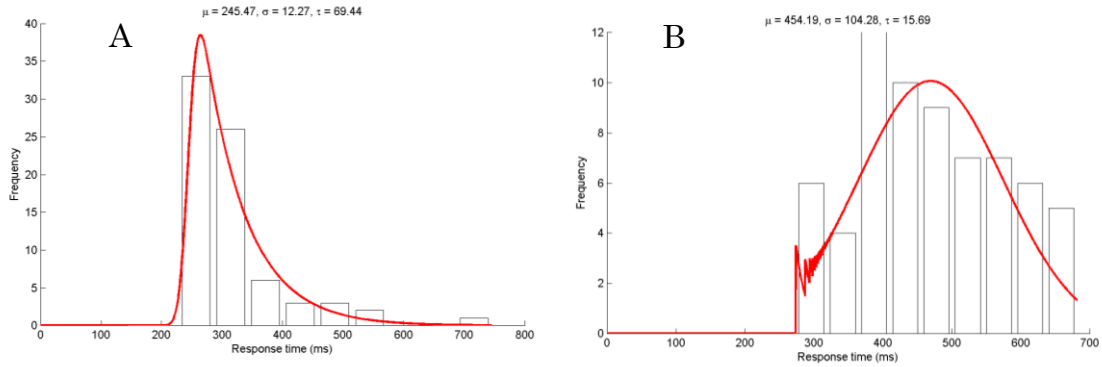

Figure 17. Ex-Gaussian fitting provided by the Exgauss MATLAB toolbox. A. Example of a good ex-Gaussian fitting with parameters μ = 245.47, σ = 12.27 and τ = 69.44. B. An example of poor ex-Gaussian fitting, with parameters μ = 454.19, σ = 104.26 and τ = 15.69.

Poor ex-Gaussian fitting and high z-score outlier exclusion

When adding the high z-score outlier subjects to the ones with poor ex-Gaussian fitting, since two of those subjects met both criterions for exclusion, only one extra subject was removed from the poor ex-Gaussian fitting data subset, leaving a total of 8 subjects eliminated for this subset of data.

Data subsets

When a subject was excluded for either criterion on one task, he was also excluded for the other task. This means all data was rearranged so that only subjects with data in both tasks of the experiment (i.e., simple detection task (D_RT) and "go/no-go" task (G_RT)) remained. After removing outlier values as described above, the number of subjects remaining for each comparison are displayed in Table 2.

Table 2. Resulting total and per age group number of subjects in each data subset analysed. We note that the row with "Both" exclusion criterions applied denotes the reunion of both subsets, i.e. subjects with either one criterion met, or both.

Exclusion criterion	Total # of subjects	# subjects old	# subjects young
High z-score	62	32	30
Poor ex-Gaussian fitting	58	29	29
Both	57	28	29

We decided to utilize the data subset with the exclusion of both types of outliers for further analyses, with a total of 57 subjects.

2.2.3 Empirical RT data analysis

The aim of this analysis was to study, on the empirical data, how task condition affected the ex-Gaussian parameters of the reaction time distributions. To study the effect each condition has on the resulting ex-Gaussian parameters (a visual representation of which can be found on Figure 15), we performed a repeated measures ANOVA for each ex-Gaussian parameter. For all repeated measures ANOVA tests, the age group of the subjects was included as a between-subjects factor, and the type of task performed by all subjects was defined as a within-subjects factor.

This provided descriptive statistics (mean and standard deviation) for each factor combination (D_RT_{young}, D_RT_{old}, G_RT_{young}, G_RT_{old}), the resulting significance of effect for both within-subject and between-subject factors on the ex-Gaussian parameters, and figure plots were then created to provide a visual representation of these dynamics.

2.3 Linear ballistic accumulator

In order to be able to compare our proposed model to previously established response time models, we attempted to fit our empirical reaction time data using the linear ballistic accumulator model. A MATLAB® toolbox, LBA (https://github.com/smfleming/LBA), was used for fitting the LBA model. This toolbox's code is adapted from Scott Brown's R code for fitting the LBA, provided in Brown & Heathcote (2008).

As previously stated, the LBA is a choice RT model, meaning it was designed for at least two choices, i.e. two possible responses, two independent evidence accumulators. Our empirical reaction time data, described above, is a collection of reaction times associated with two different task conditions: a simple reaction time task, requiring the detection of an auditory stimulus, and a go/no-go task

requiring the discrimination between two different auditory stimuli and an overt response only to one (the "go") stimulus. Given the nature of these two task conditions, and the small number of errors committed by the participants, no reaction time for "wrong" responses could be fit in the model: errors in the simple reaction time were misses (failures to respond); and errors in the go/no-go task, were misses to the "go" stimulus or responses to the "no-go" stimulus, and in this second case the errors were too infrequent to be modelled successfully. Therefore, changes had to be considered in the LBA model in order to apply it. The main change we needed to apply was that only one evidence accumulator would exist for our data, since all our responses were deemed as "correct" (when you simply detect a stimulus and produce a reaction time value, there is no wrong response; when you only respond for one of the two presented stimuli – as in a go/no-go task – you only obtain the RTs for the detection of the "go" stimulus). The LBA also considers the option for different conditions, as for different task difficulty levels that can differ from trial to trial. In our case, there was only one "condition" per task, hence its value was set to 1 in our LBA toolbox adapted scripts.

To estimate LBA parameters from data, the LBA toolbox uses the maximum likelihood estimation objective function, which is used to quantify the resemblance between data and model, therefore allowing a search for the best-fitting set of LBA parameters. To begin the search for the best-fitting set of parameters, the LBA requires an initial set of parameters, referred to as the starting point. A computer-driven search is then performed, changing parameters until a set is identified as providing the best value for the objective function. The choice of initial parameters has been shown to be of importance, sometimes referred to as "something of an art", requiring experience and experimentation (Donkin, Averell, Brown, & Heathcote, 2009). For this reason, it was attempted both by sequential manual choice of the user and by randomly defined (within certain constraints) in MATLAB® and computed for optimization (i.e. run several times only to return the set of initial parameters that provided the best fit).

Our adapted toolbox scripts, in likeness to the original, returned, as a result, the best-fitting set of LBA parameters and a plot figure combining LBA model predictions (in a line plot) and the histogram of the data.

2.4 Fitting the model to empirical results

Having real, experimental data to compare our model results to, we wanted to find our best-fitting model parameter sets for each combination of experimental conditions. An initial manual search for a set of model parameters that lead to results that resembled those found on empirical ex-Gaussian parameters showed that some of our results didn't seem to be too far off from this achievement, which motivated us to perform an automated search.

2.4.1 Automate search for best-fitting parameters

Our aim was to find the best-fitting model parameters for each task condition and each subject's group. To accomplish this, we decided to find the set of model parameters that minimized the sum of squared errors of prediction for all ex-Gaussian parameters. The sum of squared errors (SSE) is the sum of the squares of deviations of predicted data from actual empirical values, and can be used as a measure of discrepancy between empirical data and an estimation model. The lower the SSE, the better a model fits the data. To calculate the sum of the squared errors we used the formula below:

$$SSE = \left(\mu_{exp} - \mu_{model}\right)^2 + \left(\sigma_{exp} - \sigma_{model}\right)^2 + \left(\tau_{exp} - \tau_{model}\right)^2$$

, where SSE is the sum of squared errors, μ_{exp}, σ_{exp} and τ_{exp} are the mean ex-Gaussian parameters obtained from empirical data, and μ_{model}, σ_{model} and τ_{model} are the resulting ex-Gaussian parameters from the model.

A custom script, `find_best_parameters.m`, was created using MATLAB® to automate this process and allow iteration through all model tests, each with their set of parameters. This script begins by allowing the user to define the means for each ex-Gaussian parameter in each of the four combinations of experimental conditions (DRT_{young}, DRT_{old}, GRT_{young}, GRT_{old}), which were previously obtained. It creates three matrices (one for each ex-Gaussian parameter) with 100 rows and number of columns equal to the total number of models to be imported. It then iterates through the selected models and imports each of the 100 resulting scripts (from the 100 runs described above), in each iteration. The 100 resulting ex-Gaussian parameter sets per model are then averaged, and the sums of squared errors can be calculated. Four SSEs are calculated per iteration, one for each combination of experimental conditions in the empirical data. These SSEs are added to their respective matrices, which also save the number of the model test they belong to, and are, at last, sorted by crescent order of the sum of squared errors. Therefore, running this script allows us to obtain four matrices, one for each combination of experimental conditions, all sorted by crescent order of SSE value. Selecting the first row gives us the model parameters with the minimum SSE value.

Upon running the script each time, model tests were run with values of parameters between those that best fit a particular condition, searching for changes in the best-fitting parameter sets. This allowed a more precise tuning of the model parameters that best represented the empirical data. Since our MATLAB® script provided an ordered list of the model tests whose parameter sets lead to the smallest SSEs, we were able to attempt a manual optimization of these best-fitting parameter sets. By comparing differences in parameter values between the model tests on top of each list (one list per experimental task condition), it allowed us to run the model for parameter values close to them, run the `find_best_parameters.m` script including those model tests, and search for differences in the resulting model tests list. In these extra model tests, each parameter (f, N and dt) was varied at specific intervals (i.e. with specific increment values). Differences in f were done with 0.2 Hz increments, N with increments of 1, and dt with increments of 1 ms.

To provide an example, Table 3 displays the resulting best-fitting sets of parameters, for each experimental task condition, after the first attempted search.

Table 3. Sets of parameters that minimized the sum of squared errors (SSE) for each experimental condition combination (DRT_{young}, DRT_{old}, GRT_{young}, GRT_{old}) in the first run of this automate search.

Condition	**Best-fitting model parameters**			**SSE**
	***f* (Hz)**	***N***	***dt* (ms)**	
DRT_{young}	10	10	20	153.607
DRT_{old}	13	10	20	61.915
GRT_{young}	13	25	10	386.080
GRT_{old}	12.2	25	10	519.466

2.5 Statistical analysis

Descriptive data statistics and repeated measures ANOVA were performed using IBM SPSS Statistics 24.0. Graphs were obtained using both SPSS and Microsoft Excel (2016).

2.5.1 Repeated measures ANOVA – considerations

For results to be able to reflect reality, the repeated measures ANOVA test requires some assumptions to be met. This is true for all but one, the condition of sphericity, who needs to be tested. Sphericity means that the population variances of all possible different scores are equal, and is tested with Mauchly's test, which is included in SPSS' repeated measures ANOVA output. For all repeated measures ANOVA tests performed, whenever the condition of sphericity could not be

assumed, corrections to the degrees of freedom were applied. For Greenhouse-Geisser sphericity estimates (ξ) above 0.75, the Huynh-Feldt correction was used. For those under this value, the Greenhouse-Geisser correction was applied (Field, 2013).

3 Results

3.1 Simulation of reaction time distributions

Here, we will describe how our computational model outputs depend on the model's input parameters.

After running the computational model, we obtained a distribution of reaction times for each set of parameters. Next, we used the Exgauss MATLAB® toolbox to fit an ex-Gaussian distribution to these data. The toolbox provided successful ex-Gaussian fittings to the data for most of the parameters studied (see Figure 18 for an example). These results indicate that, by modelling progressive neuronal onset activity dependent on the phase of alpha oscillations, we can obtain simulated RT data with a distribution shape that resembles those obtained for experimental data – an ex-Gaussian distribution (Ratcliff R. , 1979).

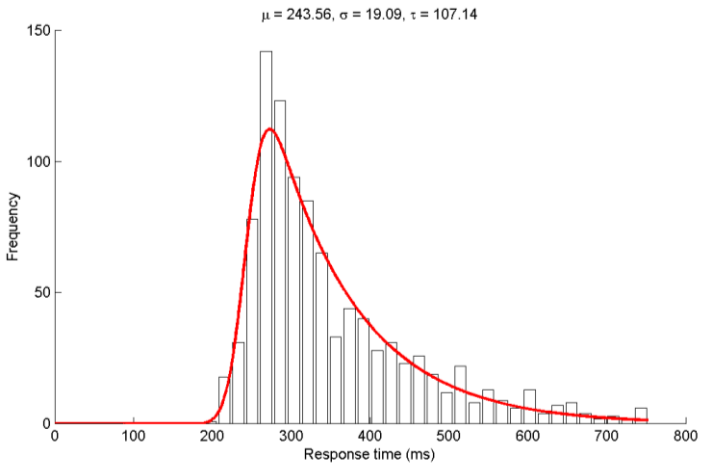

Figure 18. Example of histogram and probability density function (PDF) line plots for the model run with f = 8.4 Hz, N = 15 and dt = 10 ms. Resulting ex-Gaussian parameters can be seen in the title, with μ = 243.56, σ = 19.09 and τ = 107.14.

Nevertheless, for some parameter combinations the fitting with the ex-Gaussian distribution was poor, as demonstrated by Figure 19's example plot. Specifically, for dt = 5 ms and N = 10 brain areas, the resulting RT distribution was not an ex-Gaussian distribution, and, therefore, the resulting fitting was of poor quality. This was true for all 100 subject runs of the model with these specifications. For dt = 5 ms and other N values, there were some sporadic cases where the ex-Gaussian fitting was also poor, as in the particular case shown in Figure 20. This lead to the discarding of further studies with model parameter dt set at 5 ms.

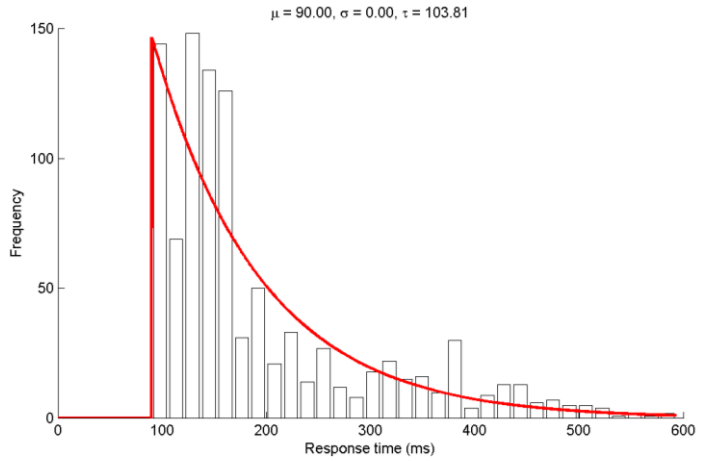

Figure 19. Histogram and PDF line plots for the model run with f = 8 Hz, N = 10 and dt = 5 ms. Resulting ex-Gaussian parameters can be seen in the title, with μ = 90.00, σ = 0.00 and τ = 103.81.

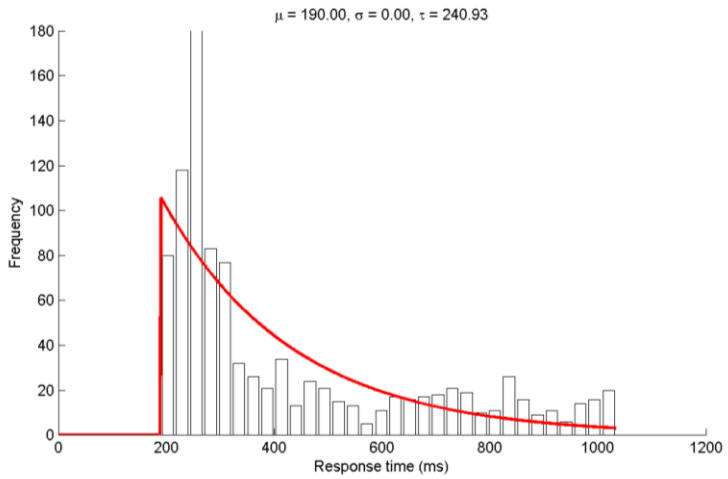

Figure 20. Histogram and PDF line plots for the model run with f = 8 Hz, N = 30 and dt = 5 ms. Resulting ex-Gaussian parameters can be seen in the title, with μ = 90.00, σ = 0.00 and τ = 240.93.

3.1.1 Model parameters' effect on ex-Gaussian parameters

To study how the tested model parameters, alpha frequency (*f*), number of cortical areas (*N*) and stimulus travelling time between areas (*dt*), influence the resulting ex-Gaussian parameters, a repeated measures ANOVA was performed for each ex-Gaussian parameter, with these model parameters as within-subject factors, using a subset of data with the parameter specifications indicated on Table 4. This subset of data used results from a total of 54 sets of model parameters, all with 100 repetitions (subjects).

Table 4. Parameter value specifications in the subset of data used to perform a repeated measures ANOVA to test the effect of all parameters and their interactions on the ex-Gaussian parameters.

Parameter	Minimum	Maximum	Increment
f (Hz)	8	13	1
N	10	20	5
dt (ms)	10	20	5

Tables with the resulting descriptive statistics (mean and standard deviation) for μ, σ, and τ values for each parameter combination can be found in Appendix A.I.

3.1.1.1 Effect of frequency (*f*) on μ values

When studying the effect of frequency on μ values, degrees of freedom were corrected using Huynh-Feldt estimates of sphericity ($\xi = 0.907$). Results showed a significant main effect of frequency on μ (i.e. the mean of the normal distribution portion of the ex-Gaussian distribution), $F_{(4.533,\ 448.755)} = 6666.904$, $p < 0.001$.

Using MS Excel, plots were generated for a visual representation of the effect each model parameter has on each ex-Gaussian parameter.

Plots of μ vs. frequency were generated for models with dt = 10 ms and N between 10 and 30, with 5 area increments. Figure 21 displays the resulting plot for a model run with dt = 10 ms and N = 20 brain areas. Mu (μ) values were shown to decrease with increasing alpha-band frequency, as can be seen in the plot.

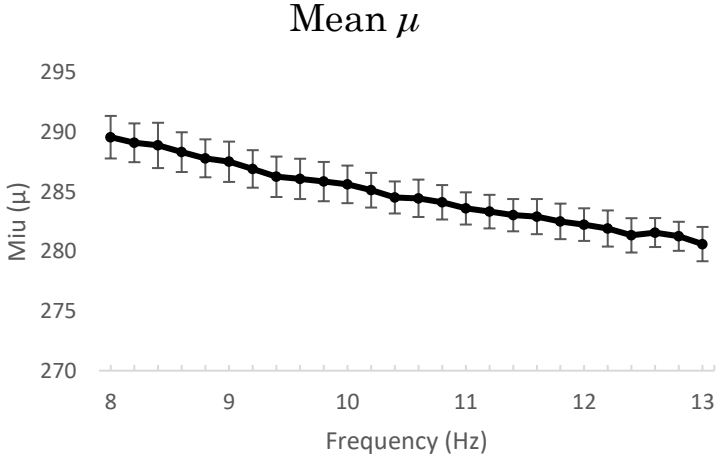

Figure 21. Mean μ values vs. frequency (Hz) for N = 20 and dt = 10 ms. Standard deviation (SD) error bars are also represented in the plot.

3.1.1.2 Effect of the number of brain areas (N) on μ values

For this study, degrees of freedom were corrected using Huynh-Feldt estimates of sphericity (ξ = 0.809). Results showed a significant main effect of the total number of brain areas to process the stimulus on μ values, $F_{(1.618,\ 160.144)}$ = 1677948.167, $p < 0.001$.

As an example, plots for μ vs. N were created for models with dt = 10 ms and frequency values ranging from 8 to 13 Hz, with 1 Hz increments. Figure 22 displays the resulting plot for the model run with dt = 10 ms and f = 8 Hz. Results show that, with an increasing number of brain areas to process the stimulus, μ values also increase.

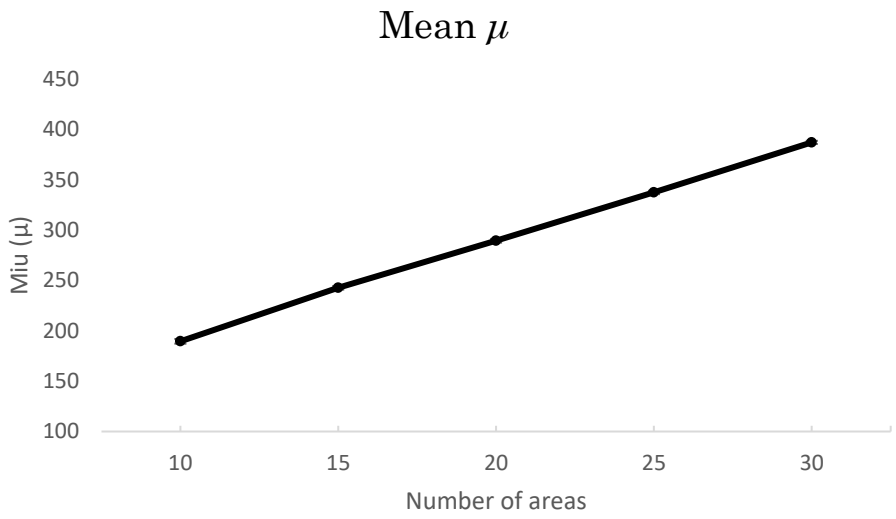

Figure 22. Mean μ values vs. number of areas for f = 8 Hz and dt = 10 ms. Standard deviation (SD) error bars are also represented in the plot (albeit too small to be visible).

3.1.1.3 Effect of the time between brain areas (dt) on μ values

In this study, Greenhouse-Geisser estimates of sphericity (ξ = 0.737) were used to correct the degrees of freedom. Results showed a significant main effect of the time needed for a stimulus to be sent between brain areas on μ values, $F_{(1.474,\ 145.953)} = 2094369.211$, $p < 0.001$.

Figure 23 displays the μ vs. dt plot for the model run with f = 10 Hz and N = 15 brain areas, as an example. The plot displays a positive relationship between μ and dt, being that an increase in the time distance between brain areas results in an increase in the mean of the normal portion of the resulting ex-Gaussian distribution of RT's.

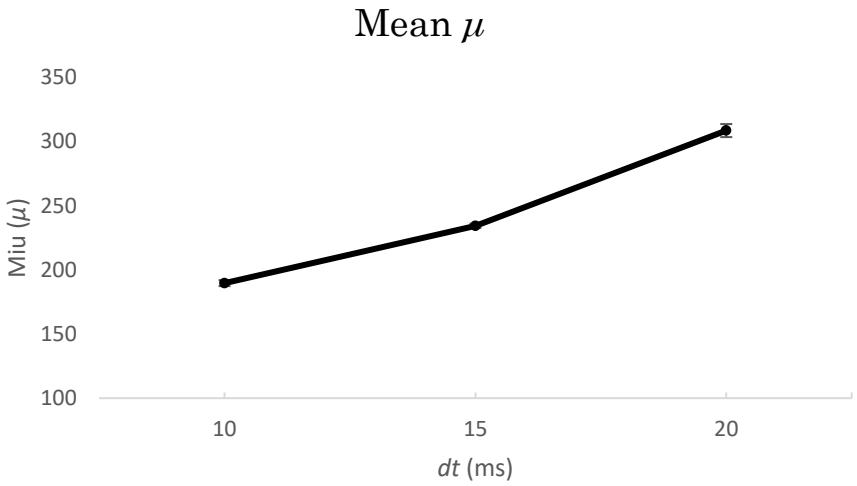

Figure 23. Mean μ values vs. time needed for the stimulus to be sent between brain areas (dt) for f = 8 Hz and N = 10 brain areas. Standard deviation (SD) error bars are also represented in the plot (albeit too small to be visible).

3.1.1.4 Effect of parameter interactions on μ values

The interaction between frequency and the number of brain areas on μ was found to be significant, $F_{(7.250,\ 717.772)} = 101.581$, $p < 0.001$, although from simple plot analysis no clear interaction appears to be visible (plot lines appear to be parallel to each other). Greenhouse-Geisser estimates of sphericity ($\xi = 0.725$) were used for this study.

Figure 24 displays how μ vs. frequency varies across different N parameter values. μ decreases with increasing alpha frequency, and this change in μ is the same for all values of the total number of brain locations.

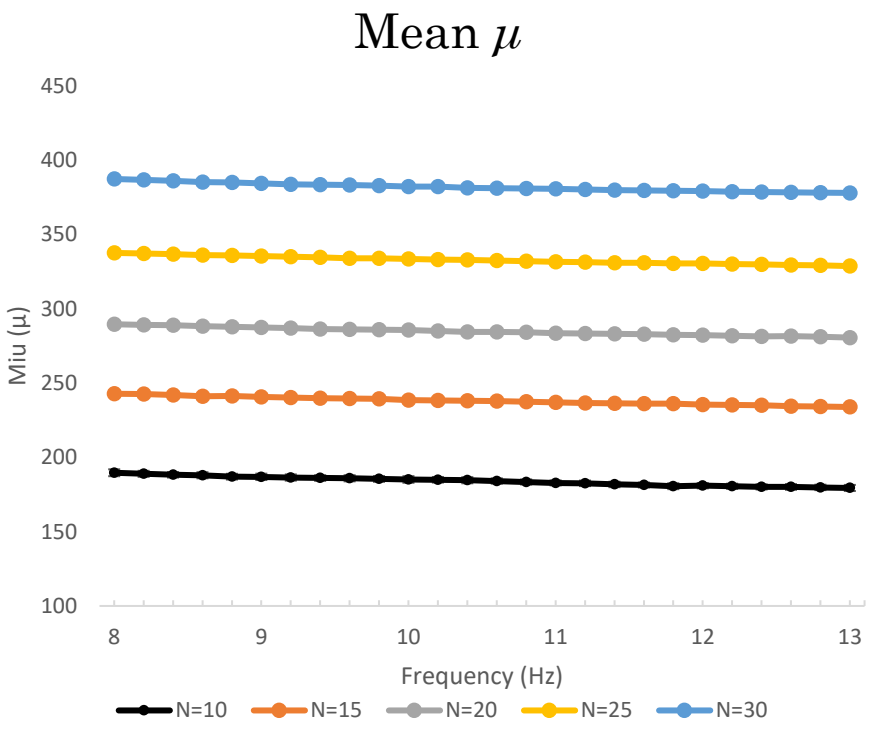

Figure 24. Mean μ values vs. frequency (Hz) over different numbers of brain areas (N). dt equal to 10 ms in these model variations. Standard deviation (SD) error bars are represented for each line plot (albeit too small to be visible).

The effect of the interaction between parameter f and dt on μ values was also shown to be significant, $F_{(6.414,\ 635.005)} = 1580.622$, $p < 0.001$. Once more, Greenhouse-Geisser estimates of sphericity ($\xi = 0.641$) were used to correct the degrees of freedom.

Figure 25 displays how μ vs. frequency varies across different dt parameter values. This variation appears to be relatively consistent across the different dt values, although, for dt = 20 ms, it appears to be slightly larger for lower frequencies.

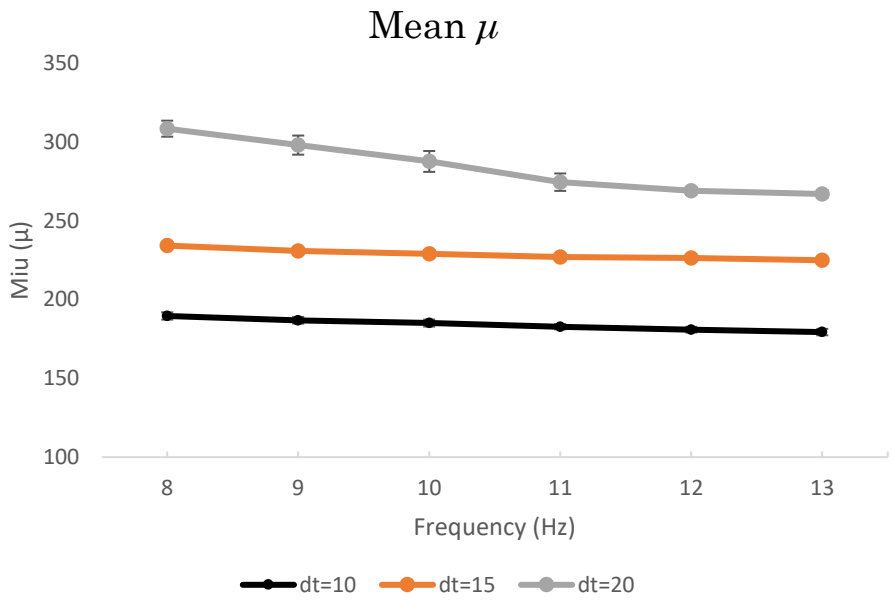

Figure 25. Mean μ values vs. frequency (Hz) over different between-areas time intervals (*dt*). *N* equal to 10 brain areas in these model variations. Standard deviation (SD) error bars are represented for each line plot (albeit some too small to be visible).

The interaction between the total number of brain areas and the time needed to send a stimulus between them was, likewise, shown to have a significant effect on μ values, $F_{(2.133,\ 211.198)} = 95303.303$, $p < 0.001$. Greenhouse-Geisser estimates of sphericity ($\xi = 0.533$) were used to correct the degrees of freedom.

Figure 26 shows how μ vs. number of areas varies across different values of *dt*. This variation appears to be relatively consistent across the different *dt* values.

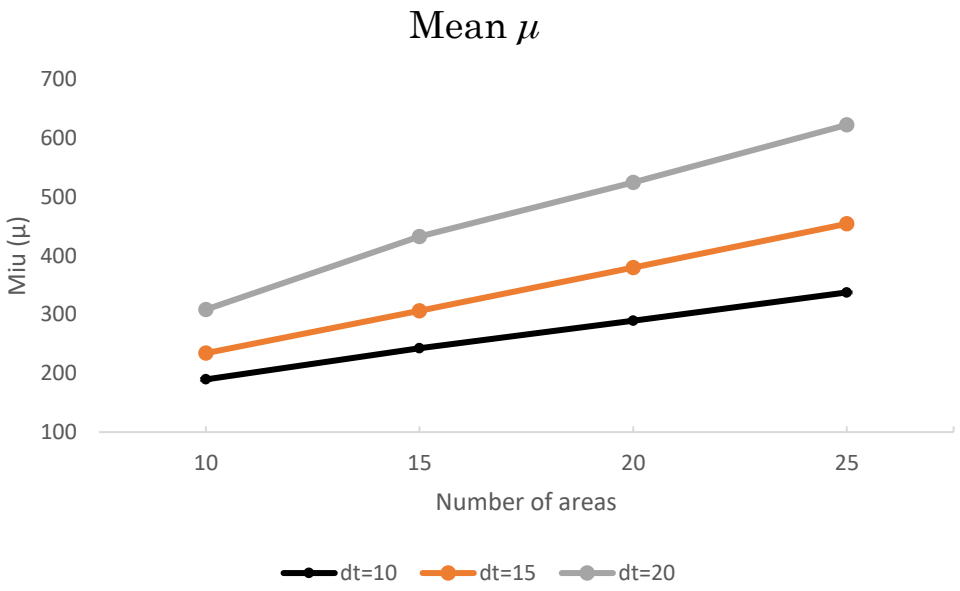

Figure 26. Mean μ values vs. total number of brain areas over different between-areas time intervals (*dt*). Frequency is set at 8 Hz in these model variations. Standard deviation (SD) error bars are represented for each line plot (albeit too small to be visible).

Furthermore, the interaction between all model parameters studied (*f*, *N* and *dt*) was also studied for effects on μ values. Results showed there was indeed a significant effect resulting from the interaction of all model parameters studied on μ values, $F_{(9.393,\ 929.876)} = 88.666$, $p < 0.001$. For this study, Greenhouse-Geisser estimates of sphericity ($\xi = 0.470$) were once again used to correct the degrees of freedom.

To further study these effects of model parameters on μ values, separate repeated measures ANOVA tests were also performed, all confirming the presented results.

3.1.1.5 Effect of frequency on σ values

After performing a repeated measures ANOVA to study the effect of the model parameters on σ values, results showed a significant main effect of

frequency on σ values, $F_{(4.432,\ 438.804)} = 2029.586$, $p < 0.001$. Degrees of freedom were corrected using Huynh-Feldt estimates of sphericity ($\xi = 0.886$).

Plots of σ vs. frequency were generated for models with dt = 10 ms and N between 10 and 30, with 5 area increments. Figure 27 displays the resulting plot for a model run with dt = 10 ms and N = 20 brain areas, as an example. Sigma (σ) values were shown to decrease with increasing frequency of the simulated alpha-band oscillations, as can be seen in the plot.

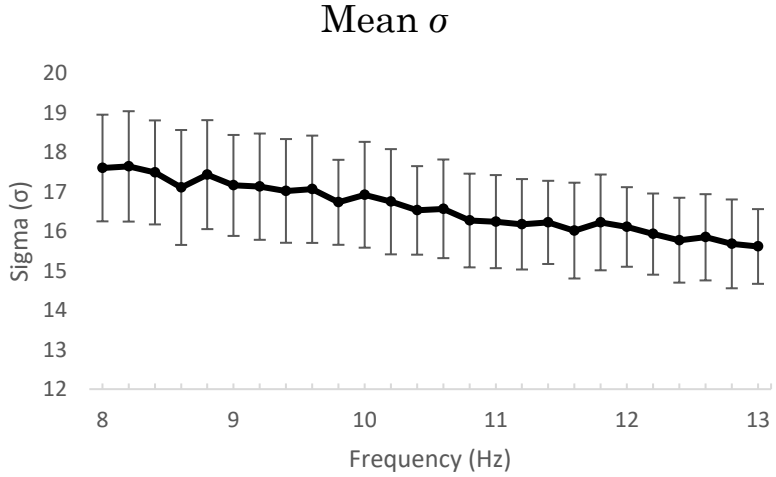

Figure 27. Mean σ values vs. frequency (Hz) for N = 20 and dt = 10 ms. Standard deviation (SD) error bars are also represented in the plot.

3.1.1.6 Effect of the number of brain areas (N) on σ values

Studying the effect of parameter N on σ values, degrees of freedom were corrected using Huynh-Feldt estimates of sphericity ($\xi = 0.941$). Results showed a significant main effect of the total number of brain areas on the standard deviation of the normal portion of the ex-Gaussian distribution (σ), $F_{(1.881,\ 186.250)} = 5390.018$, $p < 0.001$.

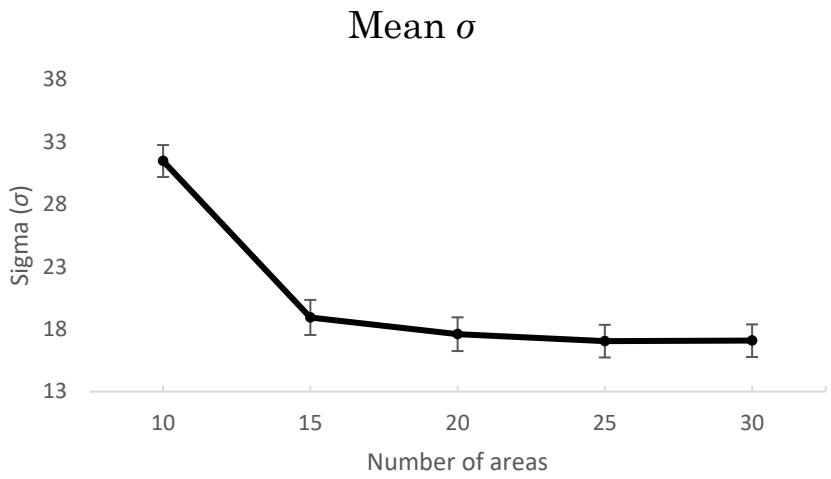

Figure 28. Mean σ values vs. number of areas for f = 8 Hz and dt = 10 ms. Standard deviation (SD) error bars are also represented in the plot.

Plots for σ vs. N were created for models with dt = 10 ms and frequency values ranging from 8 to 13 Hz, with 1 Hz increments. Figure 28 displays the resulting plot for the model run with dt = 10 ms and f = 8 Hz. Results show that, with an increasing number of brain areas to process the stimulus, σ values appear to decrease exponentially.

3.1.1.7 Effect of the time between brain areas (dt) on σ values

For this study, Greenhouse-Geisser estimates of sphericity ($\xi = 0.725$) were used to correct the degrees of freedom. Results showed a significant main effect of dt on σ values, $F_{(1.450,\ 143.561)} = 42331.111$, $p < 0.001$.

Figure 29 displays the σ vs. dt plot for the model run with f = 10 Hz and N = 15 brain areas. The plot displays a slight decrease between the first two dt values (10 and 15 ms) and a significant increase for the last dt value, equal to 20 ms.

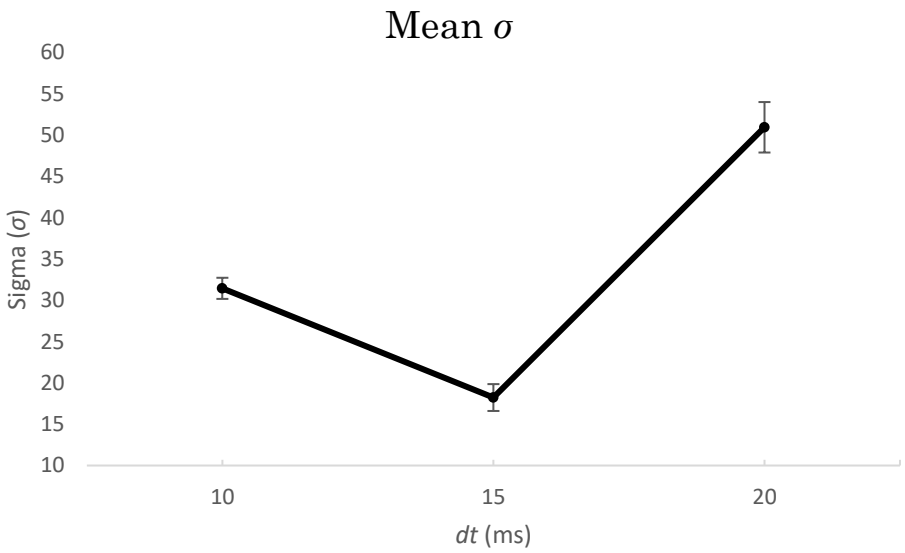

Figure 29. Mean σ values vs. time needed for the stimulus to be sent between brain areas (dt) for f = 8 Hz and N = 10 brain areas. Standard deviation (SD) error bars are also represented in the plot.

3.1.1.8 Effect of parameter interactions on σ values

Each combination of parameter interactions was studied for possible effects on σ values. The interaction between frequency and the number of brain areas was shown to have a significant effect on σ values, $F_{(6.867,\ 679.876)} = 330.962$, $p < 0.001$. Degrees of freedom were corrected using Greenhouse-Geisser estimates of sphericity ($\xi = 0.687$).

Figure 30 displays how σ vs. frequency varies across different N parameter values. σ variation across frequency appears to be substantially different for $N = 10$.

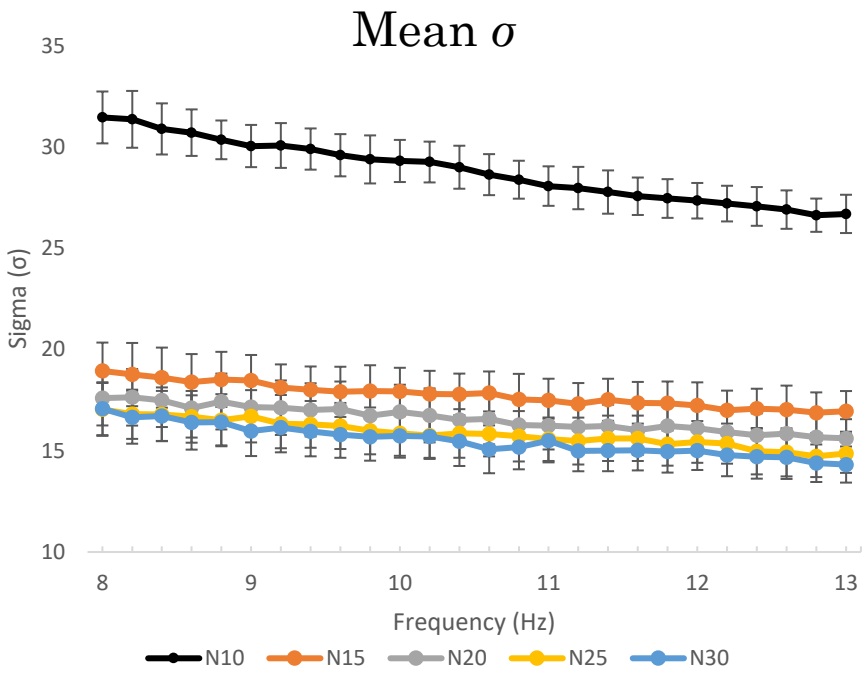

Figure 30. Mean σ values vs. frequency (Hz) over different numbers of brain areas (N). dt equal to 10 ms in these model variations. SD error bars are represented for each line plot.

A significant effect on σ values was found for the interaction between frequency and the time between brain areas, $F_{(6.227,\ 616.442)} = 848.470$, $p < 0.001$. Degrees of freedom were corrected using Greenhouse-Geisser estimates of sphericity ($\xi = 0.623$).

Figure 31 displays how σ vs. frequency varies across different dt parameter values. As seen in Figure 29, from dt = 10 ms to dt = 15 ms, σ values appear to decrease consistently, but the same cannot be said for dt = 20 ms, were σ values are higher and with a different type of variation across frequency values.

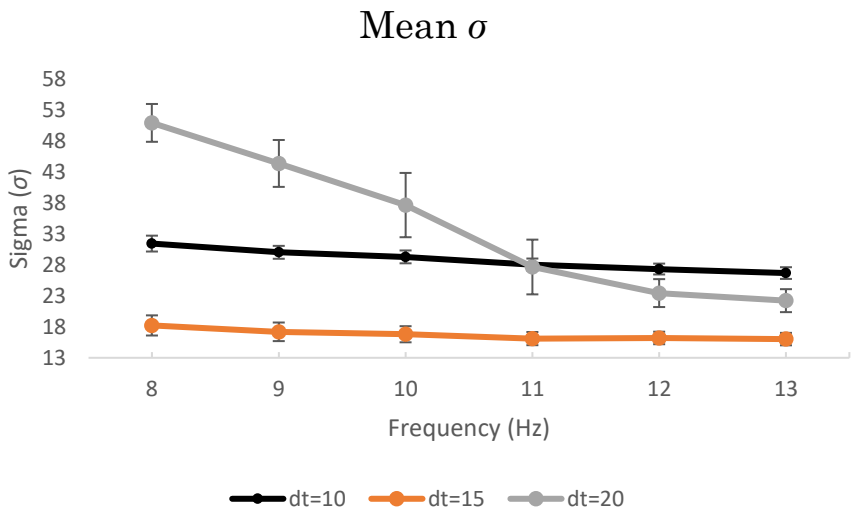

Figure 31. Mean σ values vs. frequency (Hz) over different between-areas time intervals (dt). N equal to 10 brain areas in these model variations. Standard deviation (SD) error bars are represented for each line plot.

The interaction between the total number of brain areas and the time it takes for a stimulus to be sent between them was also found to have a significant effect on σ values, $F_{(2.239,\ 221.689)} = 2012.916$, $p < 0.001$. Degrees of freedom were corrected using Greenhouse-Geisser estimates of sphericity ($\xi = 0.560$).

Figure 32 shows how σ vs. number of areas varies across different values of dt. This variation appears to be quite substantial across different dt values, although, for high number of areas, the difference between $dt = 10$ ms and $dt = 20$ ms appears to be very small.

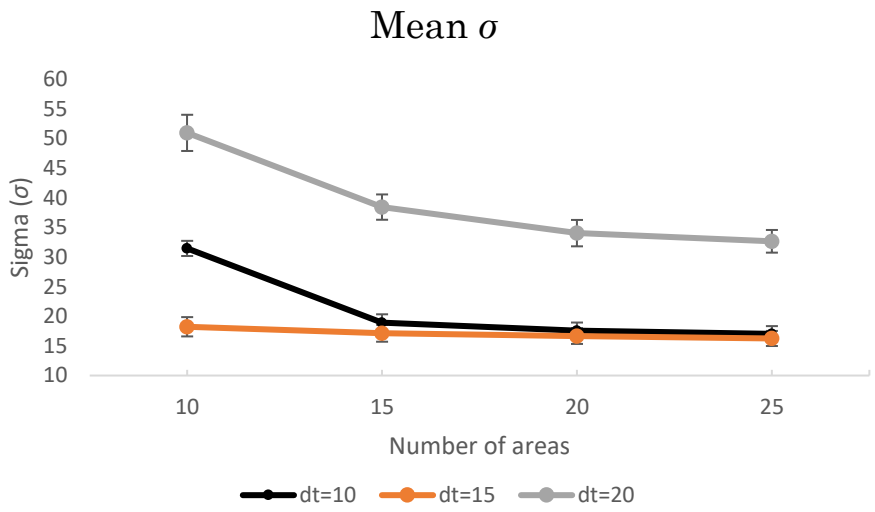

Figure 32. Mean σ values vs. total number of brain areas over different between-areas time intervals (dt). Frequency is set at 8 Hz in these model variations. Standard deviation (SD) error bars are represented for each line plot (albeit some too small to be visible).

Moreover, the interaction between all model varying parameters was also shown to have a significant effect on σ values, i.e. on the standard deviation of the normal portion of the ex-Gaussian distribution, $F_{(10.049,\ 994.860)} = 255.656$, $p < 0.001$.

3.1.1.9 Effect of frequency (f) on τ values

After performing a repeated measures ANOVA to study the effect of the model parameters on τ values, results showed a significant main effect of frequency on τ values, $F_{(4.755,\ 470.705)} = 21383.716$, $p < 0.001$. Degrees of freedom were correct using Huynh-Feldt estimates of sphericity ($\xi = 0.951$).

Plots of τ vs. frequency were generated for models with dt = 10 ms and N between 10 and 30, with 5 area increments. Figure 33 displays the resulting plot for a model run with dt = 10 ms and N = 20 brain areas. The mean and standard deviation of the exponential portion of the distribution, tau (τ), was likewise shown to decrease with increasing frequency.

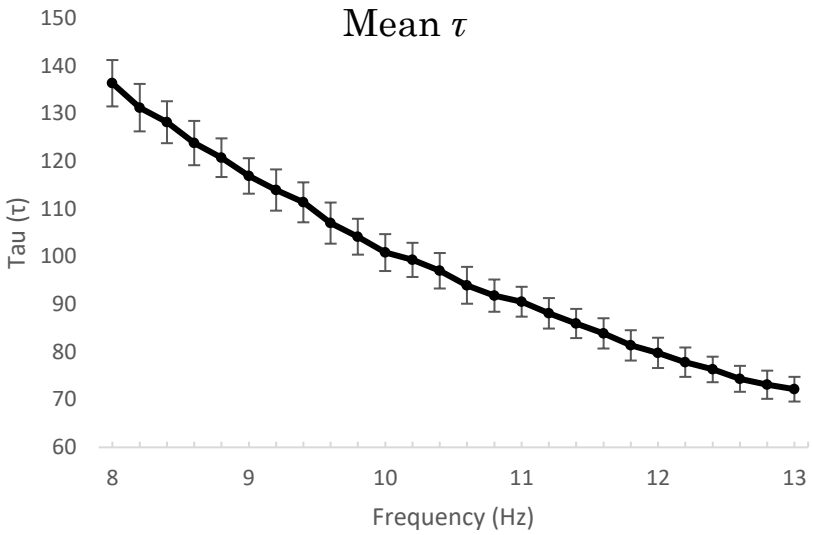

Figure 33. Mean τ values vs. frequency (Hz) for N = 20 and dt = 10 ms. SD error bars are also represented in the plot.

3.1.1.10 Effect of the number of brain areas (N) on τ values

Results showed a significant main effect of the total number of brain areas on τ values, $F_{(2, 198)} = 25138.861$, $p < 0.001$.

Plots for τ vs. N were created for models with dt = 10 ms and frequency values ranging from 8 to 13 Hz, with 1 Hz increments. Figure 34 displays the resulting plot for the model run with dt = 10 ms and f = 8 Hz. Results show that, with an increasing number of brain areas to process the stimulus, τ values appear to increase logarithmically.

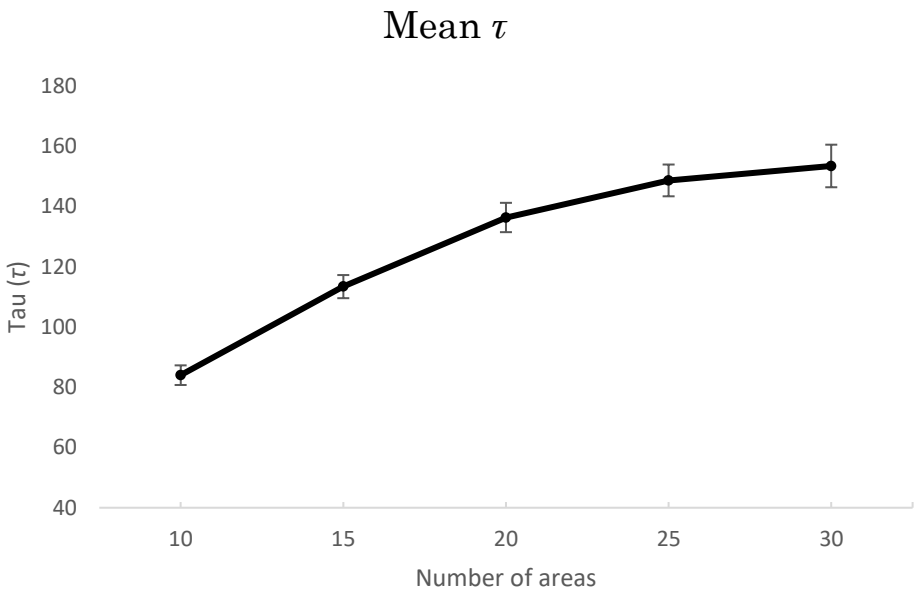

Figure 34. Mean τ values vs. number of areas for f = 8 Hz and dt = 10 ms. Standard deviation (SD) error bars are also represented in the plot.

3.1.1.11 Effect of the time between brain areas (dt) on τ values

Results showed a significant main effect of parameter dt on τ values, $F_{(2, 198)} = 12133.848$, $p < 0.001$.

Figure 35 displays the τ vs. dt plot for the model run with f = 10 Hz and N = 15 brain areas. The plot displays a slight increase between the first two dt values (10 and 15 ms) and a significant decrease for the last dt value (of 20 ms).

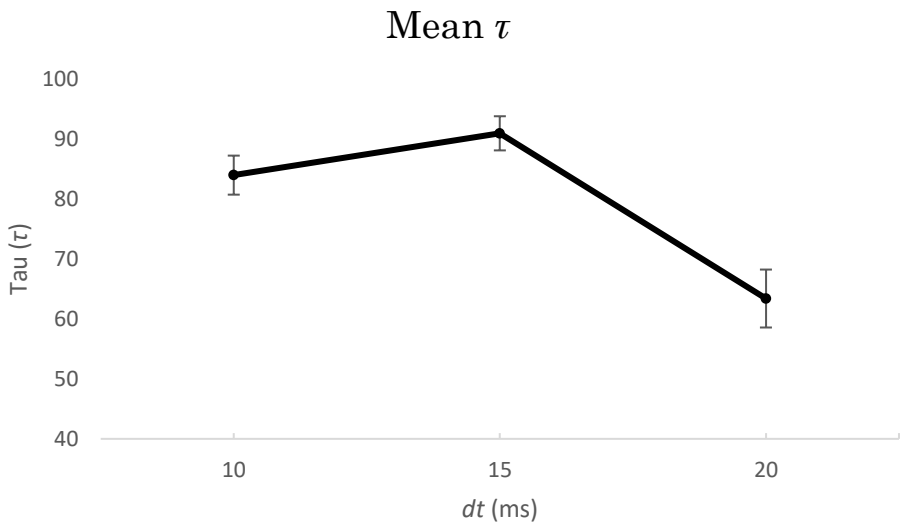

Figure 35. Mean τ values vs. time needed for the stimulus to be sent between brain areas (dt) for f = 8 Hz and N = 10 brain areas. Standard deviation (SD) error bars are also represented in the plot.

3.1.1.12 Effect of parameter interactions on τ values

Each combination of parameter interactions was studied for possible effects on τ values. The interaction between frequency and the number of brain areas was shown to have a significant effect on τ values, $F_{(9.067,\ 897.677)} = 404.646$, $p < 0.001$. Degrees of freedom were corrected using Huynh-Feldt estimates of sphericity ($\xi = 0.907$).

Figure 36 displays how τ vs. frequency varies across different N parameter values. Mean τ values appeared to decrease consistently with increasing frequency across all tested N values, although for higher numbers of areas mean τ values appear to be more proximate. This is consistent with the logarithmic growth τ values display on Figure 34.

Studying the effect of the interaction between frequency and the time between brain areas on τ values, degrees of freedom were corrected using Huynh-Feldt estimates of sphericity ($\xi = 0.904$). Results showed a significant effect of the interaction between f and dt on τ values, $F_{(9.041,\ 895.053)} = 632.145$, $p < 0.001$.

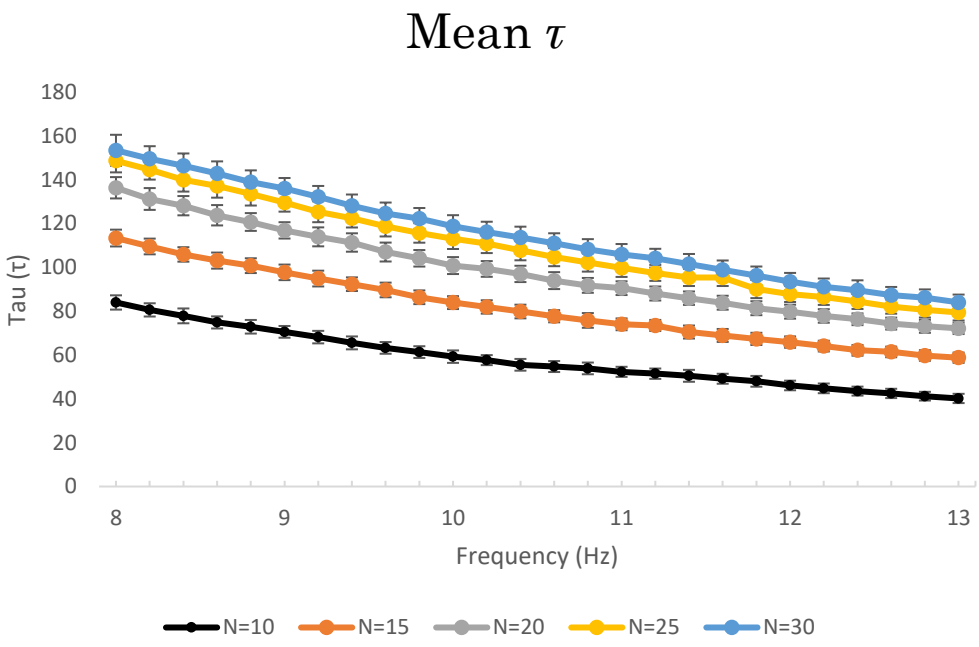

Figure 36. Mean τ values vs. frequency (Hz) over different numbers of brain locations (N). dt equal to 10 ms in these model variations. SD error bars are represented for each line plot.

Figure 37 displays how τ vs. frequency varies across different dt parameter values. As seen in Figure 35, from dt = 10 ms to dt = 15 ms, τ values appear to decrease consistently, but the same cannot be said for dt = 20 ms, were τ values dependency on frequency is different.

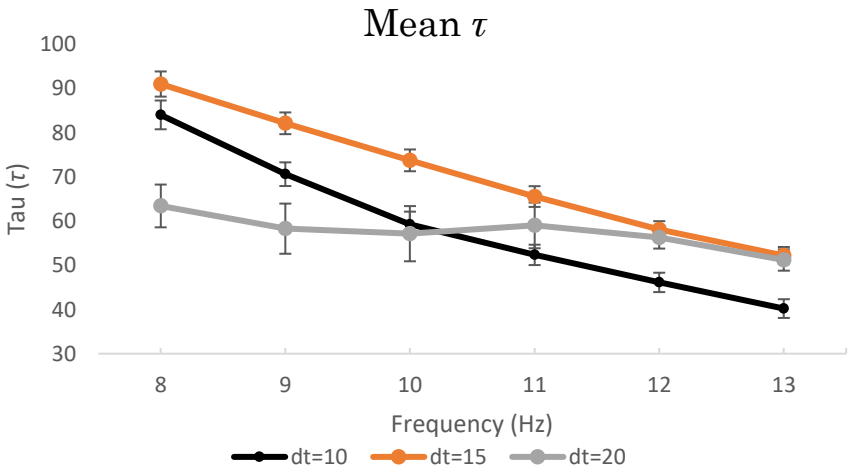

Figure 37. Mean τ values vs. frequency (Hz) over different between-areas time intervals (dt). N equal to 10 brain areas in these model variations. Standard deviation (SD) error bars are represented for each line plot.

The interaction between the number of brain areas that process the stimulus and the time needed to send the stimulus between brain areas was also found to have a significant effect on τ values, $F_{(3.740,\ 370.281)} = 2688.919$, $p < 0.001$. Degrees of freedom were also corrected using Huynh-Feldt estimates of sphericity ($\xi = 0.935$).

Figure 38 shows how τ vs. number of areas varies across different values of dt. This variation appears to relatively consistent for dt values between $dt = 10$ ms and $dt = 20$ ms, but not for $dt = 15$ ms.

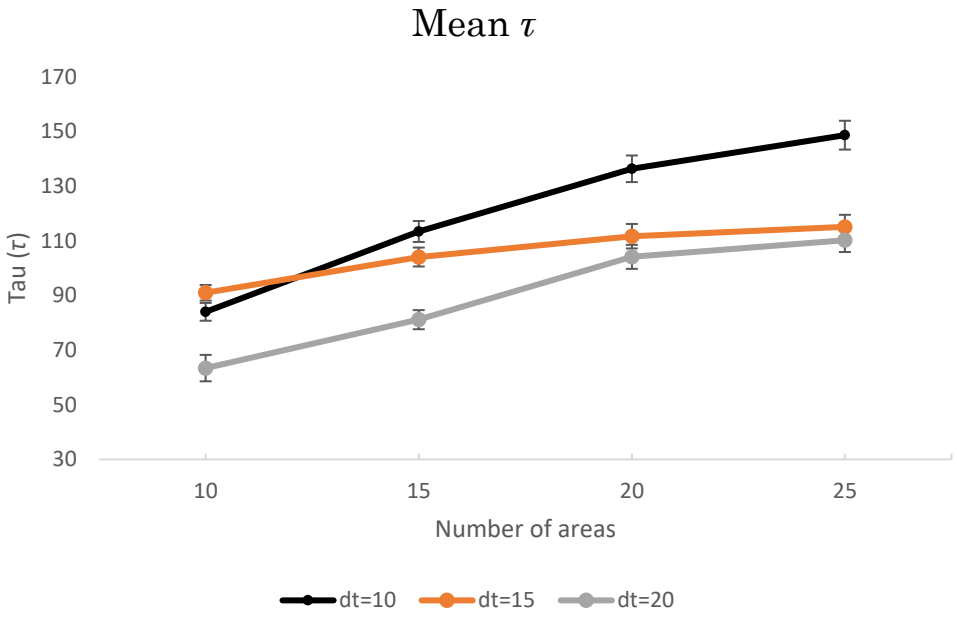

Figure 38. Mean τ values vs. total number of brain areas over different between-areas time intervals (dt). Frequency is set at 8 Hz in these model variations. Standard deviation (SD) error bars are represented for each line plot.

Finally, we studied the effect of the interaction between all varying parameters (f, N and dt) on τ values. Results showed a significant effect of this interaction on the mean and standard deviation of the exponential portion of the ex-Gaussian distribution (τ), $F_{(14.108,\ 1396.688)} = 85.967$, $p < 0.001$. Degrees of freedom were corrected using Greenhouse-Geisser estimates of sphericity ($\xi = 0.705$).

3.1.2 Interim summary

Our analyses showed that increasing alpha frequency leads to a decrease in μ (that represents the average reaction time value for the Gaussian component of the distribution), a decrease in σ (the variability) and a decrease in τ (the exponential part or tail of the distribution). To provide a visual example of these differences, histogram plots of RT data obtained for different frequency values can be seen in Figure 39. With increasing frequency (from A – B), we can see a decrease in the mean RT, in the variability of responses (A plot has a wider distribution than plot B) and in the exponential tail of the distribution (B plot has a smaller number of abnormally long reaction times). These observations suggest that increasing alpha frequency leads to faster and less variable reaction times.

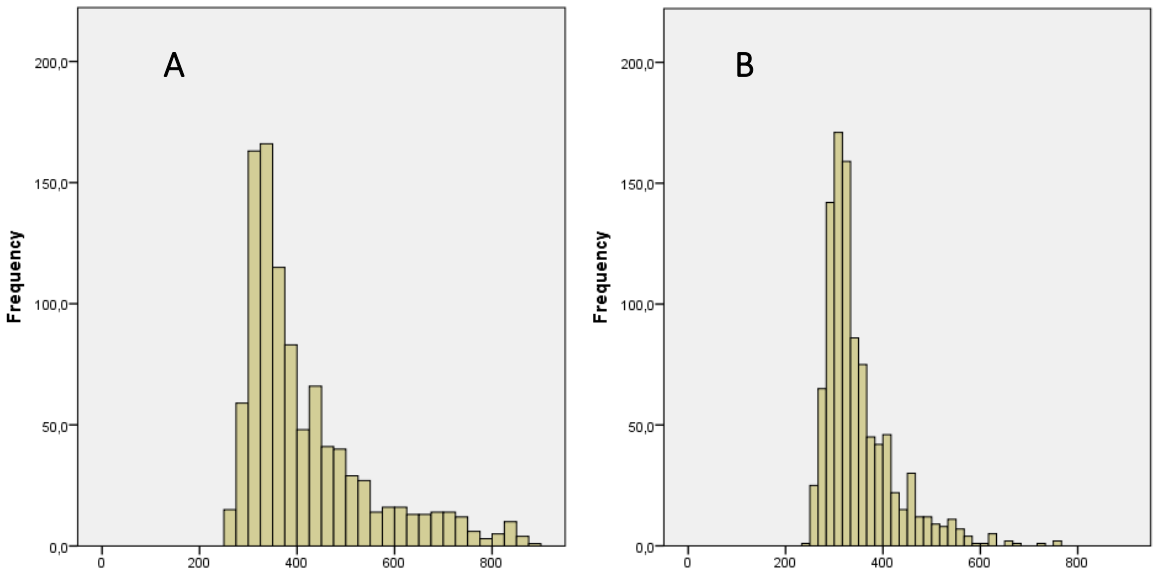

Figure 39. Histogram plots for simulated RT data obtained for the model run with $N = 10$, $dt = 10$ ms and different frequencies. A. Results obtained for frequency equal to 8 Hz, with a mean RT of 420.59 ms and standard deviation of 136.155 ms. B. Results obtained for frequency equal to 13 Hz, with mean RT equal to 349.77 ms and standard deviation equal to 73.45 ms.

Furthermore, increasing the number of areas involved in the signal processing increased μ and τ but decreased σ, suggesting that increasing the number of areas increased the mean reaction time, as expected, decreased the variability of the Gaussian part of the distribution but increased the exponential part of the distribution, suggesting that it increased the number of particularly slow reactions. A visual example of these differences can be observed in the plot histograms of Figure 40. With increasing number of areas, there is a clear increase in the mean reaction time, and increase in the number of extreme (long) responses, and a narrower distribution for the normal part of the distribution.

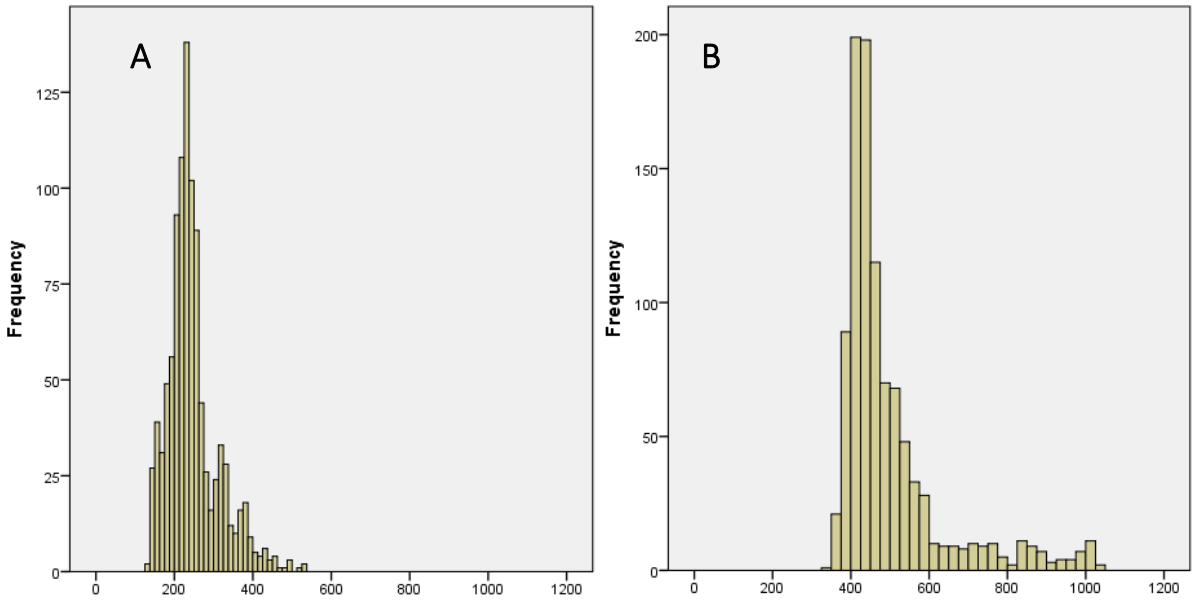

Figure 40. Histogram plots for simulated RT data obtained for the model run with f = 10 Hz, dt = 10 ms and different N values. A. Results obtained for N = 10, with a mean RT of 245.59 ms and standard deviation of 65.114 ms. B. Results obtained for N = 30, with mean RT equal to 497.19 ms and standard deviation equal to 135.219 ms.

Finally, changing the time it takes for information to travel between brain nodes (dt) had a more complex effect on reaction time distributions. Increasing dt appears to increase μ and σ, decrease τ, suggesting longer reaction times with increasing number of areas involved, as expected, increased variability on the Gaussian part of the curve but a decrease on the number of particularly long reaction times. Figure 41 displays histogram plots that provide a visual example for these differences. With increasing dt, there is a clear decrease in the number

of extreme (long) responses, and a clear increase in the mean RT. No clear visual differences can be spotted in terms of variability of the RTs.

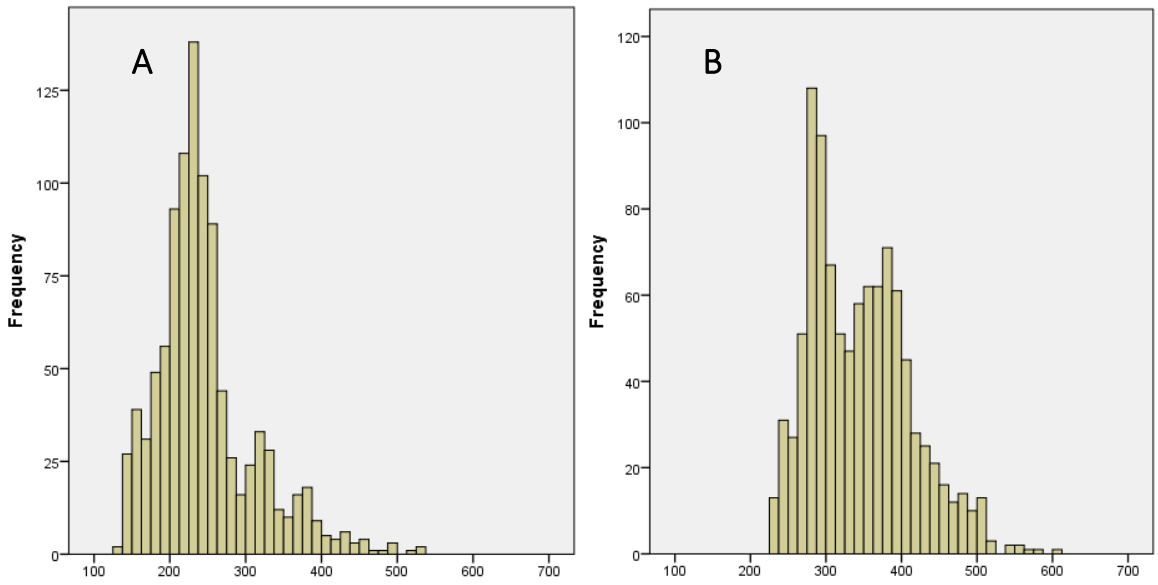

Figure 41. Histogram plots for simulated RT data obtained for the model run with f = 10 Hz, N = 10 ms and different dt values. A. Results obtained for dt = 10 ms, with a mean RT of 245.59 ms and standard deviation of 65.114 ms. B. Results obtained for dt = 20 ms, with mean RT equal to 344.71 ms and standard deviation equal to 66.956 ms.

3.2 Analysis of empirical reaction time data

3.2.1 Effect of group and task type on empirical ex-Gaussian parameters

3.2.1.1 Expected results

Based on current literature, one could expect significant differences in the RT data distributions for tasks of different levels of complexity. Studies have shown that, when processing more complex stimuli (Hochstein & Ahissar, 2002) (Okada, et al., 2010), or when faced with indecision (Kaufman, Churchland, Ryu, & Shenoy, 2015) (Ratcliff & McKoon, 2008), subjects take more time to respond,

due to the need of more processing in these cases than when simply responding to detect the presence of a simple sensory stimulus. This suggests we should expect a significant increase in mean RT for the more complex task (go/no-go), when compared to the simple detection RT task, in the variability of RTs and, possibly, in the number of abnormally long reaction times. This would mean an increase in μ, σ and τ for the go/no-go task RT data (when compared to the simple RT task). How RTs vary with age has also been an interest point for many researchers, and studies show RTs tend to slow with age, although this slowing has been mainly attributed to pathological alterations in the brain and slower motor responses. Nonetheless, studies with healthy young and older adults have shown significant differences in RT distributions, namely that the performance of older adults was slower (higher μ), more variable (higher σ), and more extreme (higher τ) (McAuley, Yap, Christ, & White, 2006), so the same differences should be expected in our results.

3.2.1.2 Effect of group and task type on μ values

Table 5 provides a résumé of the descriptive statistics resulting from SPSS's repeated measures ANOVA, namely mean and standard deviation. We can observe that the average μ values were higher for younger subjects compared to the older subjects, in both detection and go/no-go tasks. This tells us that the younger subjects took, on average, more time to complete each task than their older counterparts. This result was unexpected as it is reported that older adults take longer to respond in sensorimotor tasks.

Furthermore, for all subject groups, the average amount of time each subject took to respond (related to μ) was larger for the go/no-go task than for the simple detection task. This was expected, since the latter involved a simple stimulus detection while the former involved stimulus discrimination before response decision. Figure 42 shows a bar plot for average μ values with standard

deviation error bars. It is clear that for both age groups, mean μ was higher for the go/no-go task.

Table 5. Descriptive statistics for μ values separated by factor combinations. DRT and GRT represent the simple detection and go/no-go types of task, respectively. N stands for the sample size.

Task	Age group	Mean	Std. Deviation	N
DRT	Young	285.791	49.154	29
	Old	260.296	42.306	28
	Total	273.267	47.290	57
GRT	Young	325.784	51.323	29
	Old	320.980	58.507	28
	Total	323.424	54.528	57

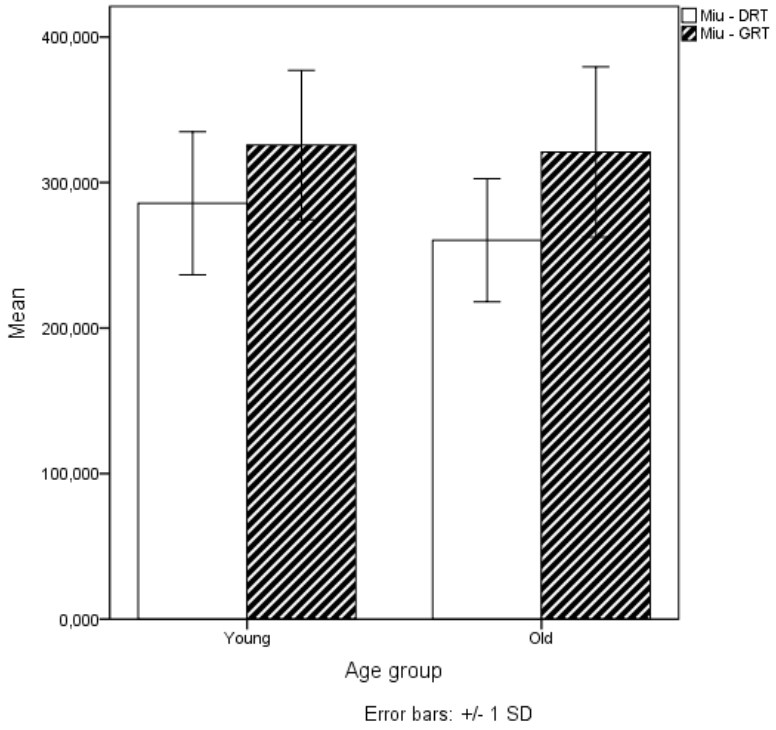

Figure 42. Bar plot for average μ values resulting from empirical data. Error bars represent ± 1 standard deviation (SD). For both age groups, mean μ ("miu") values are higher for the go/no-go (GRT) task than for the simple detection (DRT).

Statistical results showed that the type of task had a significant effect on μ values, $F_{(1, 55)} = 94.494$, $p < 0.001$, which can be justified by the larger average μ values we see for the go/no-go task, when compared to the simple detection task. A marginally significant effect was found for the interaction between the type of task and the age group of the subjects, $F_{(1, 55)} = 3.991$, $p = 0.051$. This is reflected on the larger difference between task type in the older group in relation to the younger group. As a between-subjects factor, results showed no significant effect of age group on μ, $F_{(1, 55)} = 1.498$, $p = 0.226$.

3.2.1.3 Effect of group and task type on σ values

Table 6 provides a résumé of the descriptive statistics resulting for σ values, namely mean and standard deviation. For the simple detection task, mean σ

values were higher for younger individuals than for their older counterparts. However, the same cannot be said for the go/no-go task, where subjects from the older group obtained the biggest mean σ values. Overall, mean σ values were larger for the go/no-go task, suggesting a bigger variability of the normal part of the distribution for the more complex task.

Table 6. Descriptive statistics for σ values separated by factor combinations. DRT and GRT represent the simple detection and go/no-go types of task, respectively. N stands for the sample size.

	Age group	**Mean**	**Std. Deviation**	**N**
DRT	Young	28.233	13.791	29
	Old	20.899	11.221	28
	Total	24.630	13.019	57
GRT	Young	33.829	16.199	29
	Old	36.226	28.788	28
	Total	35.006	23.070	57

Figure 43 displays a bar plot for average σ values with standard deviation error bars. For both age groups, mean σ was higher for the go/no-go task. It is also noticeable a larger standard deviation of the mean for σ values of an older age performing the go/no-go task.

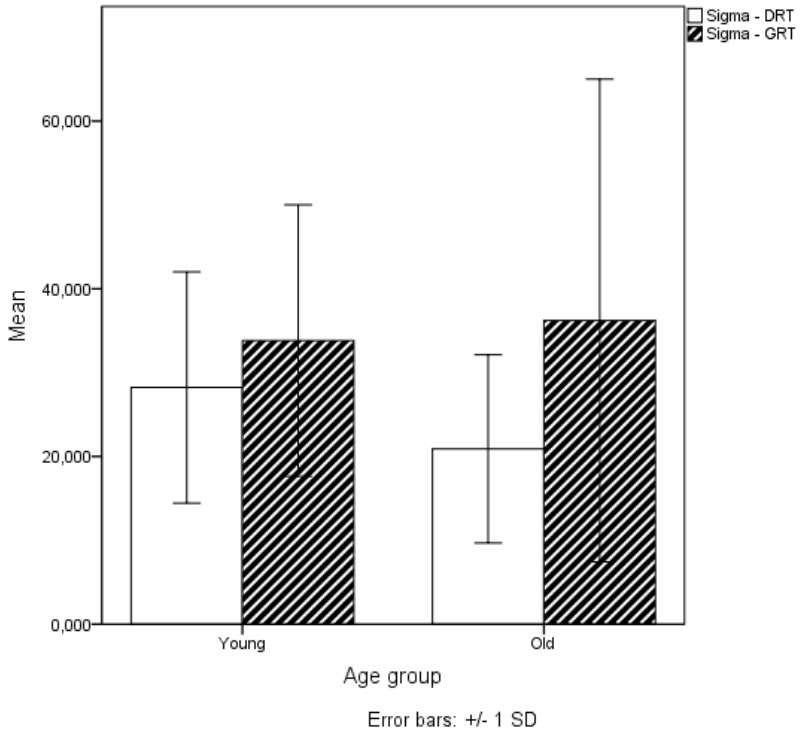

Figure 43. Bar plot for average σ values resulting from empirical data. Error bars represent ± 1 standard deviation (SD). For both age groups, mean σ ("sigma") values are higher for the go/no-go (GRT) task than for the simple detection (DRT).

Statistical results showed the type of task performed had a significant effect on σ values, $F_{(1, 55)} = 13.099$, $p = 0.001$, but no significant effect was found for the interaction between the type of task and the age group, $F_{(1, 55)} = 2.834$, $p = 0.098$. As a between-subjects factor, results showed no significant effect of age group on σ values, $F_{(1, 55)} = 0.377$, $p = 0.542$, which is justified by the variability in sigma values within each group for each task condition.

3.2.1.4 Effect of group and task type on τ values

Table 7 provides a résumé of the descriptive statistics resulting for τ values, namely mean and standard deviation. For the simple detection task, τ values for the younger subjects were, on average, larger than for the older subjects. On the other hand, the opposite occurred for the go/no-go task, where the older subject

group's mean τ values were bigger than those of their younger counterparts. For both age groups, mean τ values were larger for the go/no-go task than for the simple detection. This suggests an overall increase in the number of particularly slow reactions when going from the simple detection task to the, more complex, go/no-go task. Figure 44 shows a bar plot for average τ values with standard deviation error bars.

Table 7. Descriptive statistics for τ values separated by factor combinations. DRT and GRT represent the simple detection and go/no-go types of task, respectively. N stands for the sample size.

Task	Age group	Mean	Std. Deviation	N
DRT	Young	64.931	24.705	29
	Old	54.980	20.648	28
	Total	60.043	23.150	57
GRT	Young	75.202	22.653	29
	Old	86.200	30.383	28
	Total	80.604	27.064	57

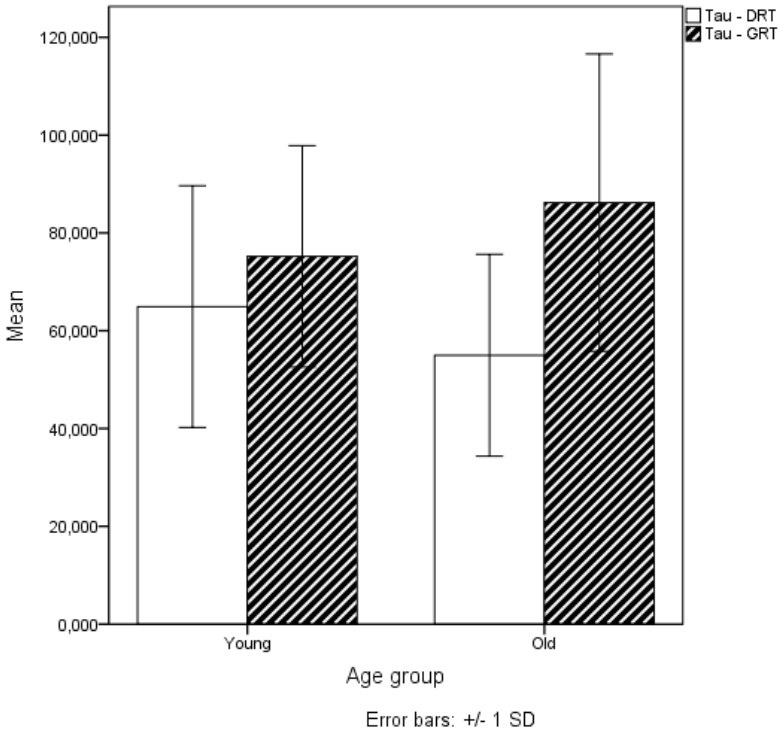

Figure 44. Bar plot for average τ values resulting from empirical data. Error bars represent ± 1 standard deviation (SD). For both age groups, mean τ ("tau") values are higher for the go/no-go (GRT) task than for the simple detection (DRT).

Statistical results showed a significant main effect of the type of task on τ values, $F_{(1, 55)} = 30.624$, $p < 0.001$. This reflects the difference seen on average τ between task types. The interaction between the type of task performed and the age group of the subject was also found to be significant, $F_{(1, 55)} = 7.807$, $p = 0.007$, reflecting the larger difference between tau values in the go/no-go task in comparison to the detection task, in the older group in comparison to the younger group. As a between-subjects factor, results showed no significant effect of age group on τ values, $F_{(1, 55)} = 0.377$, $p = 0.542$, which is justified by the disparities seen on how mean τ varies between age groups in each task.

3.2.1.5 Interim summary

Overall, our analyses show that there is a significant main effect of the type of task performed, and all parameters (μ, σ, τ) were, on average, higher for the go/no-go task, which is more complex than the detection task. Although μ values were, on average, higher for younger subjects on both tasks, results did not show a significant effect of the age group on μ values. In fact, the age group of the subjects did not detain a significant effect on any ex-Gaussian parameter. The interaction between the type of task and the age group of the subject that performs it was marginally significant for mean μ and significant for mean τ values.

Together these results suggest that an increasing complexity of the task increases mean reaction time, the variability of the Gaussian part of the distribution, and the number of particularly slow reactions (provided by the exponential portion of the distribution). Although the age group alone does not have a significant effect on the ex-Gaussian parameters, its interaction with the type of task somehow affects the number of particularly slow reactions, as seen through Figures 42 and 44, where the differences in these parameters, between tasks, were higher for older subjects than for their younger counterparts. Although this difference can also be seen in Figure 43, the high values of standard deviation for the mean σ values probably impede the significance of the interaction between age group and task type for σ values.

Thus, in conclusion, although older people had a better performance in the simple RT task, their performance deteriorated more (was slower and more variable) in the go/no-go task than the performance of younger people.

3.3 Fitting the linear ballistic accumulator

Our adapted LBA model scripts were unable to provide good fitting for most of our empirical RT data. Examples of the LBA model output are represented in Figure 45, and represent the majority of output results obtained by our adapted LBA toolbox scripts.

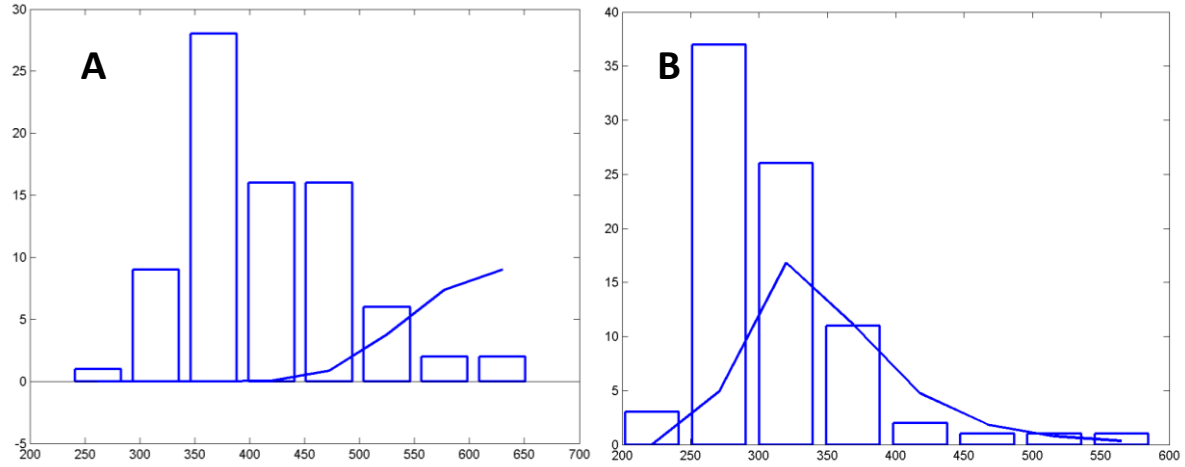

Figure 45. Two case results for fitting the LBA model to our empirical data. Plots represent reaction time data histograms and model predictions (line plots) for two different subjects. A. Extreme case of poor LBA model fitting. B. Although a better fit to the data when compared to figure A, these LBA model predictions are likewise representative of a poor fitting to the data. Plots were generated using the LBA MATLAB® toolbox.

The poor fitting of our empirical data to the LBA model results further emphasized the need for a different model to explain reaction time variability in tasks requiring a single response output.

3.4 Fitting our model to empirical results

To fit our model to the empirical results, an automate search was run in MATLAB® to obtain the sets of model parameters that provided the minimal sum of squared errors, for each combination of experimental factors. The resulting best-fitting sets of model parameters for each experimental task condition are displayed in Table 8.

Table 8. Final sets of parameters that best minimized the sum of squared errors (SSE) for each experimental factor combination (DRT_{young}, DRT_{old}, GRT_{young}, GRT_{old}).

Condition	**Best-fitting model parameters**			**SSE**
	***f* (Hz)**	***N***	***dt* (ms)**	
DRT_{young}	10.4	10	20	79.866
DRT_{old}	12.8	10	19	37.194
GRT_{young}	12	23	12	202.798
GRT_{old}	11.8	24	11	271.357

As can be seen in the SSE column on Table 8, results for the DRT task incurred lower values of sum of squared errors, hence higher resemblance between the model results and the empirical data, than those for the GRT task. This could be because the model was indeed designed to reproduce the mathematics of processing a simple stimulus and indicating its detection, instead of considering a "choice" factor. With that being said, a choice task would still involve the reception of a stimulus, its processing throughout a number of areas, and the decision to press the "detection" button.

These results suggest that, in a simple detection task, the main difference between younger and older subjects lies on the frequency of the alpha oscillations that modulate their neuronal activity. For the go/no-go task, no major differences were apparent between the sets of parameters that best fit the younger and older

groups. A slight difference in frequency (0.2 Hz), a slight difference in the number of cortical areas (1 area of difference), and a slight difference in the stimulus travelling time between areas (1 ms).

Between the types of task, DRT and GRT, results showed major differences in the number of areas (*N*) and stimulus travelling time between areas (*dt*), where, for a the more complex task (GRT), *N* appears to double its DRT resulting value, and *dt* appears to decrease to half its DRT resulting value. These results suggest that, for a more complex task, more areas are required to process the stimulus, but with a smaller average stimulus travelling time between them. This could indicate a bigger proximity between the cortical areas that process this stimulus in a more complex paradigm.

Since, with these results, we were able to obtain an ordered list of model tests that best fit each experimental task condition, we sought for major differences between the best-fitting tests for each condition. No major differences were found between these "best-fitting" sets, and hence we considered the first on the list to be satisfying. The top sets of model parameters in the final, ordered, list are presented in Appendix A.IV.

In order to have a better notion of which modelled ex-Gaussian parameters were farthest from the empirically found values, for each condition, we also analysed the squared errors separately, and saw, for each "winning" set of parameters, which parameter(s) had the biggest squared error and, hence, least resembled the empirical ex-Gaussian parameters that define the experimental RT data distribution. The squared errors for each ex-Gaussian parameter, for each condition, are displayed in Table 9. It is noticeable that, for the simple detection task, the ex-Gaussian parameter that was most different between simulated and empirical data was τ. For the go/no-go task, it was σ that most differed between modelled and empirical data.

Table 9. Separate squared errors (for μ, σ and τ) for each of the best-fitting sets of model parameters within each experimental condition (DRT_{young}, DRT_{old}, GRT_{young}, GRT_{old}).

	Squared error		
	μ	***σ***	***τ***
DRT_{young} (f = 10.4, N = 10, dt = 20)	21.887	20.236	37.742
DRT_{old} (f = 12.8, N = 10, dt = 19)	9.152	2.633	25.409
GRT_{young} (f = 12, N = 23, dt = 12)	62.768	137.653	2.378
GRT_{old} (f = 11.8, N = 24, dt = 11)	1.821	269.499	0.038

4 Discussion

4.1 Fitting the LBA model to simple RT data

The adaptation of the linear ballistic accumulator to fit our simple detection RT data was shown to be unsuccessful. We believe there are several reasons that may justify these results. By removing both the "competitive" component of the model, by having only one evidence accumulator, and the accuracy component, due to the absence of right or wrong responses, we may have changed the model sufficiently for it not to work. However, when studying the mathematics of the model, we could not find a mathematical justification for this influence, since each accumulator is processed independently and the accuracy component served only to, independently, calculate a different accumulator of "wrong" responses. Nonetheless, this reason gained strength when we ran our adapted scripts with the example data from the LBA toolbox (using only RT data for the correct responses) and were still unable to generate good model predictions.

Our data sample size could have also influenced the poor quality of the model fittings, since most of our datasets had a sample size below 100 observations (average sample size was 69.5 observations). Studies have shown that sample sizes of at least 100 observations are necessary for plausible parameter estimation, although using much larger samples is highly motivated (Donkin, Averell, Brown, & Heathcote, 2009). In an attempt to study if this was affecting our results, we joined data from 10 subjects for LBA model fitting, although no improvement was seen on the results. It is, however, worth noting that we gathered data from 10 different subjects, not a sample size 10 times larger for one subject, which could also contribute to the poor fitting, due to eventual inter-individual differences in the RT data.

We recognize that a major setback in our LBA fitting was the choice of a good starting point (i.e. initial parameters). We addressed several different

approaches to select starting points for model fitting, based on the literature (Donkin, Brown, & Heathcote, 2011). Among those approaches, we chose parameters that had been shown to produce reasonable predictions in choice RT data, performed repeated searches, where each new search used the best-fitting set of parameters from the last as the starting point, and iterated through 100 different start points, where the one leading to the best fit (in that search) was then used as the start point in the following search. None of these led to reasonable model predictions to our data.

Upon the obtained results, we arrived at the conclusion that using the linear ballistic accumulator model to fit our simple RT data was not a good path, and abandoned this pursue. These results emphasized the need for a computational model capable of explaining reaction time variability in tasks with single response output.

4.2 Computational model of the effect of alpha oscillatory phase on the timing of motor responses

4.2.1 Phase of alpha oscillations and RT data

By modelling a progressive stimulus processing dependent on the phase of alpha-band oscillations, we were able to obtain simulated RT data that resembled the overall shape of RT distributions found in observed data (an ex-Gaussian distribution), which goes in agreement with the conclusion made by Coon et al. (2016) that alpha oscillatory phase modulates the timing of neuronal activity and, therefore, resulting behaviour.

We suggest further studies could be made by changing the phase interval in the optimal window for stimulus processing from 120-240º to 90-240º in the model design. This suggestion comes from the fact that, although the optimal phase window was mainly between 120-240º (our modelled phase value range) in

Coon et al.'s study, their results suggested that activity onset might also occur between 90º and 240º. Further studies are also encouraged by altering the model's definition of a constant alpha band frequency throughout all task-related cortical areas. Although studies show cortical activity with frequency in the alpha band can be prominent throughout the cortex, and rhythms with a frequency of oscillation within the alpha band are shown to be related to activity in our modelled areas (for sensory stimulus processing) (Coon, et al., 2016) (Niedermeyer & Lopes da Silva, 1982) (Klimesch, 1999), they also show that different cortical regions may have oscillatory activity with different peak alpha frequency values, which our model currently does not consider.

4.2.2 Model parameters influence RT data and the shape of their ex-Gaussian distributions

All model parameters were shown to have a significant effect on the ex-Gaussian parameters that define the resulting distributions of our simulated RT data. The same was true for every interaction between them.

Our analyses showed that increasing alpha frequency leads to a decrease in μ (which represents the mean of the Gaussian portion of the distribution), σ (the standard deviation of the Gaussian portion of the distribution) and τ (the mean and standard deviation of the exponential part of the distribution, i.e. the tail seen in ex-Gaussian distributions). These results suggest that increasing alpha frequency leads to faster, less variable, and with fewer particularly long reaction times. Peak alpha frequency has been shown to decline with age (Niedermeyer & Lopes da Silva, 1982) (Klimesch, 1999), particularly when cerebral pathology is involved. Response times have been shown to slow (i.e. increase) with old age, with their RT distributions also reported to be wider. This suggests that, for elderly subjects performing a RT task, their increased average reaction time (that would reflect on higher μ values) and wider distribution of RTs (that would reflect on higher σ values) could be a consequence of their lower peak alpha frequency.

Moreover, our results suggest that increasing the number of cortical areas that process the stimulus increases the mean reaction time, as would be expected, decreases the variability of the simulated RTs, but increases the number of particularly slow reactions. Increasing N lead to increases in both μ and τ, and a decrease in σ. The decrease in σ was exponential, while the increase in τ was of a logarithmic nature, suggesting diminished variability in these parameters as N increases. It is generally understood that, when processing more complex sensory information, the brain not only takes more time to elaborate a response, but also requires more cortical areas to process stimuli, as demonstrated by studies that clarified the hierarchical organization of various sensory systems (Hochstein & Ahissar, 2002) (Okada, et al., 2010) (Savic, Gulyas, Larsson, & Roland, 2000). Furthermore, studies have shown that moments of behavioural indecision are accompanied by moments of neural indecision, where neural activity changed its location between locations related to different choices (Kaufman, Churchland, Ryu, & Shenoy, 2015). These results suggest that, for a more complex sensory input, or for different levels of indecision, information processing would be transmitted by either more cortical areas or "back-and-forth" between choice-related cortical areas, in moments of indecision (which could, in our model, reflect on higher values of N being associated with higher μ and τ values). Our results seem to agree with these speculations.

Changes in the stimulus travelling time between cortical areas (dt) had more complex effects on the ex-Gaussian parameters. Increasing dt resulted in increases in the mean RT, as expected, but had more complex effects in σ and τ. Overall, increasing dt appears to increase σ and decrease τ, but not in a linear manner. With all other parameters fixed, varying dt from 10 ms to 15 ms lead to a slight decrease in σ and a slight increase in τ, but values for dt = 20 ms showed opposite results, with a large increase for mean σ and a large decrease for τ. Further studies, with a wider range of values for dt, would be necessary to have a better notion of how this parameter affects the variability and tail of the RT ex-Gaussian distribution.

4.3 Empirical RT data

4.3.1 Task type influences RT data and the shape of their ex-Gaussian distributions

We showed that the type of task performed has a significant main effect on the ex-Gaussian parameters and, hence, on the overall values and shape of the RT distributions. Specifically, our analyses demonstrated that all parameters were, on average, higher for the go/no-go task than for the simple detection task. This suggests that increasing task complexity leads to an increase in all ex-Gaussian parameters. An increase in complexity would, therefore, result in longer reactions (higher μ), as expected, that could be explained by an increased number of areas (N) used for processing or by an increased average time for stimulus travelling between areas (dt), as previous results suggest. A need for a higher number of cortical areas for processing would be compatible with a more complex task. An increase in σ with increased complexity suggests higher variability in the reaction times for more complex tasks, which could be, for example, explained by a bigger component of indecision from the subject, related with a more complex decision. We showed that higher values of σ are associated with dt values either equal to 10 ms or 20 ms (or in close proximity to these), and with a decrease in f or N. Increased task complexity also leads to increases in τ and can, therefore, be associated with more abnormally long reaction times. From our previous results, we saw that an increase in N leads to higher τ values, which intensifies the argument for higher numbers of cortical areas being associated with the stimulus processing in a more complex task. Increasing τ values can also be the result of decreases in alpha frequency, suggesting the possibility that subjects with lower alpha frequency rhythms might have a tendency for presenting more extreme values of reaction times.

No ex-Gaussian parameter was solely significantly affected by the age group of the subjects. However, the interaction between both factors, age group and type

of task, was shown to be significant for τ and μ values (although, for the latter, it was marginally significant, p = 0.051), where we were able to see that the differences in these parameters, between tasks, were higher for older subjects than for their younger counterparts. This may suggest that older subjects have a more difficult adaptation to the complex task than to the simple one (since average reactions increase more with higher task complexity and lead to more abnormally long reactions than for younger subjects). Although, by analysing Figure 43, we can also notice a higher variation (in mean σ) between tasks for older subjects, the interaction between age group and the type of task was not significant. It is also apparent the high standard deviation for mean GRT task σ values of older subjects, which could justify the non-significance of this interaction.

Overall, our results showed that the complexity of the task performed has a significant effect on the overall values and shape of the RT ex-Gaussian distribution, which suggests significant differences in the model parameters would be obtained if we tried to model the stimulus processing for both tasks.

4.4 Fitting our model to empirical reaction time data

We were able to find sets of model parameters that lead to RT distributions that best resembled those obtained empirically. It is, however, worth mentioning that these sets of parameters were not the result of an automatic search algorithm that, by itself, tests the model for different parameters and returns those that provide the best results, but of manual model tests, with sets of parameters chosen by the user, that are then automatically processed in order to find the best fitting results. Searching with an automatic search algorithm might provide a more thorough adjustment of our model's parameters.

Our best-fitting sets of parameters were relatively similar within the same task (between age groups), and noticeably different between task types, as would be expected based on the results for the ex-Gaussian fitting to empirical RT data. The quality of the fitting was assessed by the sum of squared errors (SSE) between

the parameters, and the lowest (hence best) values for SSE were discovered for the model fitting a simple detection task. For this task, the main difference (in the model parameters) between age groups was in the frequency of alpha oscillations, where for younger subjects this value was much smaller (= 10.4 Hz) than for the older subjects (= 12.8 Hz). Alpha peak frequency has been shown to decrease with older age (Clark, et al., 2004), which does not reflect on our results. However, this decrease has been shown to reflect some degree of cerebral pathology, and healthy individuals appear to show little to no decline in alpha frequency (Niedermeyer & Lopes da Silva, 1982) (Grandy, et al., 2013). It is also worth noting that the subjects in our older age group were between 52 and 70 years old and, hence, not representative of an elderly age. However, this would still not explain an increase in alpha frequency for this group of subjects. N was equal to 10 cortical areas in both age groups, and dt was equal to 20 ms for the younger group and 19 ms to their older counterparts. For the go/no-task, no major differences were apparent between age groups.

When comparing the results between tasks, the main discovery is that our computational model was able to fit both tasks with changes in parameters that, in our perspective, appear to make sense. When increasing task complexity (i.e. comparing GRT task results to those obtained for the DRT task), our results suggest that more cortical areas would be needed to process the stimulus (higher N – approximately double), and that these areas would be in closer proximity (lower dt – approximately half) to each other. Given what we know about the cortical processing of auditory sensory data, namely that more areas in the auditory cortex are required for discrimination between different stimuli than for simple sound detection, and that these are in close cortical proximity to each other, these results seem to be in agreement with what would be expected to change in the stimulus processing, when comparing the simple detection of an auditory stimulus with a more complex auditory discrimination task paradigm.

The smaller SSE values for the simple detection compared to the go/no-go task could be explained by the fact that our computational model was, indeed, designed to reproduce the mathematics behind the processing of a simple auditory

stimulus, with no consideration for a "choice" factor. Since the more complex, go/no-go, task introduces a component of choice between pressing or not pressing a button, depending on the stimulus itself, this could introduce a bigger indecision factor on whether to press the button.

We were able to detect, for each task, which simulated ex-Gaussian parameters (i.e. obtained from simulated RT data) were most different from those obtained in the empirical RT data fitting. For the simple detection task, the biggest fitting differences appear to be in the tail of the ex-Gaussian distribution, i.e. in the number of abnormally long reactions. For the go/no-go task, the biggest fitting differences occurred in σ values, hence, in the overall variability of reaction times. In here, the difference between empirical and simulated data was highest suggesting that the model had difficulty in modelling the Gaussian variability of the go/no-go RT data.

Overall, we were pleased with the resemblance between our simulated RT data and real RT data, as well as with the model's adaptation to the different tasks. Further studies with variations in all model parameters are encouraged, as well as for a wider permissive window of phase-modulated neuronal activity (90-240º), and for application to RT data from sensorimotor tasks using different sensory input (e.g. visual). Particularly, we encourage testing different values of the constant time parameters, t_0 and t_{exe}, which are for sensory information arrival at the cortex and motor execution purposes, respectively. Different ranges of t_0 values would be encouraged considering the different range of values proposed by existing literature (Mahajan & McArthur, 2012) (Jain, Bansal, Kumar, & Singh, 2015). t_{exe} represents the time needed for motor execution only, but, since our literature-based chosen value was selected, for lack of a known value, from the fastest recorded motor response, this parameter could prove to be higher, in reality. Alterations in these values could affect the results, particularly for the number of cortical areas involved in the performance of the sensorimotor task (N) and in the time it takes for information spike volleys to be sent from one area to the next (dt).

5 Conclusions & future work

The high within-subject variability in human behavioural response timing, when repeatedly performing the same task, has long encouraged researchers to uncover the underlying mechanisms of cognition and sensory stimulus processing. Current reaction time models attribute the source of this variability to variability in the evidence accumulation process, before making a response. Yet, recent findings suggest that the phase of alpha oscillations in the brain modulates the timing of neuronal population activity, opening the possibility that RT variability arises from variability in the timing of information transmission in the brain. We computed a model focusing on this very aspect, and are overall pleased with the resemblance between our model's simulated data and real RT data, namely in the successful fitting of our RT distributions (which has long been considered a critical test for a RT model's success).

Our results appear to be in agreement with what would be expected in what comes to change in RT distributions between tasks of different complexity, namely the increasing number of cortical areas that would be involved in sensory stimulus processing for more complex tasks and the closer proximity these areas would have from each other. Our model parameters seem to have the expected effects on the RT distribution (i.e. their ex-Gaussian parameters), such as, by lowering alpha frequency, increasing the mean reaction times, which could be expected considering the studies relating activity in lower alpha frequency (e.g. in children and elderly adults) to longer reaction times. Although no significant main effect was found for the age group of the subjects in the empirical RT data, a significant interaction was shown between age group and type of task, and higher variability was shown for older subjects in both tasks, which goes in agreement with reported literature.

Our results support the hypothesis that variability in the timing of human behaviour, at least when considering the cortical processing of a simple sensory

stimulus, can be explained by an alpha-band phase-dependent modulation of the timing of neuronal population activity.

Further studies are encouraged for variations in the model parameters, such as the constant times considered for sensory input to the cortex and motor response execution, as are for changes in some assumptions made by the model, namely in attributing the same frequency value for alpha activity in all task-related cortical areas. Studies altering the permissive window of phase-modulated neuronal population activity, to include the entirety of the through's descending slope (90-240º). This computational model was designed to be applied to RT data originated from different types of sensory input, such as visual, and testing it for RT data originated from tasks involving other types of sensory input could help further analyse whether modulation by alpha phase-dependent neuronal population activity can explain variability in response times in all sensory systems.

6 References

Andrews, S., & Heathcote, A. (2001). Distinguishing common and task-specific processes in word identification: a matter of some moment? *J Exp Psychol Learn Mem Cogn, 27*(2), 514-544.

Bates, J. A. (1951). Electrical activity of the cortex accompanying movement. *The Journal of Physiology, 113*, 240-257.

Ben-David, B. M., Eidels, A., & Donkin, C. (2014). Effects of Aging and Distractors on Detection of Redundant Visual Targets and Capacity: Do Older Adults Integrate Visual Targets Differently than Younger Adults? *PLoS ONE, 9*(12), e113551.

Berger, H. (1929). Über das Elektrenkephalogramm des Menschen. *Archiv für Psychiatrie und Nervenkrankheiten, 87*(1), 527-570.

Brown, S., & Heathcote, A. (2005). A ballistic model of choice response time. *Psychological Review, 112*(1), 117-128.

Brown, S., & Heathcote, A. (2008). The Simplest Complete Model of Choice Response Time: Linear Ballistic Accumulation. *Cognitive Psychology, 57*(3), 153-178.

Clark, C. R., Veltmeyer, M. D., Hamitlon, R. J., Simms, E., Paul, R., Hermens, D., & Gordon, E. (2004). Spontaneous alpha peak frequency predicts working memory performance across the age span. *Internantional Journal of Psychophysiology, 53*, 1-9.

Coon, W., Gunduz, A., Brunner, P., Ritaccio, A., Pesaran, B., & Schalk, G. (2016). Oscillatory phase modulates the timing of neuronal activations and resulting behavior. *NeuroImage*(133), 294-301.

Donkin, C., Averell, L., Brown, S., & Heathcote, A. (2009). Getting more from accuracy and response time data: Methods for fitting the linear ballistic accumulator. *Behavior Research Methods, 41*(4), 1095-1110.

Donkin, C., Brown, S., & Heathcote, A. (2011). Drawing conclusions from choice response time models: A tutorial using the linear ballistic accumulator. *Journal of Mathematical Psychology, 55*(2), 140-151.

Dykiert, D., Der, G., Starr, J. M., & Deary, I. J. (2012). Age Differences in Intra-Individual Variability in Simple and Choice Reaction Time: Systematic Review and Meta-Analysis. *PLoS ONE, 7*(10), e45759.

Ehret, G. (1997). The auditory cortex. *J Comp Physiol A, 181*, 547-557.

Field, A. (2013). *Discovering Statistics Using IBM SPSS Statistics.* London: SAGE Publications Ltd.

Fisher, C. R., Walsh, M. M., Blaha, L. M., & Gunzelmann, G. (2015). ACT-R and LBA Model Mimicry Reveals Similarity Across Modeling Formalisms. *CogSci*, 710-715.

Fries, P. (2005). A mechanism for cognitive dynamics: neuronal communication through neuronal coherence. *Trends in Cognitive Sciences, 9*(10), 474-480.

Gottsdanker, R. (1982). Age and Simple Reaction Time. *Journal of Gerontology, 37*(3), 342-348.

Grandy, T. H., Werkle-Bergner, M., Chicherio, C., Schmiedek, F., Lövdén, M., & Lindenberger, U. (2013). Peak individual alpha frequency qualifies as a stable neurophysiological trait marker in healthy younger and older adults. *Psychophysiology, 50*, 570-582.

Haegens, S., Nácher, V., Luna, R., Romo, R., & Jensen, O. (2011). α-Oscillations in the monkey sensorimotor network influence discrimination performance by rhythmical inhibition of neuronal spiking. *Proc. Natl. Acad. Sci., 108*(48), 19377-19382.

Hanslmayr, S., Volberg, G., Wimber, M., Dalal, S. S., & Greenlee, M. W. (2013). Prestimulus Oscillatory Phase at 7 Hz Gates Cortical Information Flow and Visual Perception. *Current Biology, 23*, 2273-2278.

Heathcote, A., & Brown, S. (2002). Quantile maximum likelihood estimation of response time distributions. *Psychonomic Bulletin & Review, 9*(2), 394-401.

Heathcote, A., Popiel, S. J., & Mewhort, D. J. (1991). Analysis of Response Time Distributions: An Example Using the Stroop Task. *Psychological Bulletin, 109*(2), 340-347.

Heathcote, A., Popiel, S. J., & Mewhort, D. J. (1991). Analysis of Response Time Distributions: An Example Using the Stroop Task. *Psychological Bulletin, 109*(2), 340-347.

Herrmann, C. S., Munk, M. H., & Engel, A. K. (2004). Cognitive functions of gamma-band activity: memory match and utilization. *Trends in cognitive sciences, 8*(8), 347-355.

Hochstein, S., & Ahissar, M. (2002). View from the Top: Hierarchies and Reverse Hierarchies in the Visual System. *Neuron, 36*, 791-804.

Hyman, R. (1953). Stimulus information as a determinant of reaction time. *Journal of Experimental Psychology, 45*(3), 188.

Jain, A., Bansal, R., Kumar, A., & Singh, K. (2015). A comparative study of visual and auditory reaction times on the basis of gender and physical activity levels of medical first year students. *International Journal of Applied and Basic Medical Research, 5*(2), 124-127.

Kahana, M. J. (2006). The Cognitive Correlates of Human Brain Oscillations. *The Journal of Neuroscience, 26*(6), 1669-1672.

Kaufman, M. T., Churchland, M. M., Ryu, S. I., & Shenoy, K. V. (2015). Vacillation, indecision and hesitation in moment-by-moment decoding of monkey motor cortex. *eLife, 4*, e04677.

Kelly, C., Foxe, J. J., & Garavan, H. (2006). Patterns of Normal Human Brain Plasticity After Practice and Their Implications for Neurorehabilitation. *Archives of Physical Medicine and Rehabilitation, 87*(12), 20-29.

Klimesch, W. (1999). EEG alpha and theta oscillations reflect cognitive and memory performance: a review and analysis. *Brain Research Reviews, 29*, 169-195.

Klimesch, W., Sauseng, P., & Hanslmayr, S. (2007). EEG alpha oscillations: The inhibition-timing hypothesis. *Brain Research Reviews, 53*, 63-88.

Klimesch, W., Sauseng, P., Hanslmayr, S., Gruber, W., & Freunberger, R. (2007). Event-related phase reorganization may explain evoked neural dynamics. *Neuroscience and Behavioral Reviews, 31*, 1003-1016.

Luce, R. D. (1986). *Response times: Their role in inferring elementary mental organization.* New York: Oxford University Press.

Mahajan, Y., & McArthur, G. (2012). Maturation of auditory event-related potentials across adolescence. *Hearing Research, 294*(1-2), 82-94.

McAuley, T., Yap, M., Christ, S. E., & White, D. A. (2006). Revising Inhibitory Control Across the Life Span: Insights From the Ex-Gaussian Distribution. *Developmental Neuropsychology, 29*(3), 447-458.

Moser, E. I., Moser, M. B., & Andersen, P. (1994). Potentiation of dentate synapses initiated by exploratory learning in rats: dissociation from brain temperature, motor activity, and arousal. *Learning & Memory, 1*, 55-73.

Niedermeyer, E., & Lopes da Silva, F. H. (1982). *Electroencephalography: Basic Principles, Clinical Applications, and Related Fields.* Lippincott Williams & Wilkins.

Okada, K., Rong, F., Venezia, J., Matchin, W., Hsieh, I.-H., Saberi, K., . . . Hickok, G. (2010). Hierarchical Organization of Human Auditory Cortex: Evidence from Acoustic Invariance in the Response to Intelligible Speech. *Cerebral Cortex, 20*(10), 2486-2495.

Parris, B. A., Dienes, Z., & Hodgson, T. L. (2013). Application of the ex-Gaussian function to the effect of the word blindness suggestion on Stroop task performance suggests no word blindness. *Frontiers in Psychology, 4*, 647.

Piccioli, Z. D., & Littleton, J. T. (2014). Retrograde BMP Signaling Modulates Rapid Activity-Dependent Synaptic Growth via Presynaptic LIM Kinase Regulation of Cofilin. *Journal of Neuroscience, 34*(12), 4371-4381.

Purves, D., Augustine, G. J., Fitzpatrick, D., Katz, L. C., LaMantia, A.-S., McNamara, J. O., & Williams, S. M. (2001). *Neuroscience.* Sinauer Associates, Inc.

Ratcliff, R. (1979). Group Reaction Time Distributions and an Analysis of Distribution Statistics. *Psychological Bulletin, 86*(3), 446-461.

Ratcliff, R. (2006). Modeling response signal and response time data. *Cognitive Psychology, 53*, 195-237.

Ratcliff, R., & McKoon, G. (2008). The Diffusion Decision Model: Theory and Data for Two-Choice Decision Tasks. *Neural Computation, 20*(4), 873-922.

Ratcliff, R., & Van Dongen, H. P. (2011). Diffusion model for one-choice reaction-time tasks and the cognitive effects of sleep deprivation. *PNAS, 108*(27), 11285-11290.

Ratcliff, R., Thapar, A., & McKoon, G. (2001). The effects of aging on reaction time in a signal detection task. *Psychology and Aging, 16*(2), 323-341.

Rousselet, G. A., Thorpe, S. J., & Fabre-Thorpe, M. (2004). How parallel is visual processing in the ventral pathway? *TRENDS in Cognitive Sciences, 8*(8), 363-370.

Savic, I., Gulyas, B., Larsson, M., & Roland, P. (2000). Olfactory Functions Are Mediated by Parallel and Hierarchical Processing. *Neuron, 26*(3), 735-745.

Schalk, G. (2015). A general framework for dynamic cortical function: the function-through-biased-oscillations (FBO) hypothesis. *Frontiers in Human Neuroscience, 9:352.*

Silvanto, J. (2015). Why is "blindsight" blind? A new perspective on primary visual cortex, recurrent activity and visual awareness. *Counsciousness and Cognition, 32*, 15-32.

Smith, P. L. (1995). Psychophysically Principled Models of Visual Simple Reaction Time. *Psychological Review, 102*(3), 567-593.

Snell, R. S. (2010). *Clinical Neuroanatomy* (7th ed.). Lippincott Williams & Wilkins.

Sourakov, A. (2009). Extraordinarily Quick Visual Startle Reflexes of Skipper Butterflies (Lepidoptera: Hesperiidae) Are among the Fastest Recorded in the Animal Kingdom. *The Florida Entomologist, 92*(4), 653-655.

Sternberg, S. (2004). Reaction-Time Experimentation. *Psychology, 600*, 301.

Thorpe, S., Delorme, A., & Van Rullen, R. (2001). Spike-based strategies for rapid processing. *Neural Networks, 14*, 715-725.

Usher, M., & McClelland, J. L. (2001). On the time course of perceptual choice: The leaky competing accumulator model. *Psychological Review, 108*, 550-592.

van Dijk, H., Schoffelen, J.-M., Osstenveld, R., & Jensen, O. (2008). Prestimulus Oscillatory Activity in the Alpha Band Predicts Visual Discrimination Ability. *The Journal of Neuroscience, 28*(8), 1816-1823.

Van Zandt, T. (2000). How to fit a response time distribution. *Psychonomic Bulletin & Review, 7*(3), 424-465.

Wessinger, C., VanMeter, J., Tian, B., Van Lare, J., Pekar, J., & Rauschecker, J. (2001). Hierarchical Organization of the Human Auditory Cortex Revealed by Functional Magnetic Resonance Imaging. *Journal of Cognitive Neuroscience, 13*(1), 1-7.

Appendix

A.I – Descriptive statistics for model runs varying all model parameters

Table 1. Descriptive statistics for μ values across variations in all model parameters. Obtained through SPSS.

Model parameters			**Descriptive statistics (μ)**		
***dt* (ms)**	***N***	***f* (Hz)**	**Mean**	**Std. Deviation**	**Sample Size**
10	10	8	189.63610	2.315289	100
10	10	9	186.89680	2.132793	100
10	10	10	185.12780	2.202879	100
10	10	11	182.79610	1.689894	100
10	10	12	180.95240	1.795667	100
10	10	13	179.40790	2.039473	100
10	15	8	242.79840	1.744308	100
10	15	9	240.76500	1.423557	100
10	15	10	238.56860	1.412056	100
10	15	11	237.07800	1.345738	100
10	15	12	235.56950	1.483151	100
10	15	13	233.90040	1.212888	100
10	20	8	289.57000	1.782514	100
10	20	9	287.51110	1.688859	100
10	20	10	285.61520	1.576044	100
10	20	11	283.59870	1.351171	100
10	20	12	282.24440	1.365945	100
10	20	13	280.61060	1.438376	100

15	10	8	234.31340	1.675351	100
15	10	9	230.94850	1.423198	100
15	10	10	228.99610	1.351602	100
15	10	11	227.10530	1.330084	100
15	10	12	226.36200	1.420463	100
15	10	13	225.00990	1.233840	100
15	15	8	306.51860	1.523549	100
15	15	9	303.66240	1.313057	100
15	15	10	301.03370	1.447680	100
15	15	11	299.20720	1.278345	100
15	15	12	298.20580	1.257691	100
15	15	13	296.85160	1.276636	100
15	20	8	379.99600	1.629438	100
15	20	9	377.26510	1.326006	100
15	20	10	374.86960	1.312388	100
15	20	11	372.97100	1.335341	100
15	20	12	371.84950	1.200285	100
15	20	13	370.65800	1.241962	100
20	10	8	308.50870	5.090547	100
20	10	9	298.08890	6.062109	100
20	10	10	287.73230	6.631049	100
20	10	11	274.56240	5.534237	100
20	10	12	269.06260	2.441501	100
20	10	13	267.06140	2.463828	100
20	15	8	432.63830	2.668756	100
20	15	9	425.79070	2.555781	100
20	15	10	419.40040	2.141465	100
20	15	11	413.43140	1.960281	100
20	15	12	408.06440	2.267022	100
20	15	13	404.81400	2.015786	100
20	20	8	524.79300	2.799343	100

20	20	9	518.75590	2.447907	100
20	20	10	512.91900	2.173786	100
20	20	11	506.66850	2.128738	100
20	20	12	502.06840	2.016155	100
20	20	13	498.58090	1.823896	100

Table 2. Descriptive statistics for σ values across variations in all model parameters. Obtained through SPSS.

Model parameters			**Descriptive statistics (σ)**		
***dt* (ms)**	***N***	***f* (Hz)**	**Mean**	**Std. Deviation**	**Sample Size**
10	10	8	31.45801	1.280697	100
10	10	9	30.04559	1.042337	100
10	10	10	29.30877	1.039892	100
10	10	11	28.06857	.975106	100
10	10	12	27.34534	.876952	100
10	10	13	26.69469	.945196	100
10	15	8	18.93848	1.403318	100
10	15	9	18.46393	1.265318	100
10	15	10	17.92794	1.168897	100
10	15	11	17.49258	1.064199	100
10	15	12	17.23819	1.138801	100
10	15	13	16.94426	1.004121	100
10	20	8	17.59846	1.350032	100
10	20	9	17.15746	1.278220	100
10	20	10	16.92097	1.339663	100
10	20	11	16.24134	1.178467	100
10	20	12	16.10614	1.007232	100
10	20	13	15.61214	.945834	100
15	10	8	18.23267	1.627867	100
15	10	9	17.20197	1.500946	100
15	10	10	16.80834	1.302278	100
15	10	11	16.10411	1.065097	100
15	10	12	16.20743	1.014421	100
15	10	13	16.02392	1.007662	100

15	15	8	17.14142	1.428633	100
15	15	9	16.18785	1.048204	100
15	15	10	15.72345	1.079785	100
15	15	11	14.98558	1.031288	100
15	15	12	14.82136	1.053710	100
15	15	13	14.61019	1.035690	100
15	20	8	16.67183	1.336949	100
15	20	9	15.92841	.919837	100
15	20	10	15.22492	1.079380	100
15	20	11	14.41876	1.054786	100
15	20	12	14.35327	.871443	100
15	20	13	14.11886	.983296	100
20	10	8	50.96269	3.056975	100
20	10	9	44.40967	3.789905	100
20	10	10	37.67879	5.194406	100
20	10	11	27.67500	4.422328	100
20	10	12	23.45763	2.255221	100
20	10	13	22.23700	1.855786	100
20	15	8	38.43466	2.136320	100
20	15	9	36.03205	1.826892	100
20	15	10	34.38117	1.807530	100
20	15	11	32.33680	1.650833	100
20	15	12	30.21733	1.782403	100
20	15	13	29.63869	1.565117	100
20	20	8	34.03964	2.226479	100
20	20	9	31.43001	1.840553	100
20	20	10	29.83760	1.823685	100
20	20	11	27.79457	1.635874	100

20	20	12	26.16540	1.486150	100
20	20	13	25.29537	1.243252	100

Table 3. Descriptive statistics for τ values across variations in all model parameters. Obtained through SPSS.

Model parameters			**Descriptive statistics (τ)**		
***dt* (ms)**	***N***	***f* (Hz)**	**Mean**	**Std. Deviation**	**Sample Size**
10	10	8	84.01186	3.257428	100
10	10	9	70.60031	2.677612	100
10	10	10	59.28388	2.847217	100
10	10	11	52.34683	2.302820	100
10	10	12	46.12455	2.190687	100
10	10	13	40.20196	2.117676	100
10	15	8	113.41400	3.838885	100
10	15	9	97.76178	3.553781	100
10	15	10	83.94637	2.940449	100
10	15	11	74.03539	2.690827	100
10	15	12	65.92987	2.588078	100
10	15	13	58.80279	2.337345	100
10	20	8	136.36340	4.865765	100
10	20	9	116.91910	3.721525	100
10	20	10	100.85031	3.868808	100
10	20	11	90.54143	3.134152	100
10	20	12	79.81731	3.176602	100
10	20	13	72.19407	2.590355	100
15	10	8	90.98975	2.850158	100
15	10	9	82.11033	2.460294	100
15	10	10	73.72875	2.465089	100
15	10	11	65.54018	2.343847	100
15	10	12	58.07748	1.891709	100

15	10	13	52.19521	1.938657	100
15	15	8	104.07402	3.469319	100
15	15	9	94.13160	2.852301	100
15	15	10	86.14120	2.761443	100
15	15	11	77.67847	2.630866	100
15	15	12	69.82034	2.471624	100
15	15	13	62.65480	2.404148	100
15	20	8	111.68860	4.479591	100
15	20	9	100.83898	3.862266	100
15	20	10	91.99733	3.168848	100
15	20	11	82.96352	3.132761	100
15	20	12	75.06675	2.698630	100
15	20	13	67.05466	2.725383	100
20	10	8	63.41783	4.835173	100
20	10	9	58.27813	5.674339	100
20	10	10	57.14543	6.242201	100
20	10	11	59.01075	5.164453	100
20	10	12	56.29033	2.518543	100
20	10	13	51.19106	2.413889	100
20	15	8	81.13905	3.493782	100
20	15	9	69.39704	3.224995	100
20	15	10	61.35585	3.142113	100
20	15	11	54.74893	2.498521	100
20	15	12	50.02420	2.897944	100
20	15	13	44.48432	2.491262	100
20	20	8	104.13475	4.395130	100
20	20	9	90.63122	3.817990	100
20	20	10	80.73760	3.286608	100

20	20	11	73.53054	3.084991	100
20	20	12	66.70667	2.941405	100
20	20	13	60.57905	2.542333	100

A.II – Custom MATLAB® scripts

Example model script

Example script for the model run with $f = 10.6$ Hz, $N = 15$, and $dt = 10$ ms.

```
% Number of areas (N): 15
% Amplitude (A): 1
% Frequency of discretization (f_disc): 1000 (Hz)
% Time for stimulus to reach the brain (t0): 30 (ms)
% Time from area to area (dt) = 10 (ms)
% Frequency of alpha band in ALL areas: 10.6 (Hz)
% Alpha-wave phase of oscillation: changes each area
% Time for motor execution purposes (t_exe): 15 (ms)

N = 15;
A = 1;
f_disc = 1000;
t0 = 30/1000; %(s)
dt = 10/1000; %(s)
f = 10.6;
t_exe = 15/1000; %(s)
% time vector
t = 0 : (1/f_disc) : 1; %(s)

% generate phases for each area:
phi = zeros(1,N);
for i = 1:N
    phi(i) = generate_random_phase();
end

% generate alpha waves for each area:
y = zeros(N,length(t));
for i=1:N
    y(i,:) = generate_wave(A, f, t, phi(i));
end



% calculate times at which stimulus can occur
% function in_trough_at() receives t, ti, y, A as input, with ti being the
% time at which stimulus reaches this location, and so the first possible
% instant of stimulus propagation occurrence
t_response = zeros(1,N);
for i = 1:N
    if (i == 1)
        % if we talk about the first area, ti = t0
        t_response(i) = in_trough_at(t, t0, y(i,:), A);
    else
        ti = t_response(i-1) + dt; % time at which stimulus propagates +
time of travel between areas
        t_response(i) = in_trough_at(t, ti, y(i,:), A);
    end
end
% We consider that the stimulus is sent to the subject at t = 0
rt = t_response(N) + t_exe;
```

generate_random_phase( )

Function to generate a random phase offset for an oscillatory wave.

```
function [phi] = generate_random_phase()
    % in degrees
    phi_d = (360-0).*rand(1) + 0;
    % change to radians
    phi = degtorad(phi_d);
end
```

generate_wave( )

Function to generate an oscillatory wave, given its needed parameters.

```
function y = generate_wave(A, f, t, phi)
    y = A * cos(2 * pi * f * t + phi);
end
```

in_trough_at( )

Function that returns the time at which excitation can occur at the receiving cortical location.

```
function [ time_trough] = in_trough_at( t, ti, y, A )
%IN_TROUGH_AT(t,ti, y, A) Returns the time at which the oscillation can
%   provoke excitation at the receiving location.
%   You INPUT the time vector (t), the initial time(ti) at which you want to
begin the search at the receiving location, the y vector (the function) and
the amplitude (A) of that oscillation.
%   It RETURNS the time when excitation can occur at the receiving site

time = ti;
initial = find( t == ti );
y_threshold = A*cosd(120);

for i = initial : length(t)
    if(t(i) > t(end))
        break;
    end

    if(y(i) <= y_threshold)
        time = t(i);
        break;
    end
end
time_trough = time;
end
```

get_1000rt( )

Function that returns 1000 RT values from the model run with a specific set of parameters

```
function result = get_1000rt(i)
    % Get 1000 RT values to be able to produce an histogram.
    % Input number # of model ( file 'model_rt_#.m' )

    % Because MATLAB resets the rand state at startup, rand generates
    % the same sequence of numbers in each session unless you change the
value
    % of the state input:
    rand('twister', sum(1000*clock));
    randn('state', sum(1000*clock));

    RT = zeros(1,1000);
    freq = cell(1,1000);
    phase = cell(1,1000);

    script = '';
    if (i < 10)
        script = strcat('model_rt_00', num2str(i));
    elseif (i >= 10 && i < 100)
        script = strcat('model_rt_0', num2str(i));
    elseif (i >= 100)
        script = strcat('model_rt_', num2str(i));
    end

    for ii = 1:1000
        run(script);
        RT(ii) = rt*1000; % get result in ms
        freq{ii} = num2cell(f, [1 2]);
        phase{ii} = num2cell(phi, [1 2]);
    end

    result = struct('rt', RT, 'freq', {freq}, 'phase', {phase});

end
```

model2csv.m

Script that creates a *.csv* file for each data (*.mat*) file that has been created.

```
function model2csv()

    % I want to go through all the model folders, all runs, and create an
    % .csv file for all data .mat files that have been created
    %
    names = [];
    first_model = 1;
    last_model = 199;

    number_models = last_model - first_model + 1;

    excelRT = zeros(100, 1000);
    excelMiu = zeros(100, number_models);
    excelSigma = zeros(100,number_models);
    excelTau = zeros(100, number_models);

    for i = first_model : last_model
        if (i < 10)
            foldername                                                    =
strcat('C:\Users\Lea\Documents\University\Biomedical                Engineering
(MSc)\Thesis\Projecto   Maria   Ribeiro\Test   Runs\TEST   RUN   -   RT   alpha
model\Model_00', num2str(i), '\');
        elseif (i >= 10 && i < 100)
            foldername                                                    =
strcat('C:\Users\Lea\Documents\University\Biomedical                Engineering
(MSc)\Thesis\Projecto   Maria   Ribeiro\Test   Runs\TEST   RUN   -   RT   alpha
model\Model_0', num2str(i), '\');
        elseif (i > 100)
            foldername                                                    =
strcat('C:\Users\Lea\Documents\University\Biomedical                Engineering
(MSc)\Thesis\Projecto   Maria   Ribeiro\Test   Runs\TEST   RUN   -   RT   alpha
model\Model_', num2str(i), '\');
        end
        for ii = 1:100
            filename = foldername;
            filename  =  strcat(filename,  'Run_',  num2str(ii),  '\result_',
num2str(ii), '.mat');
            data = load(filename);
            excelRT(ii,:) = data.rt;
            excelMiu(ii,(i-first_model+1)) = data.miu;
            excelSigma(ii,(i-first_model+1)) = data.sigma;
            excelTau(ii,(i-first_model+1)) = data.tau;
        end


        if (i < 10)
            csvFilenameRT   =   strcat(foldername,   'model_00',   num2str(i),
'_rt.csv');
            csvFilenameMiu   =   strcat(foldername,   'model_00',   num2str(i),
'_miu.csv');
            csvFilenameSigma  =  strcat(foldername,  'model_00',  num2str(i),
'_sigma.csv');
            csvFilenameTau   =   strcat(foldername,   'model_00',   num2str(i),
'_tau.csv');
        elseif (i >= 10 && i < 100)
```

```
            csvFilenameRT   =   strcat(foldername,   'model_0',   num2str(i),
'_rt.csv');
            csvFilenameMiu   =   strcat(foldername,   'model_0',   num2str(i),
'_miu.csv');
            csvFilenameSigma   =   strcat(foldername,   'model_0',   num2str(i),
'_sigma.csv');
            csvFilenameTau   =   strcat(foldername,   'model_0',   num2str(i),
'_tau.csv');
        elseif (i > 100)
            csvFilenameRT   =   strcat(foldername,   'model_',   num2str(i),
'_rt.csv');
            csvFilenameMiu   =   strcat(foldername,   'model_',   num2str(i),
'_miu.csv');
            csvFilenameSigma   =   strcat(foldername,   'model_',   num2str(i),
'_sigma.csv');
            csvFilenameTau   =   strcat(foldername,   'model_',   num2str(i),
'_tau.csv');
        end

        csvwrite(csvFilenameRT, excelRT');
        csvwrite(csvFilenameMiu, excelMiu);
        csvwrite(csvFilenameSigma, excelSigma);
        csvwrite(csvFilenameTau, excelTau);

    end

end
```

all_data_into_csv.m

Script that creates a *.csv* file containing all data, for the model run with fixed *dt* at 10 ms, but varying *f* and *N*.

```
temp_miu_array = zeros(100,1);
temp_sigma_array = zeros(100,1);
temp_tau_array = zeros(100,1);
% number_of_runs, number_of_N * number_of_f
MIU = zeros(100, 5*26);
SIGMA = zeros(100, 5*26);
TAU = zeros(100, 5*26);

for i = 1:5 % Number of areas
    for j = 1:26 % Number of different frequencies per area

        if (i==1) % N=10, models start at 1
            model = j;
            for run = 1:100
                if (j < 10)
                    directory                                                    =
strcat('C:\Users\Lea\Documents\University\Biomedical                    Engineering
(MSc)\Thesis\Projecto   Maria   Ribeiro\Test   Runs\TEST   RUN   -   RT   alpha
```

```
model\Model_00',    num2str(j),    '\Run_',    num2str(run),    '\result_',
num2str(run), '.mat');
                elseif (j >= 10 && j < 100)
                    directory                                                =
strcat('C:\Users\Lea\Documents\University\Biomedical            Engineering
(MSc)\Thesis\Projecto   Maria   Ribeiro\Test   Runs\TEST   RUN   -   RT   alpha
model\Model_0', num2str(j), '\Run_', num2str(run), '\result_', num2str(run),
'.mat');
                end
                temp = load(directory);
                temp_miu_array(run) = temp.miu;
                temp_sigma_array(run) = temp.sigma;
                temp_tau_array(run) = temp.tau;
            end
        elseif (i==2) % N=15, models start at #28 (ID)
            model = j + 27;
            for run = 1:100
                if (model < 100)
                    directory                                                =
strcat('C:\Users\Lea\Documents\University\Biomedical            Engineering
(MSc)\Thesis\Projecto   Maria   Ribeiro\Test   Runs\TEST   RUN   -   RT   alpha
model\Model_0',    num2str(model),    '\Run_',    num2str(run),    '\result_',
num2str(run), '.mat');
                elseif (model >= 100)
                    directory                                                =
strcat('C:\Users\Lea\Documents\University\Biomedical            Engineering
(MSc)\Thesis\Projecto   Maria   Ribeiro\Test   Runs\TEST   RUN   -   RT   alpha
model\Model_',    num2str(model),    '\Run_',    num2str(run),    '\result_',
num2str(run), '.mat');
                end
                temp = load(directory);
                temp_miu_array(run) = temp.miu;
                temp_sigma_array(run) = temp.sigma;
                temp_tau_array(run) = temp.tau;
            end
        elseif (i==3) % N=20, models start at #55
            model = j + 54;
            for run = 1:100
                if (model < 100)
                    directory                                                =
strcat('C:\Users\Lea\Documents\University\Biomedical            Engineering
(MSc)\Thesis\Projecto   Maria   Ribeiro\Test   Runs\TEST   RUN   -   RT   alpha
model\Model_0',    num2str(model),    '\Run_',    num2str(run),    '\result_',
num2str(run), '.mat');
                elseif (model >= 100)
                    directory                                                =
strcat('C:\Users\Lea\Documents\University\Biomedical            Engineering
(MSc)\Thesis\Projecto   Maria   Ribeiro\Test   Runs\TEST   RUN   -   RT   alpha
model\Model_',    num2str(model),    '\Run_',    num2str(run),    '\result_',
num2str(run), '.mat');
                end
                temp = load(directory);
                temp_miu_array(run) = temp.miu;
                temp_sigma_array(run) = temp.sigma;
                temp_tau_array(run) = temp.tau;
            end
        elseif (i==4) % N=25, models start at #82
            model = j + 81;
            for run = 1:100
                if (model < 100)
```

```
                    directory                                                =
strcat('C:\Users\Lea\Documents\University\Biomedical                Engineering
(MSc)\Thesis\Projecto   Maria   Ribeiro\Test   Runs\TEST   RUN   -   RT   alpha
model\Model_0',    num2str(model),    '\Run_',    num2str(run),    '\result_',
num2str(run), '.mat');
                elseif (model >= 100)
                    directory                                                =
strcat('C:\Users\Lea\Documents\University\Biomedical                Engineering
(MSc)\Thesis\Projecto   Maria   Ribeiro\Test   Runs\TEST   RUN   -   RT   alpha
model\Model_',    num2str(model),    '\Run_',    num2str(run),    '\result_',
num2str(run), '.mat');
                end
                temp = load(directory);
                temp_miu_array(run) = temp.miu;
                temp_sigma_array(run) = temp.sigma;
                temp_tau_array(run) = temp.tau;
            end
        elseif (i==5) % N=30, models start at #108
            model = j + 107;
            for run = 1:100
                directory                                                =
strcat('C:\Users\Lea\Documents\University\Biomedical                Engineering
(MSc)\Thesis\Projecto   Maria   Ribeiro\Test   Runs\TEST   RUN   -   RT   alpha
model\Model_',    num2str(model),    '\Run_',    num2str(run),    '\result_',
num2str(run), '.mat');

                temp = load(directory);
                temp_miu_array(run) = temp.miu;
                temp_sigma_array(run) = temp.sigma;
                temp_tau_array(run) = temp.tau;
            end
        end

        % 'temp_X_array' has now all the X's from ONE RUN, for 1 value of
        % N and 1 value of f

        column = j + (i-1)*26;

        MIU(:, column) = temp_miu_array;
        SIGMA(:, column) = temp_sigma_array;
        TAU(:, column) = temp_tau_array;

    end
end

foldername   =   'C:\Users\Lea\Documents\University\Biomedical   Engineering
(MSc)\Thesis\Projecto Maria Ribeiro\Test Runs\TEST RUN - RT alpha model\';
miu_filename = strcat(foldername, 'miu_all_data.csv');
sigma_filename = strcat(foldername, 'sigma_all_data.csv');
tau_filename = strcat(foldername, 'tau_all_data.csv');

csvwrite(miu_filename, MIU);
csvwrite(sigma_filename, SIGMA);
csvwrite(tau_filename, TAU);
```

find_best_parameters.m

Script used to generate ordered tables (one for each experimental condition) from minimum to maximum SSE, returning SSE values and the respective model they belong to.

```
% To find the model parameters that provide the closest empirical fitting
% (closest resemblance to ex-Gaussian parameters), we calculate the squared
% error differences between model and empirical parameters and then search
% for its minimal value.

% We have 4 combinations of empirical values:
% DRT old
% DRT young
% GRT old
% GRT young

% To do this, MATLAB must load every .m model results file, find the
% average ex-Gaussian values for the 100 runs per model, calculate the
% squared error differences for each of the 4 condition combinations and
% add them to the respective matrix, along with the model number (the
% iteration number, i).

% After doing this for all models, the matrix must be ordered for crescent
% squared error values

clear all;

first_model = 1;
last_model = 241;
% three models cannot be processed (the ones with random frequency): 27, 54,
81
miu = zeros(100, last_model);
sigma = zeros(100, last_model);
tau = zeros(100, last_model);
% NOTE: for simplicity we create the matrices as if all models are imported.
% Then we eliminate columns 27, 54 and 81

% The same logic as above to create the final squared error matrices
error_drt_old = zeros(last_model, 2);
error_drt_young = zeros(last_model, 2);
error_grt_old = zeros(last_model, 2);
error_grt_young = zeros(last_model, 2);

% To be able to, then, see which parameter is diverging the most (i.e.
% causing the biggest error), we create matrices for each parameter error:
% MIU
miu_error_drt_old = zeros(last_model,2);
miu_error_drt_young = zeros(last_model,2);
miu_error_grt_old = zeros(last_model,2);
miu_error_grt_young = zeros(last_model,2);
% SIGMA
sigma_error_drt_old = zeros(last_model,2);
sigma_error_drt_young = zeros(last_model,2);
sigma_error_grt_old = zeros(last_model,2);
sigma_error_grt_young = zeros(last_model,2);
```

```
% TAU
tau_error_drt_old = zeros(last_model,2);
tau_error_drt_young = zeros(last_model,2);
tau_error_grt_old = zeros(last_model,2);
tau_error_grt_young = zeros(last_model,2);

% Define the average empirically obtained ex-Gaussian parameters:
drt_old_miu = 260.296;
drt_old_sigma = 20.899;
drt_old_tau = 54.980;

drt_young_miu = 285.791;
drt_young_sigma = 28.233;
drt_young_tau = 64.931;

grt_old_miu = 320.980;
grt_old_sigma = 36.226;
grt_old_tau = 86.200;

grt_young_miu = 325.784;
grt_young_sigma = 33.829;
grt_young_tau = 75.202;


for i = first_model:last_model
    if (i==27 || i==54 || i==81)
        % skip
        continue;
    end

    if (i < 10)
        foldername  =  strcat('C:\Users\Lea\Documents\University\Biomedical
Engineering (MSc)\Thesis\Projecto Maria Ribeiro\Test Runs\TEST RUN - RT alpha
model\Model_00', num2str(i), '\');
    elseif (i >= 10 && i < 100)
        foldername  =  strcat('C:\Users\Lea\Documents\University\Biomedical
Engineering (MSc)\Thesis\Projecto Maria Ribeiro\Test Runs\TEST RUN - RT alpha
model\Model_0', num2str(i), '\');
    elseif (i >= 100)
        foldername  =  strcat('C:\Users\Lea\Documents\University\Biomedical
Engineering (MSc)\Thesis\Projecto Maria Ribeiro\Test Runs\TEST RUN - RT alpha
model\Model_', num2str(i), '\');
    end

    for ii = 1:100
        filename = foldername;
        filename  =  strcat(filename,  'Run_',  num2str(ii),  '\result_',
num2str(ii), '.mat');
        data = load(filename);
        miu(ii, i) = data.miu;
        sigma(ii, i) = data.sigma;
        tau(ii, i) = data.tau;
    end

    % When we get to this point, the column corresponding to the current
    % model is complete with the data. We can now calculate the 4 different
    % squared error differences
    average_miu = mean(miu(:, i));
    average_sigma = mean(sigma(:, i));
```

```
    average_tau = mean(tau(:, i));

    current_miu_error_drt_old = (average_miu - drt_old_miu)^2;
    current_miu_error_drt_young = (average_miu - drt_young_miu)^2;
    current_miu_error_grt_old = (average_miu - grt_old_miu)^2;
    current_miu_error_grt_young = (average_miu - grt_young_miu)^2;

    current_sigma_error_drt_old = (average_sigma - drt_old_sigma)^2;
    current_sigma_error_drt_young = (average_sigma - drt_young_sigma)^2;
    current_sigma_error_grt_old = (average_sigma - grt_old_sigma)^2;
    current_sigma_error_grt_young = (average_sigma - grt_young_sigma)^2;

    current_tau_error_drt_old = (average_tau - drt_old_tau)^2;
    current_tau_error_drt_young = (average_tau - drt_young_tau)^2;
    current_tau_error_grt_old = (average_tau - grt_old_tau)^2;
    current_tau_error_grt_young = (average_tau - grt_young_tau)^2;

    % total sum of squares errors (SSE):
    current_error_drt_old       =       current_miu_error_drt_old       +
current_sigma_error_drt_old + current_tau_error_drt_old;
    current_error_drt_young     =     current_miu_error_drt_young     +
current_sigma_error_drt_young + current_tau_error_drt_young;
    current_error_grt_old       =       current_miu_error_grt_old       +
current_sigma_error_grt_old + current_tau_error_grt_old;
    current_error_grt_young     =     current_miu_error_grt_young     +
current_sigma_error_grt_young + current_tau_error_grt_young;

    % Put values into final matrices
    error_drt_old(i, :) = [i, current_error_drt_old];
    error_drt_young(i, :) = [i, current_error_drt_young];
    error_grt_old(i, :) = [i, current_error_grt_old];
    error_grt_young(i, :) = [i, current_error_grt_young];

    miu_error_drt_old(i, :) = [i, current_miu_error_drt_old];
    miu_error_drt_young(i, :) = [i, current_miu_error_drt_young];
    miu_error_grt_old(i, :) = [i, current_miu_error_grt_old];
    miu_error_grt_young(i, :) = [i, current_miu_error_grt_young];

    sigma_error_drt_old(i, :) = [i, current_sigma_error_drt_old];
    sigma_error_drt_young(i, :) = [i, current_sigma_error_drt_young];
    sigma_error_grt_old(i, :) = [i, current_sigma_error_grt_old];
    sigma_error_grt_young(i, :) = [i, current_sigma_error_grt_young];

    tau_error_drt_old(i, :) = [i, current_tau_error_drt_old];
    tau_error_drt_young(i, :) = [i, current_tau_error_drt_young];
    tau_error_grt_old(i, :) = [i, current_tau_error_grt_old];
    tau_error_grt_young(i, :) = [i, current_tau_error_grt_young];

end

% Now we must eliminate lines/columns that correspond to the eliminated
% models
miu(:, 27) = [];
miu(:, 54-1) = [];
miu(:, 81-2) = [];

sigma(:, 27) = [];
sigma(:, 54-1) = [];
sigma(:, 81-2) = [];
```

```
tau(:, 27) = [];
tau(:, 54-1) = [];
tau(:, 81-2) = [];

error_drt_old(27, :) = [];
error_drt_old(54-1, :) = [];
error_drt_old(81-2, :) = [];

error_drt_young(27, :) = [];
error_drt_young(54-1, :) = [];
error_drt_young(81-2, :) = [];

error_grt_old(27, :) = [];
error_grt_old(54-1, :) = [];
error_grt_old(81-2, :) = [];

error_grt_young(27, :) = [];
error_grt_young(54-1, :) = [];
error_grt_young(81-2, :) = [];


% Time to sort the rows in the error matrices:
sorted_error_drt_old = sortrows(error_drt_old, 2);
sorted_error_drt_young = sortrows(error_drt_young, 2);
sorted_error_grt_old = sortrows(error_grt_old, 2);
sorted_error_grt_young = sortrows(error_grt_young, 2);
```

A.III – Sets of parameters for all tested model variations

Table 4. All parameter combinations tested in our computational model. The models were given an identification number (ID) for practical purposes. Models with * were eliminated from analysis, for having been designed with a different paradigm, which was not pursued. This resulted in 238 models apt for analysis.

ID	*f* (Hz)	*N*	*dt* (ms)
1	8	10	10
2	8.2	10	10
3	8.4	10	10
4	8.6	10	10
5	8.8	10	10
6	9	10	10
7	9.2	10	10
8	9.4	10	10
9	9.6	10	10
10	9.8	10	10
11	10	10	10
12	10.2	10	10
13	10.4	10	10
14	10.6	10	10
15	10.8	10	10
16	11	10	10
17	11.2	10	10
18	11.4	10	10
19	11.6	10	10
20	11.8	10	10
21	12	10	10
22	12.2	10	10
23	12.4	10	10
24	12.6	10	10
25	12.8	10	10
26	13	10	10
27*	8 – 13	10	10
28	8	15	10

29	8.2	15	10
30	8.4	15	10
31	8.6	15	10
32	8.8	15	10
33	9	15	10
34	9.2	15	10
35	9.4	15	10
36	9.6	15	10
37	9.8	15	10
38	10	15	10
39	10.2	15	10
40	10.4	15	10
41	10.6	15	10
42	10.8	15	10
43	11	15	10
44	11.2	15	10
45	11.4	15	10
46	11.6	15	10
47	11.8	15	10
48	12	15	10
49	12.2	15	10
50	12.4	15	10
51	12.6	15	10
52	12.8	15	10
53	13	15	10
54*	8 – 13	15	10
55	8	20	10
56	8.2	20	10
57	8.4	20	10
58	8.6	20	10
59	8.8	20	10
60	9	20	10
61	9.2	20	10
62	9.4	20	10
63	9.6	20	10
64	9.8	20	10
65	10	20	10

66	10.2	20	10
67	10.4	20	10
68	10.6	20	10
69	10.8	20	10
70	11	20	10
71	11.2	20	10
72	11.4	20	10
73	11.6	20	10
74	11.8	20	10
75	12	20	10
76	12.2	20	10
77	12.4	20	10
78	12.6	20	10
79	12.8	20	10
80	13	20	10
81*	8 – 13	20	10
82	8	25	10
83	8.2	25	10
84	8.4	25	10
85	8.6	25	10
86	8.8	25	10
87	9	25	10
88	9.2	25	10
89	9.4	25	10
90	9.6	25	10
91	9.8	25	10
92	10	25	10
93	10.2	25	10
94	10.4	25	10
95	10.6	25	10
96	10.8	25	10
97	11	25	10
98	11.2	25	10
99	11.4	25	10
100	11.6	25	10
101	11.8	25	10
102	12	25	10

103	12.2	25	10
104	12.4	25	10
105	12.6	25	10
106	12.8	25	10
107	13	25	10
108	8	30	10
109	8.2	30	10
110	8.4	30	10
111	8.6	30	10
112	8.8	30	10
113	9	30	10
114	9.2	30	10
115	9.4	30	10
116	9.6	30	10
117	9.8	30	10
118	10	30	10
119	10.2	30	10
120	10.4	30	10
121	10.6	30	10
122	10.8	30	10
123	11	30	10
124	11.2	30	10
125	11.4	30	10
126	11.6	30	10
127	11.8	30	10
128	12	30	10
129	12.2	30	10
130	12.4	30	10
131	12.6	30	10
132	12.8	30	10
133	13	30	10
134	8	10	15
135	9	10	15
136	10	10	15
137	11	10	15
138	12	10	15
139	13	10	15

140	8	15	15
141	9	15	15
142	10	15	15
143	11	15	15
144	12	15	15
145	13	15	15
146	8	20	15
147	9	20	15
148	10	20	15
149	11	20	15
150	12	20	15
151	13	20	15
152	8	25	15
153	9	25	15
154	10	25	15
155	11	25	15
156	12	25	15
157	13	25	15
158	8	10	20
159	9	10	20
160	10	10	20
161	11	10	20
162	12	10	20
163	13	10	20
164	8	15	20
165	9	15	20
166	10	15	20
167	11	15	20
168	12	15	20
169	13	15	20
170	8	10	5
171	8	15	5
172	8	20	5
173	8	25	5
174	8	30	5
175	8	20	20
176	9	20	20

177	10	20	20
178	11	20	20
179	12	20	20
180	13	20	20
181	9.2	10	20
182	9.4	10	20
183	9.6	10	20
184	9.8	10	20
185	10.2	10	20
186	10.4	10	20
187	10.6	10	20
188	10.8	10	20
189	11.2	10	20
190	11.4	10	20
191	11.6	10	20
192	11.8	10	20
193	12.2	10	20
194	12.4	10	20
195	12.6	10	20
196	12.8	10	20
197	12.2	21	10
198	12.2	22	10
199	8	25	20
200	12.2	23	10
201	12.2	24	10
202	12.2	24	11
203	12.2	24	12
204	12.2	24	13
205	13	24	13
206	13	24	12
207	13	24	11
208	12.8	24	11
209	12.6	24	11
210	12.4	24	11
211	12	24	11
212	11.8	24	11
213	13	23	11

214	12.8	23	11
215	12.6	23	11
216	12.4	23	11
217	12.2	23	11
218	12	23	11
219	11.8	23	11
220	10.4	11	20
221	10.4	12	20
222	12.8	11	20
223	12.8	12	20
224	10.4	10	19
225	12.8	10	19
226	10.4	10	18
227	12.8	10	18
228	12.8	10	17
229	10.4	10	17
230	12.8	11	17
231	10.4	11	17
232	12.8	12	17
233	12.2	23	12
234	12.4	23	12
235	12	23	12
236	11.8	23	12
237	10.4	23	12
238	10.2	23	12
239	10	23	12
240	10.6	23	12
241	10.8	23	12

A.IV – Listed top sets of parameters that best minimized the SSE

Table 5. Top four sets of parameters that best minimized the sum of squared errors (SSE) for experimental factor combination: DRT $_{young}$.

Position	**Best-fitting model parameters DRT $_{young}$**			**SSE**
	***f* (Hz)**	***N***	***dt* (ms)**	
#1	10.4	10	20	79.866
#2	10.2	10	20	85.222
#3	10.6	10	20	94.949
#4	10.8	10	20	117.649

Table 6. Top four sets of parameters that best minimized the sum of squared errors (SSE) for experimental factor combination: DRT $_{old}$.

Condition	**Best-fitting model parameters DRT $_{old}$**			**SSE**
	***f* (Hz)**	***N***	***dt* (ms)**	
#1	12.8	10	19	37.194
#2	12.8	11	17	55.115
#3	12.8	10	20	56.240
#4	12.6	10	20	60.268

Table 7. Top four sets of parameters that best minimized the sum of squared errors (SSE) for experimental factor combination: GRT $_{young}$.

Condition	Best-fitting model parameters GRT young			SSE
	f **(Hz)**	***N***	***dt*** **(ms)**	
#1	12	23	12	202.798
#2	12.2	23	12	207.900
#3	12.4	23	12	208.316
#4	11.8	23	12	215.845

Table 8. Top four sets of parameters that best minimized the sum of squared errors (SSE) for experimental factor combination: GRT $_{old}$.

Condition	Best-fitting model parameters GRT old			SSE
	f **(Hz)**	***N***	***dt*** **(ms)**	
#1	11.8	24	11	271.357
#2	12	24	11	279.166
#3	12.4	24	11	294.058
#4	12.2	24	11	306.197